(ATINER)

Athens Journal of Sciences

(ATINER)

Volume 6, Issue 3, September 2019

Articles

Front Pages

OSMAN ISMAIL, AZMI SEYHUN KIPCAK & IBRAHIM DOYMAZ

Drying of Okra by Different Drying Methods: Comparison of Drying time, Product Color Quality, Energy Consumption and Rehydration

CAROLIN NEUGEBAUER

Sedimentation Processes in the Black Sea during the Last Glacial Period Deduced from Grain Size Analyses on Gravity Core MSM 33/54-3 from the Eastern Anatolian Continental Margin

SEWODO AUGUSTIN DEGBE & BINGLIANG SONG

Dry Ports Development: A Pivot Strategy to Enhance Sustainable Transit Traffic via West African Corridors

UVS SESHAVATHARAM & S LAKSHMINARAYANA

A Practical Model of Godel–Planck–Hubble–Birch Universe

ATHENS INSTITUTE FOR EDUCATION AND RESEARCH
A World Association of Academics and Researchers
8 Valaoritou Str., Kolonaki, 10671 Athens, Greece.
Tel.: 210-36.34.210 Fax: 210-36.34.209
Email: info@atiner.gr URL: www.atiner.gr
(ATINER) Established in 1995 (ATINER)

Mission

ATINER is a ***World Non-Profit Association*** of Academics and Researchers based in Athens. ATINER is an independent **Association** with a **Mission** to become a forum where Academics and Researchers from all over the world can meet in Athens, exchange ideas on their research and discuss future developments in their disciplines, **as well as engage with professionals from other fields**. Athens was chosen because of its long history of academic gatherings, which go back thousands of years to *Plato's Academy* and *Aristotle's Lyceum*. Both these historic places are within walking distance from ATINER's downtown offices. Since antiquity, Athens was an open city. In the words of Pericles, **Athens*"...is open to the world, we never expel a foreigner from learning or seeing".*** ("Pericles' Funeral Oration", in Thucydides, *The History of the Peloponnesian War).* It is ATINER's **mission** to revive the glory of Ancient Athens by inviting the World Academic Community to the city, to learn from each other in an environment of freedom and respect for other people's opinions and beliefs. After all, the free expression of one's opinion formed the basis for the development of democracy, and Athens was its cradle. As it turned out, the Golden Age of Athens was in fact, the Golden Age of the Western Civilization. *Education* and *(Re)searching* for the 'truth' are the pillars of any free (democratic) society. This is the reason why *Education* and *Research* are the two core words in ATINER's name.

The Athens Journal of Sciences
ISSN NUMBER: 2241-8466- DOI: 10.30958/ajs
Volume 6, Issue 3, September 2019
Download the entire issue (PDF)

Front Pages i-viii

Drying of Okra by Different Drying Methods: Comparison of Drying time, Product Color Quality, Energy Consumption and Rehydration 155
Osman Ismail, Azmi Seyhun Kipcak & Ibrahim Doymaz

Sedimentation Processes in the Black Sea during the Last Glacial Period Deduced from Grain Size Analyses on Gravity Core MSM 33/54-3 from the Eastern Anatolian Continental Margin 169
Carolin Neugebauer

Dry Ports Development: A Pivot Strategy to Enhance Sustainable Transit Traffic via West African Corridors 183
Sewodo Augustin Degbe & Bingliang Song

A Practical Model of Godel–Planck–Hubble–Birch Universe 211
UVS Seshavatharam & S Lakshminarayana

Athens Journal of Sciences
Editorial and Reviewers' Board

President's Message

All ATINER's publications including the e-journals are open access without any costs (submission, processing, publishing, open access paid by authors, open access paid by readers etc.) and are independent of the presentations made at any of the many small events (conferences, symposiums, forums, colloquiums, courses, roundtable discussions) organized by ATINER throughout the year. The intellectual property rights of the submitted papers remain with the author.

Before you submit, please make sure your paper meets some basic academic standards, which include proper English. Some articles will be selected from the numerous papers that have been presented at the various annual international academic conferences organized by the different divisions and units of the Athens Institute for Education and Research.

The plethora of papers presented every year will enable the editorial board of each journal to select the best ones, and in so doing, to produce a quality academic journal. In addition to papers presented, ATINER encourages the independent submission of papers to be evaluated for publication.

The current issue of the Athens Journal of Sciences (AJS) is the third issue of the sixth volume (2019). The reader will notice some changes compared with the previous volumes, which I hope is an improvement. An effort has been made to include papers which extent to different fields of the Natural and Formal Sciences.

Gregory T. Papanikos, President
Athens Institute for Education and Research

8th Annual International Conference on Chemistry
20-23 July 2020, Athens, Greece

The Chemistry Unit of ATINER, will hold its **8th Annual International Conference on Chemistry, 20-23 July 2020, Athens, Greece** sponsored by the Athens Journal of Sciences. The aim of the conference is to bring together academics and researchers of all areas of chemistry and other related disciplines. You may participate as stream organizer, presenter of one paper, chair a session or observer. Please submit a proposal using the form available (https://www.atiner.gr/2020/FORM-CHE.doc).

Academic Members Responsible for the Conference

- **Dr. Ellene Tratras Contis**, Head, Chemistry Unit, ATINER & Professor of Chemistry, Eastern Michigan University, USA.
- **Dr. Nicolas Abatzoglou**, Head, Environment Unit, ATINER & Professor, Department of Chemical & Biotechnological Engineering, University of Sherbrook, Canada, Chair Pfizer, PAT in Pharmaceutical Engineering, Director GREEN-TPV and GRTP-C & Pwelcomes.

Important Dates

- Abstract Submission: **16 December 2019**
- Acceptance of Abstract: 4 Weeks after Submission
- Submission of Paper: **22 June 2020**

Social and Educational Program

The Social Program Emphasizes the Educational Aspect of the Academic Meetings of Atiner.

- Greek Night Entertainment (This is the official dinner of the conference)
- Athens Sightseeing: Old and New-An Educational Urban Walk
- Social Dinner
- Mycenae Visit
- Exploration of the Aegean Islands
- Delphi Visit
- Ancient Corinth and Cape Sounion

Conference Fees

Conference fees vary from 400€ to 2000€
Details can be found at: https://www.atiner.gr/2019fees

8th Annual International Conference on Physics
20-23 July 2020, Athens, Greece

The Physics Unit of ATINER, will hold its **7th Annual International Conference on Physics, 20-23 July 2020, Athens, Greece** sponsored by the Athens Journal of Sciences. The aim of the conference is to bring together academics and researchers of all areas of physics and other related disciplines. You may participate as stream organizer, presenter of one paper, chair a session or observer. Please submit a proposal using the form available (https://www.atiner.gr/2020/FORM-PHY.doc).

Important Dates

- Abstract Submission: **16 December 2019**
- Acceptance of Abstract: 4 Weeks after Submission
- Submission of Paper: **22 June 2020**

Academic Member Responsible for the Conference

- **Dr. Ethel Petrou**, Academic Member, ATINER & Professor and Chair, Department of Physics, Erie Community College-South, State University of New York, USA.
- **Dr. Bala Maheswaran**, Head, Electrical Engineering Unit, ATINER & Professor, Northeastern University, USA.

Social and Educational Program

The Social Program Emphasizes the Educational Aspect of the Academic Meetings of Atiner.

- Greek Night Entertainment (This is the official dinner of the conference)
- Athens Sightseeing: Old and New-An Educational Urban Walk
- Social Dinner
- Mycenae Visit
- Exploration of the Aegean Islands
- Delphi Visit
- Ancient Corinth and Cape Sounion

More information can be found here: https://www.atiner.gr/social-program

Conference Fees

Conference fees vary from 400€ to 2000€
Details can be found at: https://www.atiner.gr/2019fees

Drying of Okra by Different Drying Methods: Comparison of Drying time, Product Color Quality, Energy Consumption and Rehydration

By Osman Ismail[*], Azmi Seyhun Kipcak[†] & Ibrahim Doymaz[‡]

In this study, okra was dried and modelled with using five different drying methods exist in literature. In the methods of vacuum and hot air drying, the drying temperature of 50°C was selected, while the powers of microwave and infrared were set as 90 W and 83 W, respectively. The results were evaluated in terms of drying time, product color quality, energy consumption and rehydration. The minimum drying time was obtained by microwave drying method. Also, the energy efficiency increased with the microwave drying method. In terms of color criteria the best value was obtained by the hot-air drying method. Rehydration content of dried okra samples with hot air was higher than that of other drying methods. From the results of this study, the most efficient drying methods were determined as microwave and hot-air drying.

Keywords: *Color, Drying Methods, Rehydration, Specific Energy Consumption.*

Introduction

Okra (*Abelmoschus esculentus L. Moench*), which belongs to the family Malvaceae is an annual vegetable crop growing 3 to 6 feet tall (Pendre et al. 2012, Afolabi and Agarry 2014). According to FAO data for 2015[1], okra production all over the world was about 1104407 hectares. The major producer countries include India (530790 hectares), Nigeria (385000 hectares), Ivory Coast (50000 hectares), Cameroon (23998 hectares) and Sudan (22114 hectares). Turkey has the tenth place in the production of okra with 6099 hectares.

Among the several drying methods, in hot air drying method, which has been used widely, the lower energy efficiency and long drying times are the disadvantages (El-Mesery and Mwithiga 2012, Feng and Tang 1998, Pan et al. 2008). Open-sun drying is the most common method of crop drying in developing countries. Despite several disadvantages, open-sun drying is still used in many places throughout the world where plenty of solar radiation is available. Also it is renewable, cheap and eco-friendly. The only problem of drying open-sun is drying time is slow according to the other drying methods (Tunde-Akintunde 2011).

In recent years, attempts have been made to shorten the drying period to improve the energy efficiency of the drying process and the quality of the dried

[*]Assistant Professor, Yildiz Technical University, Turkey.
[†]Associate Professor, Yildiz Technical University, Turkey.
[‡]Associate Professor, Yildiz Technical University, Turkey.
[1] FAO Statistical Database (2015). Available from: http://faostat.fao.org/.

products. The quality of the dried products could be improved by decreasing the drying temperature or the drying time. Therefore, instead of open-sun drying, microwave, infrared, oven and vacuum drying is widely preferred (Başlar et al. 2014). Infrared drying method has so many advantages in comparison with hot air drying, because the equipment can be compact with easily controllable parameters (Sakai and Mao 2006). In microwave drying, short drying time that leads to lower energy consumption and better quality of the dried food is the most advantage among the other drying methods (İsmail and Kocabay 2016).

The increase in the population and energy needs are two important factors that trigger each other. Energy production is with increasing need in developing countries, directly proportional to the development level of the country. The food industry has the energy-dependent processes required for ensuring the freshness of foods and reliability. Heat treatment and drying are the most common processes, which use significant amount of energy for the preservation of foods. In the food industry 29% of the total energy used in the heat treatment processes and 16% is used for cooling and freezing processes. In today, various criteria are evaluated for the drying performances; such as moisture absorption rate, energy consumption and specific energy consumption (Okos et al. 1998). For this relation to decrease the energy costs is the main focus for the dehydration processes. Existing studies in the literature is very much about the drying methods of food products. Also these methods are known as the energy-consuming food preservation methods, hence to decrease the energy cost on these methods is worth of a study.

There are several factors influencing the quality parameters of dried product. Some chemical and biochemical reactions such as browning reactions and lipid oxidation might alter the final color (Okos et al. 2007). Drying conditions and physicochemical changes that occur during drying and rehydration processes seem to affect the quality properties of the rehydrated products (Rudra et al. 2008).

Processed and value added products are gaining importance in the worldwide markets. Dried okra is one of these. According to TUIK data for 2015, okra production all over the Turkey was about 31,898 tonnes. Okra is mainly exported in the form of fresh okra, dehydrated okra, canned okra and okra pickle. Dehydrated okra is considered as a potential product in world trade. In European countries, the demand for fresh and dried okra is very high. For this reason, the exports of okra play an important role in the Turkish economy. The various kinds of drying methods followed for dehydration of okra such as convective air drying, open sun drying, vacuum drying, microwave drying and infrared drying are reviewed here. These techniques are mainly used for preservation and value addition of okra. There are many studies on okra in the literature. Other studies about okra dried with different drying methods and present works are summarized in Table 1 (Afolabi and Agarry 2014, Wankhade et al. 2012, Doymaz 2011, Kocabay and Ismail 2017, Dadalı et al. 2007, Doymaz 2005, Shivharea et al. 2010, Gogus and Maskan 1999, Adom et al. 1997, Al-Sulaiman 2011, Ismail and Ibn Idriss 2013, Ajay and Fakayode 2011, Huang and Zhang 2016, Aamir and Boonsupthip 2017).

Table 1. *Studies on the Drying of Okra in the Literature*

Drying method	Pretreatment	Drying conditions (Hot air (°C) Microwave (W)	Air velocity (m/s)	Drying time min	Ref.
Hot air drying	Natural	50, 60, 70	-	600-780	Afolabi and Agarry 2014
Sun drying		-	-	7200	Afolabi and Agarry 2014
Solar drying		-	-	4320	Afolabi and Agarry 2014
Hot air drying	Natural	40	1	960	Wankhade et al. 2012
Sun drying		-	-	1380	
Solar drying		-	-	900	
Sun drying	Natural	-	-	6000	Doymaz 2011
Sun drying	Natural	-	-	1980	Kocabay and Ismail 2017
	Blanched	-	-	1080	
	Salted	-	-	1320	
Microwave drying	Natural	180, 360, 540, 720, 900	-	50, 37, 23, 20, 15	Dadalı et al. 2007
Hot air drying	Natural	50, 60, 70	1	960, 630, 480	Doymaz 2005
Hot air drying	NaCl-blanched	40, 55, 70	-	780, 540, 300	Shivharea et al. 2010
Hot air drying	Natural	60, 70, 80	1.2	860, 570, 440	Gogus and Maskan 1999
Solar tent dryer	Natural	30-60	0-0.2	2880	Adom et al. 1997
Microwave drying	Natural	75, 150, 300, 500,700, 900	-	19, 18, 17, 16, 15, 13	Al-Sulaiman 2011
Solar drying	Natural	-	-	1620	Ismail and Ibn Idriss 2013
Hot air drying	Natural	50, 60, 70	14.6	580, 560, 540	Ajay and Fakayode 2011
Vacuum freeze drying	Natural	100 Pa 45, -38 °C	-	720	Huang and Zhang 2016
Microwave vacuum drying		500	-	110	
Pulse-spouted microwave vacuum drying		500	-	95	
Microwave drying	Natural	440, 618, 800	-	7, 5, 4	Aamir and Boonsupthip 2017

As it is seen from the literature, at the sun drying the drying times were very different due to the daily temperature and solar radiation (W/m^2) in summer months (June, July and August), relative humidity, wind speed and okra thickness. The differences of the hot-air drying times are due to the relative humidity and air–flow. There is no considerable difference in microwave drying.

Hot air drying and sun drying are traditional drying technologies widely used in the drying of agricultural products for a long time, but usually recognized as time-consuming or producing lower-quality products. Microwave drying is a rather effective drying technology that has advantages over traditional drying technologies. According to the studies given in the literature, there is no study about the infrared and vacuum oven drying of okra. In the sun drying of okra the ambient temperature less than 50°C, so in this study considering the mentioned temperature 50°C is taken as the reference temperature. Hence, reduced power levels both on microwave and infrared method is used. Based on the literature, five different drying methods have been applied to the drying of the okra samples. Drying time, product color, energy consumption rehydration are examined and compared.

Methodology

Samples

Fresh okra *(Hibiscus esculentus L.)* samples, which have approximately the same length and diameter were collected from Thrace region of Turkey. The selected okra samples were cleaned with tap water to make samples free from dust and foreign materials and stored at 4.0±0.5°C in the refrigerator for about one day for the moisture equilibrium. Then, okras were removed from the refrigerator and allowed to reach to the ambient temperature. The stalk and tapered head of the cleaned samples were cut off to form a cylinder-like shape with an approximate length and weight of 50±0.3 mm and 4±0.3 g, respectively. Average diameter of okra samples was measured as 1.1±0.2 cm. Dry matter and moisture contents of the fresh samples were determined prior to drying process. To determine the initial moisture content, four identical experiments were conducted. In these experiments approximately 15±0.2 g samples were dried in an oven (Memmert UM-400, Germany) at 105℃ for 24 h (AOAC 1990). The average initial moisture content of okra was found as 84 % wet base (w.b.).

Drying Equipments and Drying Procedures

After the drying procedures explained below, all of the dried samples were packed in low density polyethylene bags.

Open-Sun Drying

Open-sun drying experiments were carried out during August 2016 (08.00 AM - 20.00 PM) in Turkey. The okra samples, about 30±0.2 g were distributed uniformly in a single layer in the sample tray, and exposed to sunlight for 12 h daily. Moisture loss and temperature of the ambient air were measured at 1 hour intervals during drying by a portable digital balance (Alfais, I2000-1, which has 0-300 g measurement range with an accuracy of ±0.1 g). When the drying time took more than 12 h, the samples during the night were packed for reducing the effect on increase in moisture content. During the drying experiments, the temperature of ambient air ranged from 32 to 45°C. The highest air temperature was reached between 10:30 AM and 14:30 PM. Drying was continued until the samples reached the desired moisture level of approximately 0.092 g water/g dry matter.

Infrared Drying

Drying experiments were carried out in a moisture analyzer with one 250 W halogen lamp (Snijders Moisture Balance, Snijders b.v., Tilburg, Holland). In the infrared drying process, samples should be separated evenly and homogeneously over the entire pan. The power level was set in control unit of equipment. The drying experiment was performed at infrared power level to 83 W. The samples of okra (approximately 30±0.2 g) were removed of dryer at a time interval of 15 min during the drying process, and their weights were measured with a digital balance (Precisa, model XB220A, Precisa Instruments AG, Dietikon, Switzerland) with an accuracy of 0.001 g. The temperature is not measured. Drying was finished when the moisture content of the samples was approximately 0.084 g water / g dry matter.

Microwave Drying

Drying experiments were carried out in a Robert Bosch Hausgerate GmbH (Germany) model microwave oven which has a maximum output of 800 W working at 2450 MHz. The microwave oven has the capability of operating at different microwave stages, from 90 W to 800 W. The area on which microwave drying was performed was 530×500×322 mm in size and consisted of a rotating glass plate 300 mm in diameter at the base of the oven. The adjustment of microwave output power and processing time was done with the aid of a digital control facility located on the microwave oven. Drying experiment was carried out at a microwave power level of 90 W. During drying experiment 30±0.2 g okra arranged as a thin layer on the rotatable plate fitted inside the microwave oven cabinet. The rotating glass plate was removed from the oven every 2 min during the drying period and moisture loss determined by weighing the plate using a digital balance. The temperature is not measured. Microwave drying continued till the moisture reduces to 0.112 g water/g dry matter of the initial moisture content.

Vacuum Oven Drying

Vacuum oven drying was performed in a laboratory type vacuum oven (Nuve EV 018, Turkey) with technical features of ~220 V, 50 Hz, 3.5 A and 800 W. The temperature of the vacuum oven has a sensitivity of 1°C, with a max temperature of 250°C. The area on which vacuum drying oven was performed was 30×20×25 cm in size. A laboratory type vacuum pump (KNF N026 1.2 AN 18, Turkey) was used in the vacuum drying operation. Its operating conditions were 220 V, 50 Hz and 0.85 A. The adjustment of vacuum value and processing temperature was done with the aid of a digital control facility located on the vacuum drying oven. The drying experiment was carried out using okra samples of weight of about 30±0.2 g and at one vacuum oven dryer at a constant temperature of 50°C and pressure of 0.1 kPa. Moisture loss in the okra samples was measured at 30 min intervals. Drying was finished when the moisture content of the samples was approximately 0.087 g water / g dry matter.

Hot-Air Drying

Drying experiments were performed in a cabinet type dryer (APV & PASILAC Limited of Carlisle, Cumbria, UK). It was constructed from stainless steel sheets formed as a rectangular tunnel of dimensions 0.54×1.4×1.02 m. The dryer consisted of a centrifugal fan to supply the airflow, an electrical heater, an air filter and a proportional temperature controller. The dryer is operated at dry bulb temperatures between 0 - 200°C. The desired drying air temperature was attained by electrical resistance and controlled by the heating control unit. The velocity of air passing through the system was measured via a 0.4-30 m/s range anemometer (model AM-4201, Lutron Electronic, Taipei, Taiwan). The airflow was measured directly in the drying chamber. The samples are dried in the perforated basket 30 cm square and 11 cm high, and moisture loss is recorded during drying by a specially developed weighing unit. This weighing unit consists of a balance (20 kg capacity), hanger rod, digital indicator and load cell (Revere Transducers Europe, Holland). The okra samples, about 50±0.3 g were distributed uniformly in a single layer in the sample tray, and then dried in hot air dryer at 50ºC air temperature and a constant air velocity of 1 m/s. Moisture loss in the okra samples was measured at 30 min intervals. Drying was finished when the moisture content of the samples was approximately 0.085 g water/g dry matter.

Color Measurement

Sample color was measured before (fresh okra) and after drying methods using a Chromameter CR-400 (Minolta, Japan). *L*, *a* and *b* values were measured to describe three dimensional color space and interpreted as follows: *L* is the brightness/lightness or whiteness ranging from no reflection for black (*L*=0) to perfect diffuse reflection for white (*L*=100). The value *a*, is the redness ranging from negative values for green to positive values for red. The value *b* is the

yellowness ranging from negative values for blue to positive values for yellow. The total change in color (ΔE) of dried samples was calculated as follows (Phoungchandang and Saentaweesuk 2011):

$$\Delta E = \sqrt{\left((L_o - L)^2 + (a_0 - a)^2 + (b_0 - b)^2\right)} \quad (1)$$

where L_o, a_o and b_o are the color values of okra samples before drying samples. Fresh okra samples were used as the reference while a higher ΔE represents a greater colour change from the reference material.

Calculation of Specific Energy Consumption

The total energy consumption of the drying process was evaluated through the Specific Energy Consumption (SEC). During drying, the electrical energy was consumed. Energy consumption of infrared radiation, microwave, hot-air convection, oven and vacuum oven with together vacuum pump was determined using a digital electric counter (Kaan, Type 111, Turkey) with 0.01 kWh precision. The specific energy consumption which is a measure of the energy needed to evaporate a unit mass of water from the product was calculated using Eq. 2 (Ismail and Kocabay 2016):

$$Q_s = \frac{Q_t}{m_w} \quad (2)$$

where Q_s is the specific energy consumption in kWh / kg water, Q_t is the consumed energy in kWh, and m_w is the mass of vaporized water in kg water.

Rehydration Experiments

Rehydration and diffusion are two important parameters in the characterization of the dried foods. Okra samples were rehydrated by immersion in distilled water at controlled room temperature. In other words, five dried okra samples introduced in a plastic mesh basket were immersed during a pre-determined time into water at 25°C using glass jar with 300 mL of water. At every 30 min intervals, okra samples were removed from water, drained, and weighed. The weights of samples were measured with an electronic digital balance. The weight change was observed at specific intervals until the equilibrium moisture content was reached. The experiments were carried out in duplicate and their average values were reported. The rehydration ratio (R_R) was calculated using Eq. 3:

$$R_R = \frac{W_t - W_{dry}}{W_{dry}} \tag{3}$$

where W_t and W_{dry} are the weight of the samples at any time (g) and the dry weight (g), respectively. Also in the rehydration experiments, the data observed were found at $p < 0.05$.

Results and Discussion

Drying Time

The effect of the different drying methods on the drying time of okra is given in Figure 1. From Figure 1 it is seen that the drying times of okra was recorded in the range of 46 min to 50 h. The maximum drying time of okra was reached by the open-sun drying method with a drying value of 50 h. Like the microwave method in which the experiments were conducted at 90 W power level, the drying time of the okra samples about 46 minutes. Other drying methods, which were conducted at a temperature of 50°C, the drying times were found as 13.5, 10 and 9.25 h for the drying methods of hot-air, vacuum and infrared drying, respectively. The drying times were determined from highest to lowest as; open-sun drying > hot-air drying > vacuum drying > infrared drying > microwave drying.

Figure 1. *The Effect of the Drying Methods on the Drying Time of Okra*

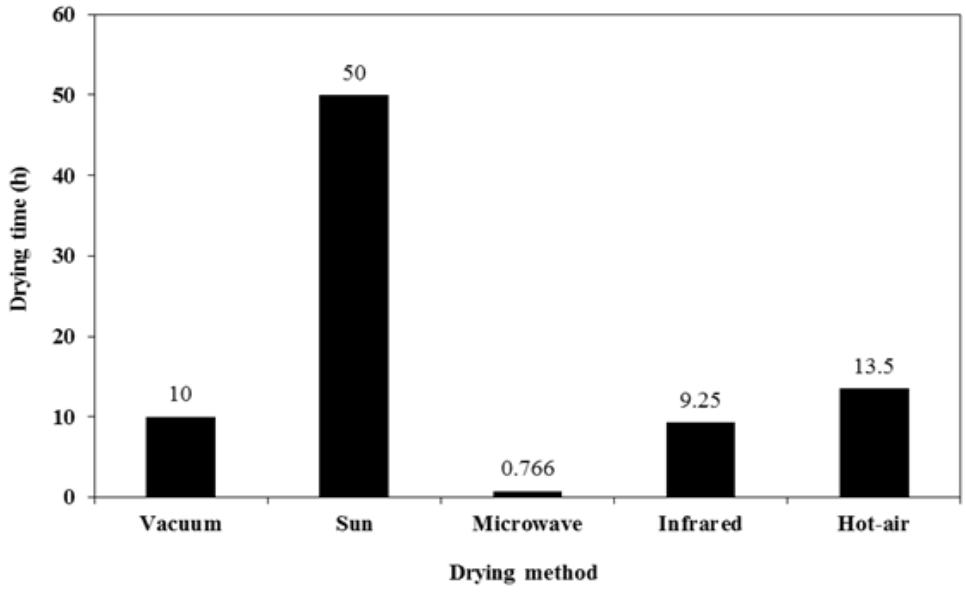

Color Analysis

Color is one of the most important factors among the food acceptability parameters. Too much color change on the food product adversely affects the food quality, which leads to decrease the marketing sales of the products. In other words, the initial quality parameter assessed by customers is the surface color of the food. The fresh okra samples *L, a* and *b* values were measured as 42.69, -3.6 and 8.34, respectively. The impact of different drying methods upon the color parameters of the dried okra samples was exhibited in Table 2.

Table 2. *Color Analysis Results of Okra*

Drying methods	**Samples**	***L****	***a***	***b***	***ΔE***
	Fresh	42.69 ± 0.99	-3.6 ± 0.84	8.34 ± 0.54	-
Vacuum oven	Dry	44.71 ± 1.03	6.80 ± 0.78	9.39 ± 0.68	10.64 ± 1.08
Open-sun	Dry	51.35 ± 1.26	11.38 ± 0.89	16.02 ± 0.65	18.93 ± 1.34
Microwave	Dry	50.21 ± 0.59	4.85 ± 0.72	15.79 ± 1.03	13.54 ± 0.94
Infrared	Dry	45.39 ± 1.04	5.39 ± 0.39	14.36 ± 0.74	11.15 ± 1.92
Hot-air	Dry	48.82 ± 1.18	3.67 ± 0.16	9.80 ± 0.90	9.62 ± 1.18

*Values are means ± SEE.

From the results of Table 2, it is seen that the fresh okra had a lightness value of 42.69. The lightness values of the dried okra samples range from 44.71 to 51.35, where the all drying methods increased the lightness. The highest lightness value was seen at the method of open-sun drying with a value of 51.35. Then, microwave and hot-air drying methods were followed with the lightness values of 50.21 and 48.82, respectively. From the *a* and *b* values results of the dried okras, it is seen that the redness and yellowness of the dried okras were increased with respect to fresh okras.

The total color change (ΔE) was calculated according to Eq. (1) using the measured *L, a* and *b* values. A larger ΔE value represents a greater change in color. Table 2 also presents the *ΔE* of the sample dried at five drying conditions. The color change of the dried okra samples was determined in terms of *ΔE*, which ranged from 9.62 to 18.93 for different drying methods. The lowest *ΔE* value is seen on the hot air drying method with a value of 9.62. Result from here, hot air dried okra showed the least color change compared to the fresh okra sample. Similar results can be seen in the literature (Mana et al. 2012, Cao et al. 2016). Since high lightness (*L*) and low total color change (ΔE) value were preferred in the food drying, hot air drying method gave better results for the preservation of the color quality.

Energy Consumption

The energy consumption values obtained using vacuum, microwave, infrared and hot-air drying of okras are given in Figure 2. When the four drying methods were compared with respect to energy consumption values, it is seen that the lowest energy consumption occurred in microwave drying method and it is followed by infrared, vacuum and hot-air drying methods. Since the energy value for open-sun drying method is zero, open-sun drying method is not included in Figure 2.

Figure 2. *Energy Consumption during the Drying of Okras*

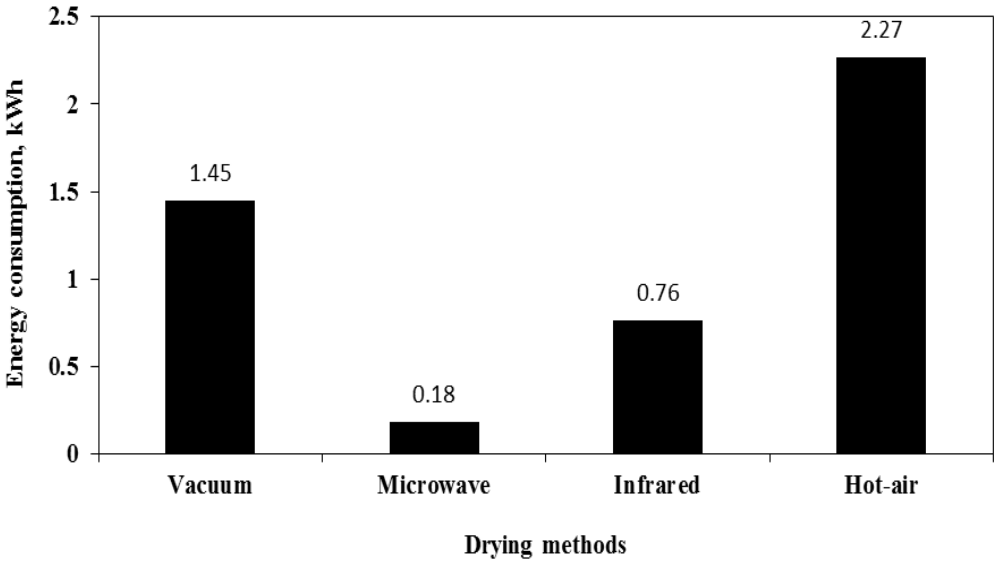

The best result was found as the microwave drying method among all drying methods considering the energy consumption values. Energy consumption of microwave method was found as 0.18 kWh. The highest value in all drying methods considering the energy consumption was seen in hot-air drying, with a value of 2.27 kWh. Other methods of infrared and vacuum oven drying energy consumption values are found as 0.76 and 1.45 kWh, respectively. As a result of this study, the drying processes carried out at low temperature and power levels, leads to a longer drying period and higher energy consumptions. These results are in agreement with the literature (El-Mesery and Mwithiga 2012).

Specific Energy Consumption

The specific energy consumption was determined, in all of the four drying methods by considering the total energy supplied to dry the okra samples from initial moisture content of about 5.25 g water / g dry matter to a final moisture content of approximately 0.07-0.12 g water / g dry matter. The specific energy consumption of the drying process under different drying methods were calculated by using Eq. (2) and given in Figure 3. As can be seen from Figure

3, the minimum energy (20.54 kWh / kg water) is needed for drying of 1 kg of okra samples at microwave drying method. The maximum energy (69.95 kWh / kg water) is needed at vacuum oven drying method. Hence microwave drying method is the most suitable method for drying fresh okra samples because of the minimum energy consumption (20.54 kWh / kg water) and drying time (46 min). The results that are found are similar to those reported by researchers for other products (Sharma and Prasad 2006, Motevali et al. 2011).

Figure 3. *Specific Energy Consumption for Drying 1 kg of Wet Product*

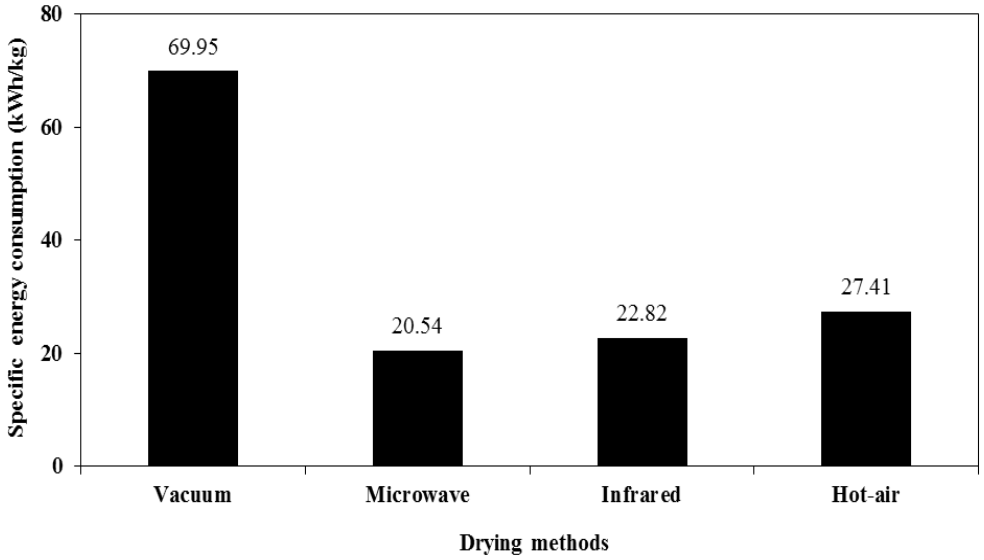

Rehydration

Rehydration process depends on structural changes in vegetal tissues and cells of food material during drying, which produces shrinkage and collapse and reduces the water absorption capacity, thereby preventing the complete rehydration of the dried product (Krokida and Philippopoulos 2005). Using Eq. (3), the rehydration content (R_R) values are calculated and are shown in Figure 4. Since there are no significance changes after 200 mins, rehydration experiments were terminated at 270 mins. As it seen from Figure 4, the rehydration contents ranged from 3.35 to 4.86 $g_{water}/g_{dry\ matter}$. The highest rehydration content of 4.86 g water / g dry matter was found in hot-air method then followed by open-sun (4.39 $g_{water}/g_{dry\ matter}$), infrared 4.29 ($g_{water}/g_{dry\ matter}$), vacuum oven (4.12 $g_{water}/g_{dry\ matter}$) and microwave (3.35 $g_{water}/g_{dry\ matter}$) methods. Similar results can be found at the studies of Moreira et al. (2008) and Mana et al. (2012).

Figure 4. *Rehydration Results of Dried Okra Samples*

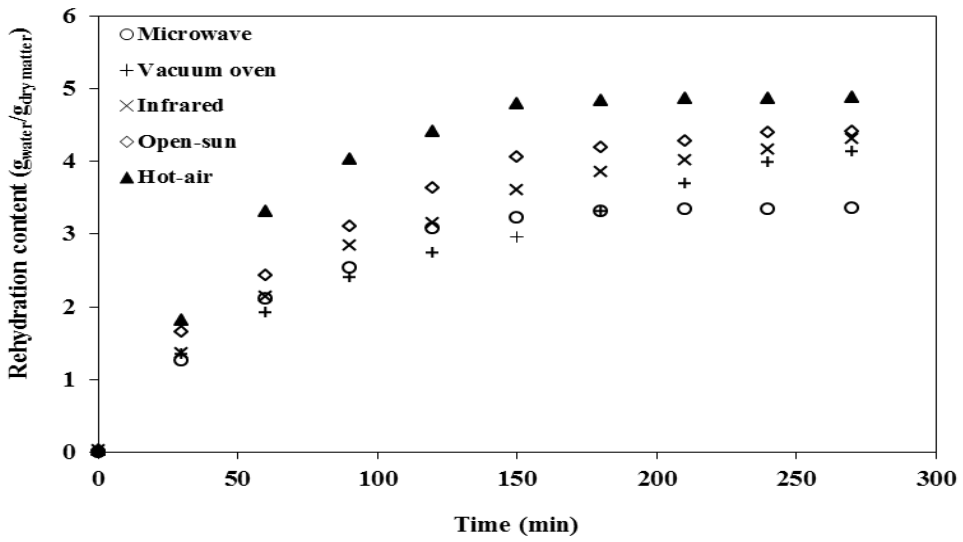

Conclusions

The growing trend on the amount of quality products and energy costs has motivated researchers to do research using different combinations of drying technologies. Based on the several conducted analyses, the best method for the drying of okra samples was found as the microwave drying method, considering the low drying time (46 min), low energy consumption (0.18 kWh) and low specific energy consumption (20.54 kWh/kg water). It can be said that this method can be applied to industry easily and can provide consumers to high-quality and uniform products. Highest rehydration contents and lowest total color change (9.62), were obtained in dried okra samples with hot air. Apart from the microwave drying method, hot air drying is also recommended for okra drying in terms of rehydration and total color change.

Nomenclature

L	Lightness
a	Greenness
b	Yellowness
t	Rehydration time (h)
ΔE	Total color change
Q_s	is the specific energy consumption in kWh / kg water
Q_t	is the consumed energy in kWh
m_w	is the mass of vaporized water in kg water
R_R	Rehydration ratio
W_t	Water content at a specific time (g water)
W_{dry}	Dry weight of product

References

Aamir M, Boonsupthip W (2017) Effect of Microwave Drying on Quality Kinetics of Okra. *Journal of Food Science and Technology* 54(5): 1239-1247.

Adom KK, Dzogbeüa VP, Ellis WO (1997) Combined Effect of Drying Time and Slice Thickness on the Solar Drying of Okra. *Journal of Science and Food Agriculture* 73(3): 315-320.

Afolabi TJ, Agarry SE (2014) Thin Layer Drying Kinetics and Modelling of Okra (Abelmoschus Esculentus (L.) Moench) Slices under Natural and Forced Convective Air Drying. *Food Science and Quality Management* 28(2014): 35-49.

Ajav E, Fakayode O (2011) Effect of Tray Loading Density on the Drying Characteristics of Okra. *Tarım Makinaları Bilimi Dergisi* 7(4): 333-337.

Al-Sulaiman MA (2011) Prediction of Quality Indices During Drying of Okra Pods in a Domestic Microwave Oven Using Artificial Neural Network Model. *African Journal of Agricultural Research* 6(12): 2680-2691.

AOAC - Official Method of Analysis (1990) Association of Official Analytical Chemists, Arlington, USA.

Başlar M, Kılıçlı M, Toker OS, Sağdıç O, Arici M (2014) Ultrasonic Vacuum Drying Technique as a Novel Process for Shortening the Drying Period for Beef and Chicken Meats. *Innovative Food Science and Emerging* Technologies 26(Dec): 182-190.

Cao ZZ, Zhou LY, Bi JF, Yi JY, Chen QQ, Wu XY, Zheng JK, Li SR (2016) Effect of Different Drying Technologies on Drying Characteristics and Quality of Red Pepper (Capsicum frutescens L.): A Comparative Study. *Journal of Science and Food Agriculture* 96(10): 3596-3603.

Dadalı G, Apar D, Ozbek B (2007) Microwave Drying Kinetics of Okra. *Drying Technology* 25(5): 917-924.

Doymaz I (2005) Drying Characteristics and Kinetics of Okra. *Journal of Food Science and Engineering* 69(3): 275-279.

Doymaz I (2011) Drying of Geen Bean and Okra Under Solar Energy. *Chemical Industry & Chemical Engineering Quarterly* 17(2): 199-205.

El-Mesery HS, Mwithiga G (2012) Comparison of a Gas Fired Hot-Air Dryer with an Electrically Heated Hot-Air Dryer in terms of Drying Process, Energy Consumption and Quality of Dried Onion Slices. *African Journal of Agricultural Research* 7(31): 4440-4452.

Feng H, Tang J (1998) Microwave Finish Drying of Diced Apples in a Spouted Bed. *Journal of Food Science* 63(4): 679-683.

Gogus F, Maskan M (1999) Water Adsorption and Drying Characteristics of Okra. *Drying Technology* 17(4-5): 883-894.

Huang JP, Zhang M (2016) Effect of Three Drying Methods on the Drying Characteristics and Quality Of Okra. *Drying Technology* 34(8): 900-911.

Ismail MA, Ibn Idriss EM (2013) Mathematical Modelling of Thin Layer Solar Drying of Whole Okra (Abelmoschus esculentus (L.) Moench) Pods. *International Food Research Journal* 20(4): 1983-1989.

İsmail O, Kocabay OG (2016) Evaluation of the Drying Methods and Conditions with respect to Drying Kinetics, Colour Quality and Specific Energy Consumption of Thin Layer Pumpkins. *Bulgarian Chemical Communications* 48(3):480-491.

Kocabay OG, Ismail O (2017) Investigation of Rehydration Kinetics of Open-Sun Dried Okra Samples. *Heat Mass Transfer* 53(6): 2155-2163.

Krokida MK, Philippopoulos C (2005) Rehydration of Dehydrated Foods. *Drying Technology* 23(4): 799-830.

Mana LV, Orikasab T, Muramatsuc Y, Tagawaa A (2012) Impact of Microwave Drying on the Quality Attributes of Okra Fruit. *Journal of Food Processing and Technology* 3(10): 186 doi:10.4172/2157-7110.1000186.

Moreira R, Chenlo F, Chaguri L, Fernandes C (2008) Water Absorption, Texture, and Color Kinetics of Air-Dried Chestnuts During Rehydration. *Journal of Food Engineering* 86(4): 584-594.

Motevali A, Minaei S, Khoshtagaza MH (2011) Evaluation of Energy Consumption in Different Drying Methods. *Energy Conversion and Management* 52(2): 1192-1199.

Okos M, Rao N, Drecher S, Rode M, Kozak J (1998) *Energy Usage in the Food Industry, American Council for an Energy-Efficient Economy*. Research Report IE981.

Okos MR, Campanella O, Narsimhan G, Singh RK, Weitnauer AC (2007) Food Dehydration. In DR Heldman, DB Lund (eds), *Handbook of Food Engineering Food Dehydration*. USA: CRC Press.

Pan Z, Khir R, Godfrey LD, Lewis R, Thompson JR, Salim A. (2008) Feasibility of Simultaneous Rough Rice Drying and Disinfestations by Infrared Radiation Heating and Rice Milling Quality. *Journal of Food Engineering* 84(3): 469-479.

Pendre NK, Nema PK, Sharma HP, Rathore SS, Kushwah SS (2012) Effect of Drying Temperature and Slice Size on Quality of Dried Okra (Abelmoschus esculentus (L.) Moench). *Journal of Food Science and Technology* 49(3): 378-81.

Phoungchandang S, Saentaweesuk S (2011) Effect of Two Stage, Tray and Heat Pump Assisted-Dehumidified Drying on Drying Characteristics and Qualities of Dried Ginger. *Food and Bioproducts Processing* 89(4): 429-437.

Rudra SG, Singh H, Basu S, Shivhar US (2008) Enthalpy Entropy Compensation during Thermal Degradation of Chlorophyll in Mint and Coriander Puree. *Journal of Food Engineering* 86(3): 379-387.

Sakai N, Mao W (2006) Infrared Heating. In DW Sun (ed), *Thermal Food Processing New Technologies and Quality Issues*. USA: CRC Press.

Sharma GP, Prasad S (2006) Specific Energy Consumption in Microwave Drying of Garlic Cloves. *EconPapers* 31(12): 1921-1926.

Shivharea US, Gupta A, Bawa AS, Gupta P (2010) Drying Characteristics and Product Quality of Okra. *Drying Technology* 18(1-2): 409-419.

Tunde-Akintunde TY (2011) Mathematical Modelling of Sun and Solar Drying of Chilli Pepper. *Renewable Energy* 36(8): 2139-2145.

Wankhade PK, Sapkal RS, Sapkal VS (2012) *Drying Characteristics of Okra Slices Using Different Drying Methods by Comparative Evaluation*. Proceedings of the World Congress on Engineering and Computer Science 2012, vol II WCECS 2012, October 24-26, 2012, San Francisco, USA.

Sedimentation Processes in the Black Sea during the Last Glacial Period Deduced from Grain Size Analyses on Gravity Core MSM 33/54-3 from the Eastern Anatolian Continental Margin

By Carolin Neugebauer[*]

Abrupt climate fluctuations within the last glacial period are recorded in several palaeoclimate archives such as Greenland ice cores and northern hemisphere sediments, both marine and terrestrial. Characterised by an abrupt warming within a few decades and followed by gradual cooling, these events – known as Dansgaard-Oeschger events (DO) - are directly related to changes in the sedimentary mechanisms for several marginal basins. Black Sea sedimentary mechanisms were mainly influenced by continental ice sheet dynamics of the northern hemisphere. Variabilities of more intense (stadial) and less intense (interstadial) glacial conditions are caused by variations in North Atlantic oceanic meridional heat transport, leading to regional climate changes (Henry et al. 2016). Thus, changes of regional climate are reflected in the grain size composition of terrestrial and marine sediments. South eastern Black Sea sediments represent well archived paleoenvironmental records of the last glacial course. As a marginal basin with its only connection to the world ocean circulation system via the Bosporus, the Black Sea experienced several periods as an isolated glacial lake, caused by sea level fall during cold DO events. To reveal the dominant modes of temperature variability between 60-30 thousand years, a sedimentary sequence of a gravity core of the south eastern Archangelsky Ridge (41°58.985' N, 36°43.845' E) is analysed with respect to several climate indicators. Laser diffractometry and statistical calculation programmes such as GRADISTAT obtained sedimentary parameters in order to estimate the dynamic and genetic reasons for the presence of numerous grain size distributions of the sediments. The process of End-member modelling has been used to assign the grain size distributions to the sedimentary mechanisms during DO events. Additionally, XRF analysis revealed the aeolian and fluviatile indicative elements of the core sequence to clarify how the regional ecosystem, especially vegetation, responded to these climate changes. As a result, the grain size distributions correspond notably with climate changes and therefore, reveal high impacts of DO events on sedimentary processes in the south eastern Black Sea region. The present study contributes a piece to the puzzle of the climate development of Southeast Europe to understand past climate mechanisms as well as to predict future climate scenarios.

Keywords: *Black Sea, Dansgaard-Oeschger Events, Grain Size Analysis, Palaeoclimate.*

Introduction

Greenland ice core records were first to show that rapid climate fluctuations during Marine Isotope Stage 3 (MIS 3, 59-29 ka years BP) impacted the North Atlantic territory during the last glacial course. These climate fluctuations are

[*]Master of Science, Germany.

known as Dansgaard-Oeschger events (DO), characterised by rapid warming over Greenland of as much as 10°C within a few decades and followed by a gradual cooling continuing for several centuries, then rapidly leading to stadial conditions (Rahmstorf 2002). Heinrich events (HE) are a climatic phenomenon that occurred during the coldest phases of DO events (Clement and Peterson 2006) and are related to massive episodic iceberg discharges from the Laurentide ice sheet (Rahmstorf 2002). They are reflected as coarse-grained layers in North Atlantic sediments; the thickness of these sediments decreases from several metres in the western Atlantic down to a few centimetres in the eastern Atlantic (Rahmstorf 2002). HE and DO events are not unrelated as Heinrich events are followed by a warm DO event, and DO events tend to get cooler until the next Heinrich event (Rahmstorf 2002). Much remains unknown about the mechanisms that lead to these climate changes. However, changes in the North Atlantic Meridional heat transport caused by freshwater release seem to be one of the main mechanisms that triggered these climate events as sea surface temperatures (SST) of the North Atlantic are closely matched with DO events in Greenland (Clement and Peterson 2006). With respect to that theory, stadial conditions are associated with weak oceanic heat transport and large sea ice extent of northern latitudes. Interstadial conditions are related to strong oceanic heat transport that extends far into the high latitudes of the North Atlantic (Wegwerth et al. 2015). The deep-water formation in the North Atlantic linked to the Atlantic Meridional Overturning Circulation may play a crucial role in triggering climate changes. Three modes of North Atlantic Ocean circulation have been estimated for the last glacial period (Rahmstorf 2002). Based on their occurrence during stadial, interstadial phases and Heinrich events, the modes are stadial mode, interstadial mode and Heinrich mode with reference to Rahmstorf (2002). These modes differ in their location of North Atlantic Deep Water formation and are all but stopped during Heinrich events (Rahmstorf 2002). The cold stadial mode is characterised by reduced deep water formation south of Iceland, during interstadial mode deep water formation increased and experienced a northward shifting into the Nordic Seas (Rahmstorf 2002). Furthermore, a strong ocean circulation led to warmer conditions in the Atlantic, melting ice sheets and freshwater supply into the North Atlantic that weakened the circulation again. Other studies suggest the collapse of northern Laurentide ice sheet, leading to increasing icebergs in the North Atlantic (Heinrich events) and thus, enhanced freshwater supply (Rahmstorf 2002). Probably, it is the interaction of all these mechanisms that may explain the abrupt climate changes during MIS 3.

The NAO (North Atlantic Oscillation) play a key role for the atmospheric and oceanic circulation pattern in the northern hemisphere and represents an index between high-pressure and low-pressure systems of the Atlantic. There are two states of the NAO: a positive NAO intensifies atmospheric circulation caused by strong subpolar low and subtropical high systems of the Atlantic Ocean, strengthening the westerlies between 45-60°N (Voelker 1999). Temperatures are increasing in northern Europe but decreasing in the Mediterranean, leading to dry winters in southern Europe (Voelker 1999) and bringing cold air to the

Black Sea (Hurrel et al. 2003). On the other hand, a negative NAO results in weakened westerlies, so that easterly and meridional wind systems predominate, leading to colder temperatures in northern Europe; southern Europe and the Black Sea experience warmer and humid conditions (Voelker 1999). However, changes in the NAO have an impact on atmospheric pattern and North Atlantic current systems (Dickson et al. 1996), such as of deep water formation and thus, may have contributed to DO events.

No less important is the question whether these events are a phenomenon of the northern hemisphere or whether they appeared with the same dramatic character globally. Recent studies demonstrate that these events are not local to Greenland (Voelker et al. 2002). These events show detectable patterns in many sediments worldwide (Figure 1). Climate fluctuations have also been detected in glacial loess deposits in China. Coarse-grained layers of loess deposits indicate cold climate intervals and are mixed with clay-rich fine-grained layers, indicating warm climate intervals (Ruddiman 2008). To identify DO events in sediments, climate fluctuations are traced by means of grain size analysis and linked to sedimentary mechanisms. Local changes in environmental conditions have a direct influence on sediment composition and grain size and actually reflect the contrast between DO stadials and DO interstadials. There are clear indications that dry and cold environmental conditions lead to high proportions of coarse aeolian fractions within a sediment (Ruddiman 2008). On the other hand, warm and humid environmental conditions increase the fine-grained fluviatile character of a sediment. These environmental conditions are dependent on prevailing wind systems and local rain fall that were intensified or limited regionally as a result of the impact of DO events.

Figure 1. *Global DO Interstadial* (left) and *Stadial* (right) *Pattern*

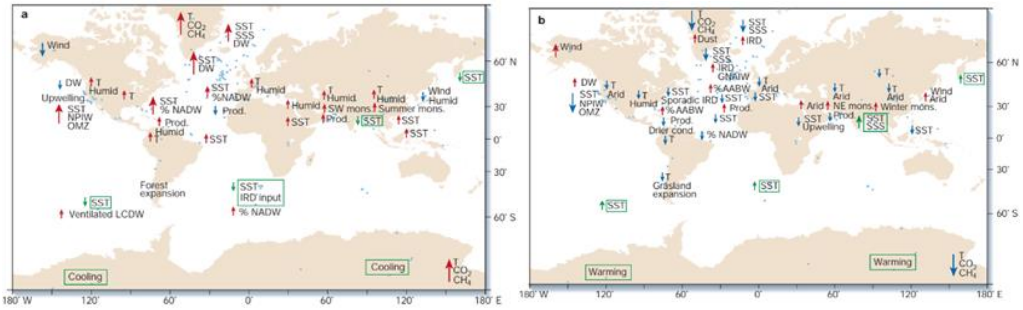

Source: Voelker et al. 2002.

The present paper aims to understand the long-range impact of North Atlantic temperature changes during DO events and the influences on sedimentation mechanisms for the study region to be demonstrated for the period between 60-30 ka years of MIS 3 by detailed grain size analyses. This study is crucial for the assessment of current and future climate changes, as global climate patterns have different regional effects whose intensities cannot yet been estimated.

Palaeoclimate Black Sea

As a marginal basin in the middle of the Eurasian continent, the Black Sea reacts very sensitively to environmental and climatic changes in the surrounding area. During the past 670,000 years, the Black Sea experienced several oscillations between brackish and limnic conditions due to sea level fluctuations which have been characterised by the constant change of interruption and connection with the Marmara Sea (Wegwerth et al. 2015). The isolated Black Sea developed to a Black Sea "Lake" during low sea level as saltwater inflows from the Marmara Sea were interrupted and both hydrological and sedimentary conditions were impacted by freshwater fluxes from the Eurasian continent in the north and the Anatolian region in the south. During MIS 3 the sea level of the Black Sea was constantly below present Bosporus sill, indicating the glacial phase of the Black Sea "Lake."

The intensity of freshwater fluxes is directly linked to the extent of the northern hemispheric ice sheets and the associated northward or southward shifted polar front. During the last glacial period the Fennoscandian ice sheet changed its extent remarkable with response to DO warming or cooling. A direct correlation with the dynamics of intermediate ice sheets is assumed, because almost all DO events occurred during past glacial periods (Rahmstorf 2002). Changes of enhanced or weakened westerly winds and fluctuations in precipitation resulted in dramatic environmental changes that can be detected in the sediments of the Black Sea.

Detailed pollen analyses of previous studies allow regional changes in vegetation in northern Anatolia to be correlated with climatic fluctuations (Shumilovskikh et al. 2014). DO interstadials are related to temperate forests due to the onset of humid conditions in northern Anatolia. On the other hand, Black Sea sediments demonstrate non-arboreal pollen during cold DO events and suggest mainly xerophytic biomes that characterised the northern Anatolian region due to arid conditions (Shumilovskikh et al. 2014). Black Sea surface temperatures reacted sensitively to North Atlantic Heinrich events as temperatures cooled down on 3°C (Wegwerth et al. 2015).

The Study Region

The Black Sea is the largest anoxic basin on earth with a characteristic stratification of the water column and a maximum water depth of 2258m. The upper 100-150 m comprise a freshwater layer that is well-oxygenated, followed by a saline water column below that has anoxic conditions (Kwiecien et al. 2009). This stratification is due to the interruption of vertical circulation caused by the freshwater input of rivers and precipitation and the influx of saline marine water from the Marmara Sea through the Bosporus that is 35 meters below sea level (Kwiecien 2009).

European largest rivers drain into the Black Sea such as the Danube and Dnieper, contributing to the positive water balance by enhanced freshwater

supply that is higher than evaporation (Wegwerth et al. 2015). Large quantities of sediments (>33%) are supplied by the large Anatolian rivers such as Kizilirmak into the south eastern Black Sea (Lericolais 2013).

The basin is surrounded by the Carpathian mountains in the west, the Pontic mountains in the south and the Caucasus in the east (Wegwerth et al. 2015).

Local Climate

The climatic conditions of the Black Sea are influenced by Europe's atmospheric circulation pattern. Main features are the westerlies, the Siberian and mid-latitude subtropical high-pressure systems as well as the Polar Front Jet and the Subtropical Jet (Wegwerth et al. 2015). Indian monsoon and Siberian high-pressure system strongly influence Mediterranean low-pressure systems that reach the Black Sea, depending on the seasonal situation of the Polar Front and Subtropical Jet (Wegwerth et al. 2015). However, the southern Black Sea region is mainly characterised by the Mediterranean climate leading to hot and dry summers and cold and wet winters. Accordingly, a positive winter NAO caused strengthened westerlies and cold and dry air is controlling the Black Sea area. A weakened NAO is leading to south westerlies and wet winters (Wegwerth et al. 2015). During summer the eastern Black Sea and north Anatolia are the most rain-laden regions due to precipitation in the Pontic mountains and Caucasus in the east (Wegwerth et al. 2015). It is precisely this climatic situation of the Black Sea that suggests regional changes in these atmospheric patterns during DO events as the change of one of these features results in the change of the other features as well (Figure 2).

Figure 2. *Atmospheric Pattern for the Black Sea Region*

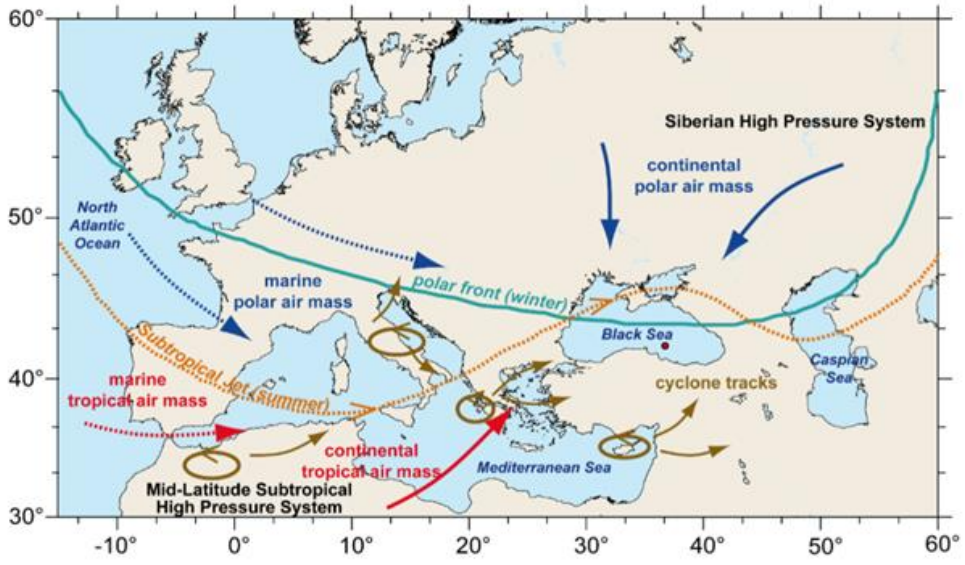

Source: Wegwerth et al. 2016.

Methods

Core Sediments

In order to reconstruct the environmental changes and the associated different sedimentary composition of the Black Sea, a sediment sequence of a gravity core from Archangelsky Ridge (41°58.985' N, 36°43.845' E) at a water depth of 382.2 m was examined for its grain size and element composition. The Archangelsky Ridge is an uplifted fault feature of the south eastern Black Sea and located within a highly tectonically active zone of the Anatolian continental margin (Wegwerth et al. 2015). The basin itself represents a part of the Para-Tethys that developed as a back-arc basin (Wegwerth et al. 2015).

Black Sea sediments contain three stratigraphic units (Unit I-III) as described by Ross (Ross et al. 1974), comprising mainly coccolith ooze (Unit I), Holocene sapropel (Unit II) and limnic clays of Unit III (Figure 3). The investigated core sequence of 353-552 cm can be assigned to the clayey sediments of Unit III, covering a time period between 60-30 ka years. Sedimentation in the south eastern Black Sea is relatively low compared to the high sedimentation rates of the western Black Sea (Wegwerth et al. 2015). The age model is based on previous investigations by Nowaczyk et al. (2012) by means of AMS 14C (accelerator mass spectroscopy).

Figure 3. *Black Sea Sediment Units I-III*

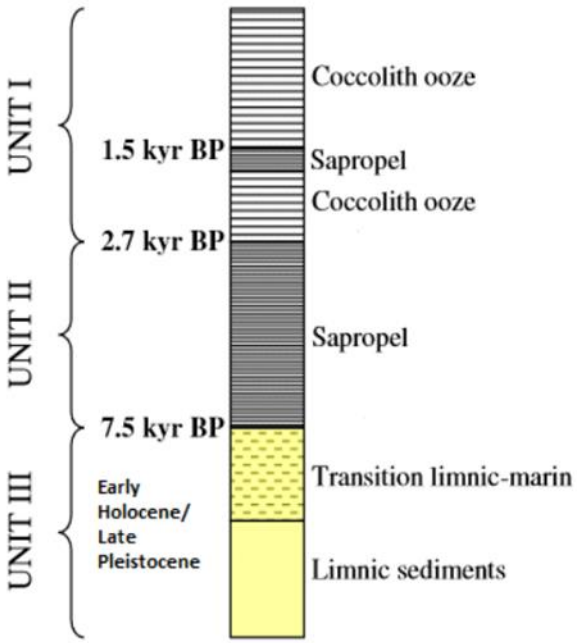

Source: Bahr 2005 (modified by the author).

Sample Preparation

First, the core sequence was sub-sampled in 1cm units and freeze-dried. Subsequently, a quantity of 120-150 mg sample material was removed. Two sample series were prepared. The laboratory procedure comprised treatment with 15 ml 33% H_2O_2 for both sample series in order to remove organic particles and the treatment with 15 ml HCl for the second one for removing calcium carbonate to determine the siliciclastic particles. Both series were heated for 1h afterwards. Furthermore, the series were filled with distilled water to keep the particles in suspension and treated with 5ml dispersed agent and sonicated for 15 minutes. Replicate samples were prepared at intervals of 10cm, showing a consistent pattern in grain size distribution.

Grain Size Analysis

Grain size fractions of the core sequence are separated into clay (<2 µm), silt (<2 µm to <62.5 µm) and sand (>62.5 µm). The sediments are classified according to the scale of Udden & Wenthworth. The grain sizes were analysed by laser diffractometry with the particle size analyser CILAS at the Institute of Baltic Sea Research in Rostock, Warnemünde (IOW). Laser diffractometry is a method based on the principle of light refraction on particles of different sizes, which produces different refraction patterns. As a result, grain sizes were summarised in grain size classes that were used for the statistical calculation program GRADISTAT that was developed by Blott and Pye (2001). It has been written for the grain size analysis with respect to statistics such as mean, mode, sorting and skewness (Blott and Pye 2001).

End-Member Modelling

The process of End-member modelling has been used to assign the grain size distribution of each sample to sedimentary mechanisms during DO events. Grain size distributions were used as input data from laser particle size analysis for the end-member modelling algorithm. The input data represent reflectance values by means of DRS (Diffuse reflectance spectroscopy) of the grains size distributions (Seidel 2015). The determination of the number of end-members refers to the number of prevailing sedimentation processes and source areas for the studied period as sediments are mainly a mixture of several sedimentation processes (Figure 4). The minimum of end-members is calculated by the coefficient of determination (r) that represents the proportion of variance of grain size classes (Prins and Weltje 1999).

Figure 4. *Number of End-Members by the Coefficient (r)*

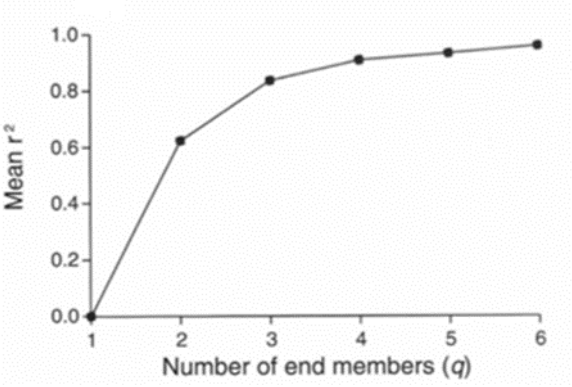

Source: Prins and Weltje 1999.

X-Ray Fluorescence

High resolution core scanning was carried out by X-ray fluorescence (XRF). XRF was used with respect to the mineral composition of the sediments. In order to exclude dilution effects by carbonate, Zr was normalised to Al. Zr is an indicator for aeolian processes and strengthened wind systems and is associated with heavy minerals. K is mainly due to weathering processes and incorporated into clay minerals, mainly deposited by river influx (Wegwerth et al. 2015).

Results

Grain Size Results

The mean varies between 4µm and 8µm and is mainly composed of cohesive fine silt size fractions. Few grains reach 16µm with a trend to the coarser silt fraction. The sorting is classified as poorly sorted with notable shifts for few samples. Poorly sorting is associated with a mixture of several grain size classes. The grain size distribution shows mainly unimodal pattern with except for few samples that show bi- and trimodal pattern, corresponding to coarser grain size due to higher amounts of sand. Coarsening of these samples corresponds to decreased clay content. Grain sizes are increasingly fluctuating between 440 cm and 550 cm core depth, indicating changed sedimentation and environmental conditions, respectively.

End-Member Modelling Results

Three predominantly end members have been obtained as minimum number of end-members for a well approximation of the grain size data. Thus, three main sedimentation mechanisms are assumed. Two end members show a similar trend in grain size classes (EM1, EM2), indicating a similar process or source. End-member 1 and 2 are classified as fine-grained. End-member 3 comprises the coarse-grained fraction and a wide range of grain size classes. Compared

with NGRIP, there are clear inverse reactions between EM1 and EM3. EM1 tends almost towards 0 compared to the maximum values of EM3. EM1 reaches maximum values during DO interstadials, maximum values of EM3 are correlated with DO stadials (Figure 5). For visualisation of the results in Figures 5 and 6, EM 1 was considered, since EM2 comprises the same grain size classes as EM1.

Figures 5 and 6. *Results Plotted to NGRIP and Ca XRF*

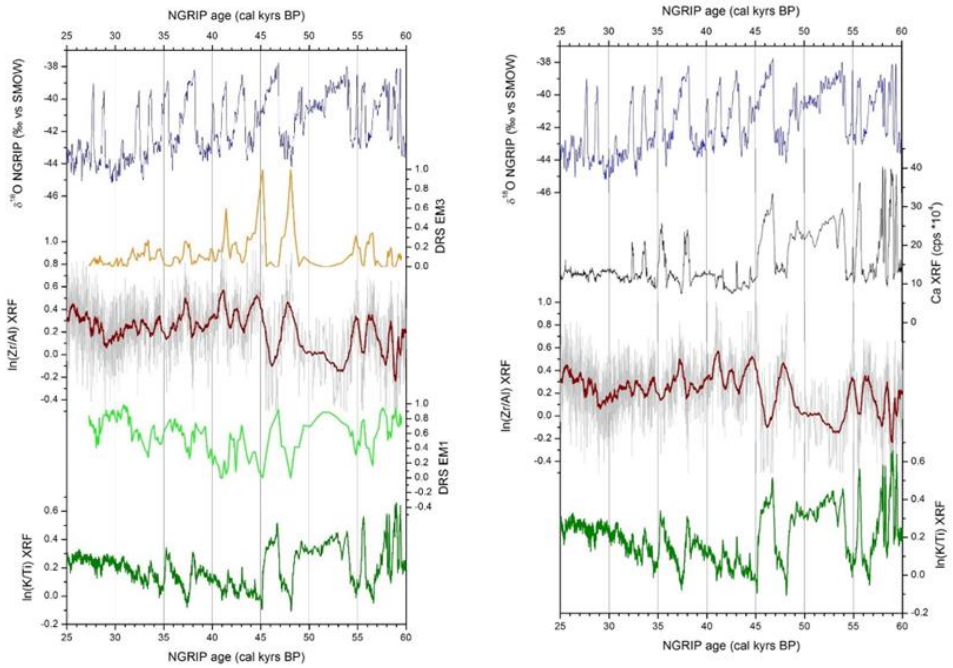

XRF Results

Ratios of ln(Zr/Al) XRF and ln(K/Ti) XRF are compared to NGRIP and the calculated end-members. Maximum peaks of ln(Zr/Al) XRF correspond to maximum peaks of EM3. Thus, the coarse-grained fraction can be correlated with high ln(Zr/Al) XRF. High ln(K/Ti) XRF is correlated with maximum values of EM1. Lowering in ln(K/Ti) XRF results in low EM1 and the fine-grained fraction (Figure 5). A clear inverse reaction between ln(Zr/Al) XRF and ln(K/Ti) XRF can be derived as well as for EM1 and EM3. Hence, high ln(Zr/Al) XRF and high EM3 correspond remarkable to cold DO events. These values are almost diminished during DO warming, when ln(K/Ti) XRF and EM1 are at highest.

Regarding Ca XRF the results correspond with climate changes detected in NGRIP. Increasing temperatures correlate with high amounts of Ca (Figure 6). Lowering in temperature agree with decreased Ca XRF. Ca is mainly originating inorganic due to increasing temperatures that lead to inorganically-precipitated carbonates as suggested by Kwiecien et al. (2009). Decreased Ca XRF is the result of inputs of terrigenous material that leads to carbonate dilution (Kwiecien

et al. 2009). However, primary productivity in the Black Sea was high during DO interstadials and low during DO stadials.

Discussion

Because high ln(Zr/Al) XRF and high EM3 match, it can be concluded that both values indicate the same sedimentary process and source, respectively. The maximum peaks of EM3 remarkable correspond to few samples with maximum shifts in their grain size for 42 ka years, 45 ka years and 47.5 ka years, demonstrating highest contents in coarse grains related to sand. The coarse-grained character of the sediments indicates aeolian supply due to arid conditions of northern Anatolia and low vegetation, raising soil erosion as well as ice-rafted debris as suggested by Shumilovskikh et al. (2014). Low primary productivity and xerophytic vegetation corresponds with these values during DO stadials (Shumilovskikh et al. 2014) and are supported by high Ca XRF results. Related to a southward shifted polar front due to ice sheet extent, European polar air masses and strengthened westerlies gained increased influence on the study region. Accordingly, less Mediterranean cyclones reached the Black Sea basin, thus, evaporation was higher than precipitation and riverine freshwater input (Wegwerth et al. 2015) (Figures 7 and 8). DO stadials mainly experienced strong winters leading to coastal ice formation and thus, explain the amounts of ice-rafted debris in southern Black Sea sediments (Wegwerth et al. 2015). There are no clear differences between HE and normal cooling DO events in the sediments detected, but highest ln(Zr/Al) XRF and EM3 at 48 ka years may notably correspond to Heinrich event 5 (HE 5). However, ice-rafted debris are not sufficiently proven in the present study. Several studies document large eastern and southeastern loess deposits during cold and dry periods that demonstrate high amounts of Zr (Buggle et al. 2008). Generally coarsening in grain sizes of loess deposits from Western Europe to the Dnieper valley is observed for 40 ka years BP by Rousseau et al. (2014). These results are similar to the present study as main coarsening of grain sizes occur between 40 ka years and 50 ka years. Rousseau et al. (2014) revealed strengthened North West winds due to northern hemisphere ice sheets. Aeolian deposits are located along rivers such as Danube, acting as source areas for sediment supply by wind systems when river flow was low (Rousseau et al. 2014). Thus, both the north of the Black Sea and Anatolia offer sources for aeolian sedimentation.

On the other hand, high ln(K/Ti) XRF corresponds with high EM1, indicating fine-grained sediments that suggest freshwater supply of rivers and may be related to enhanced riverine inflows by the Kizilirmak as well. Increased fluviatile supply may reflect melting ice in the Anatolian mountains but also of the Fennoscandian ice sheet as well as increased precipitation (Wegwerth et al. 2015). Spread of temperate and grassland biomes at 54-45 ka and 28-20 ka BP suggest humid conditions and correspond to high concentrations of freshwater and brackish dinocysts, indicating high productivity during DO interstadials as established by Shumilovskikh et al. (2014). At 54-45 ka BP, high EM1 and K are

considerably constant on the expense of EM3 and Zr, supporting the idea of warm and humid conditions for this interval and increased riverine input (Figure 5). Studies by Voelker et al. are in accordance with these results (Voelker et al. 2002) (Figure 1). Furthermore, increased fluviatile input corresponds with minimum ice extent of the Fennoscandian ice sheet (Wegwerth et al. 2015). More Mediterranean cyclones reached the Black Sea basin due to a northward shifted polar front and weakened westerlies, thus, leading to higher precipitation than evaporation for the Black Sea (Wegwerth et al. 2015) (Figures 9 and 10). Shumilovskikh et al. (2014) estimated freshening of the Black Sea surface caused by humid conditions.

However, the grain size distribution is a result of the interaction of various parameters such as changes in wind strength, sea level and local precipitation. These parameters changed in accordance with DO patterns. Glaciated Anatolian mountains may contribute to diminished freshwater supply into the southern Black Sea during DO stadials and vice versa. Pollen analysis by Shumilovskikh et al. (2014) indicates temperate and warm-temperate aboreal pollen that suggest glacial refugia in northern Anatolia. Much remains still unknown about the glaciation history of northern Anatolian mountains and its effects on sedimentation processes. Further, it is of interest to find out from where the aeolian entries come. Sources are both the European loess in the north and northern Anatolia in the south of the Black Sea. Previous studies by Wegwerth et al. (2015) have suggested aeolian indicators by the analysis of n-alkanes in the sediments, as n-alkanes represent leaf wax lipids from higher vasculant plants (Wegwerth et al. 2015). High n-alkanes indicate less vegetation cover of the source area and strengthened wind systems during cold intervals. With respect to studies by Shumilovskikh et al. (2014) these n-alkanes have their source in northern Anatolia, suggesting aeolian inputs from the south of the Black Sea.

Figures 7 and 8. *Environmental Conditions of the Black Sea during DO Stadials*

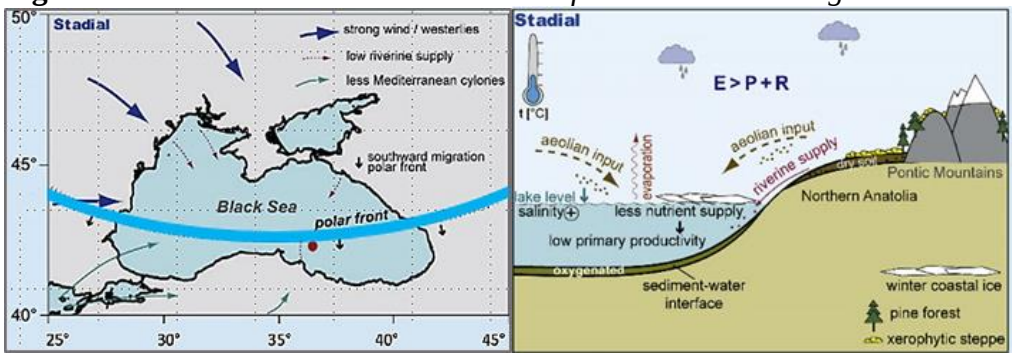

Source: Wegwerth et al. 2016 (modified by the author).

Figures 9 and 10. *Environmental Conditions of the Black Sea during DO Interstadials*

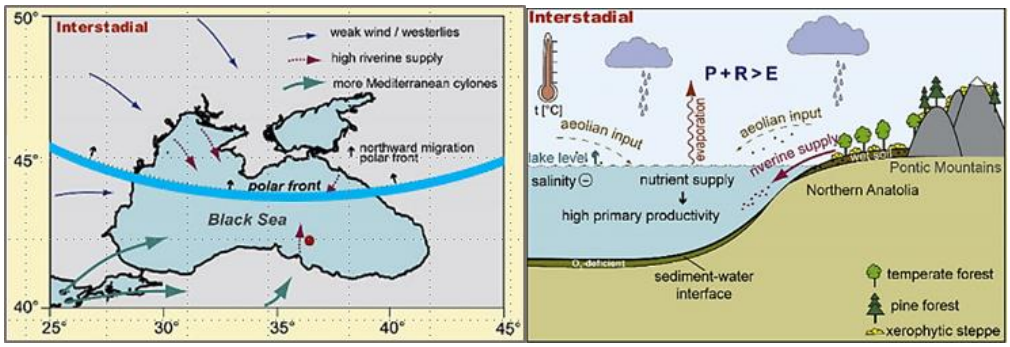

Source: Wegwerth et al. 2016 (modified by the author).

Conclusions

The present study shows clear patterns of DO events during MIS 3 in south eastern Black Sea sediments. The changes between warm and cold DO events indicate remarkable environmental changes for the Black Sea during the last glacial period. The multi-proxy application of sediment core analysis methods by means of grain size analysis, end-member modelling and XRF analysis leads to a clearer picture of the supra regional effects of DO events between 60-30 ka years BP on the Eurasian continent. DO interstadials led to warm and humid conditions with high influences of Mediterranean low-pressure systems and higher precipitation for northern Anatolia, corresponding to a mainly fluviatile character of the sediments due to freshwater inflows. On the other hand, a coarse-grained character of the sediments with aeolian-deposited elements such as Zr reflect cold and arid conditions of the environment during DO stadials due to enhanced wind systems and less vegetation cover in northern Anatolia. Thus, DO events had similar effects on inland areas as for the North Atlantic region, as previous studies by Wegwerth et al. (2015) and Voelker et al. (2002) suggested. These effects are due to changing ice sheet extents of the northern hemisphere as well as northern oceanic circulation changes and varying modes of the NAO that can be both the mechanism and consequence of DO events. This question remains still open. However, many studies are necessary to analyse past climate processes for marginal basins as they offer perfect palaeoclimate archives that may explain future climate changes for both global and regional areas as well.

References

Bahr A (2005) Late Glacial to Holocene Paleoenvironmental Evolution of the Black Sea. *Dissertation. Bremen.*

Blott SJ, Pye K (2001) Gradistat: A Grain Size Distribution and Statistics Package for the Analysis of Unconsolidated Sediments. *Earth Surface Processes and Landforms* 26(11): 1237-1248.

Buggle B, Glaser B, Zöller L, Hambach U, Marković S, Glaser I, Gerasimenko N (2008) Geochemical Characterization and Origin of Southeastern and Eastern European Loesses (Serbia, Romania, Ukraine). *Quaternary Science Reviews* 27(9-10): 1058-1075. Doi:10.1016/j.quascirev.2008.01.018.

Clement AC, Peterson LC (2008) Mechanisms of Abrupt Climate Change of the Last Glacial Period. *Reviews of Geophysics* 46(4): 1-39. Doi:10.1029/2006RG000204.

Dickson RR, Lazier J, Meincke J, Rhines P, Swift J (1996) Long-term Co-ordinated Changes in the Convective Activity of the North Atlantic. *Progress in Oceanography* 38(3): 241-295.

Henry LG, McManus JF, Curry WB, Roberts NL, Piotrowski AM, Keigwin LD (2016) North Atlantic Ocean Circulation and Abrupt Climate Change during the Last Glaciation. *Science* 353(6298): 470-474. DOI: 10.1126/science.aaf5529.

Hurrell JW, Kushnir Y, Ottersen G, Visbeck M (2003) An Overview of the North Atlantic Oscillation. In JW Hurrell, Y Kushnir, G Ottersen, M Visbeck (eds), *The North Atlantic Oscillation: Climatic Significance and Environmental Impact, Geophysical Monograph 134*. Washington DC: American Geophysical Union.

Kwiecien O, Arz HW, Lamy F, Plessen B, Bahr A, Haug GH (2009) North Atlantic Control on Precipitation Pattern in the Eastern Mediterranean/Black Sea Region during the Last Glacial. *Quaternary Research* 71(3): 375-384.

Lericolais G (2013) Late Quarternary Deep-Sea Sedimentation in the western Black Sea: New Insights from Recent Coring and Seismic Data in the Deep Basin. *Global and Planetary Change* 103(Apr): 232-247.

Nowaczyk NR, Arz HW, Frank U, Kind J, Plessen B (2012) Dynamics of the Laschamp Geomagnetic Excursion from Black Sea Sediments. *Earth and Planetary Science Letters* 351-352(Oct): 54-69.

Prins MA, Weltje GJ (1999) End-Member Modeling of Siliciclastic Grain-Size Distributions: The Late Quaternary Record of Eolian and Fluvial Sediment Supply to the Arabian Sea and its Paleoclimate Significance. In J Harbaugh (ed), *Numerical Experiments in Stratigraphy Recent Advances in Stratigraphic and Sedimentologic Computer Simulations, SEPM Special Publication* 62, 91-111. Society for Sedimentary Geology.

Rahmstorf S (2002) Ocean Circulation and Climate during the Past 120,000 Years. *Nature* 419(6903): 207-14. Doi:10.1038/nature01090.

Ross DA, Degens ET (1974) Recent Sediments of the Black Sea. In ET Degens, DA Ross (eds), *The Black Sea - Geology, Chemistry, and Biology*. Tulsa, Oklahoma, U.S.A: American Association of Petroleum Geologists.

Rousseau DD, Chauvel C, Sima A, Hatte C, Lagroix F, Antoine P, Balkanski, Y, Fuchs M, Mellett C, Kageyama M, Ramstein G, Lang A (2014) European Glacial Dust Deposits: Geochemical Constraints on Atmospheric Dust Cycle Modeling. *Geophysical Research Letters* 41(21): 7666-7674. Doi:10.1002/2014GL061382.

Ruddiman WF (2008) *Earth's Climate, Past and Future* (Second Edition) New York: WH Freeman.

Seidel M (2015) A R-based Function for Modeling of End Member Compositions. *Mathematical Geoscience* 47(8): 1-13.

Shumilovskikh LS, Fleitmann D, Nowaczyk N., Behling H, Marret F, Wegwerth A, Arz HW (2014) Orbital- and Millennial-Scale Environmental Changes between 64 and 20 ka BP Recorded in Black Sea Sediments. *Climate of the Past* 10(3): 939-954.

Voelker, Antje HL (1999) Zur Deutung der Dansgaard-Oeschger-Ereignisse in Ultra-hochauflösenden Sedimentprofilen aus dem Europäischen Nordmeer. [Dansgaard-Oeschger Events in Ultra-high Resolution Sediment Records from the Nordic

Seas] (Dissertation) Kiel: Inst. für Geowissenschaften der Christian-Albrechts-Universität.

Voelker, Antje HL (2002) Global Distribution of Centennial-Scale Records for Marine Isotope Stage (MIS) 3: A Database. *Quaternary Science Reviews* 21(10): 1185-1214.

Wegwerth A, Ganopolski A, Ménot G, Dellwig O, Kaiser J, Bard E, Lamy F, Arz HW (2015) Black Sea Temperature Response to Glacial Millennial-scale Climate Variability. *Geophysical Research Letters* 42(19): 8147-8154.

Wegwerth A, Kaiser J, Dellwig O, Shumilovskikh LS, Nowaczyk NR, Arz HW (2016) Northern Hemisphere Climate Control on the Environmental Dynamics in the Glacial Black Sea "Lake" *Quaternary Science Reviews* 135 (Mar): 41-53.

Dry Ports Development: A Pivot Strategy to Enhance Sustainable Transit Traffic via West African Corridors

By Sewodo Augustin Degbe[*] *& Bingliang Song*[†]

West Africa like many other regions in Africa, is enjoying a period of rapid growth in the past decade and within this period, its international trade has grown significantly. However, the region lacks sufficient dry ports, which can enhance a sustainable transportation of transit cargoes via the various corridors as well as relieving pressures on the seaports. The essence of this paper is to select an optimum location for the development of a dry port in West Africa based on specific factors relevant to the research objective. The center of gravity location model was applied at the landside in order to ascertain the transportation cost of goods from selected coastal ports to the hinterland markets as well selecting an optimum location for the development of dry port with a cost minimization objective. A simple forecast of demand throughput for West African landlocked countries was also applied using time series regression analysis in order to access the traffic growth rate as well as the associated capacity constraints that the ports might experience in the nearest future. Finally, SWOT analysis was used to analyze the endogenous and exogenous factors, which are deemed crucial to the development of dry port in selected West African Country.

Keywords: *Dry Port, Landlocked Countries (LLCs), Transit Traffic, West Africa.*

Introduction

Dry port development has received great attention from numerous scholars recently and its emergence is regarded as a prime outcome of the continuous increase in containerization and the growing integration between seaports and hinterland networks (Nguyen et al. 2016). As seaports' transport volume continues to grow, inland access becomes a critical factor for the seaports' competitive advantage. Thus, a progressive operation at the maritime sector and the seaport terminals without any developments in inland access by means of intermodalism is not sufficient for the whole transportation chain to function (Roso et al. 2009). The ability for countries to deliver goods and services on time and at the lowest possible cost is a key determinant of integration into the world economy today and landlocked developing countries in West Africa continue to face serious constraints and challenges in the areas of trade, transit, and overall socio-economic development. Unfortunately, just as traffic continues to grow through the transport corridor by each passing year, so are the difficulties in managing the trade.

The United Nations Convention on the Law of the Sea (UNCLOS) defined a

[*]PhD Student, Shanghai Maritime University, China.
[†]Professor, Shanghai Maritime University, China.

landlocked country as a "state or country without any access to the sea" and the permission by a coastal country for hinterland nations to transit through its seaport(s) is a permissible right. West Africa consists of twelve coastal countries with ports of relatively significant scale of operations and three landlocked countries (Burkina-Faso, Mali & Niger). Additionally, six out of the twelve coastal states provide substantial transit traffic services to the hinterland countries thus, regional corridors are predominantly important to hinterland nations because they serve as economic lifelines providing the only overland paths to global and regional markets.

Problem Statement

As business environment becomes more competitive and global than ever, service industries such as ports, are placing greater emphasis on customer satisfaction through providing quality services efficiently (Song and Cullinane 1999). The World Bank Logistics Performance Index (LPI) which is an overall LPI score measures the performance of a country's logistics based on efficiency - of arranging competitive shipments in terms of price, quality of logistics services, ability to track and trace consignments, and frequency with which shipments reach the consignee within the scheduled time (Arvis et al. 2014). According to this index, Germany, Luxembourg and Sweden are the most efficient and highly ranked LPI countries at positions 1, 2 and 3 in the 2016 LPI. In Africa, South Africa, Kenya and Egypt are the most consistent and highly ranked in logistics performance at 20, 42 and 49 positions respectively. West African countries had mixed rankings with Burkina-Faso ranked the highest at position 81 followed by Ghana, Nigeria, Togo, Cote d'Ivoire and Niger which are ranked at 86, 90, 92, 95 and 100 positions respectively. How then can the development of a dry port improve the transportation network by enhancing sustainable transit traffic which would reduce the total transport and logistics cost within the region? This research intends to unveil some comprehensive analysis which would serve as a unique tool for strategic decision making.

Research Objectives

The main objective of this research is to ascertain an optimum location where dry port(s) can be sited in West Africa and its economic impact on transit traffic designated for West African Landlocked countries. In order to achieve this goal, this study intends to address other supporting objectives which are considered crucial to the research. These objectives include; highlighting the principal factors influencing the development of dry ports, factors influencing the growth of transit traffic, hinterland transportation cost analysis for West African landlocked countries and to identify the endogenous and exogenous factors in developing a dry port in West Africa.

Literature Review

Dry Port Concept

The concept of dry ports became global in conjunction with containerization. Dry Port or Inland Clearance Depot (ICD) can be defined as: "A common user facility with public authority status, equipped with fixed installations and offering services for handling and temporary storage of any kind of goods (including containers) carried under customs transit by any applicable mode of transport, placed under customs control and with customs and other agencies competent to clear goods for home use, warehousing, temporary admissions, re-export, temporary storage for onward transit and outright export" (UNESCAP 2012).

Drivers behind the Emergence and Development of Dry Ports

Veenstra et al. (2012) ascertained that the usage of inland transport nodes has become more pragmatic considering the fact that every organization has its own individual objectives for developing dry ports. Major drivers behind the development of dry ports include; sustainable access to hinterland locations, constraints at the seaports and a means to facilitating economic zones which are considered nodes in the supply chain. Several gateway ports are currently confronted with development limitations such as diseconomies of scales, environmental issues and land availability (Roso 2005). Considering these restrictions, most seaports have delve into the development of dry ports as a solution to relieve burdens while improving in the operations through a modal slip. Thus, relocating space consuming activities to inland locations. An example of this scenario is the port of Genoa in Italy (Caballini and Gattorna 2009). Additionally, another reason for developing dry ports is to gain a competitive position through the expansion of hinterland connectivity network.

Dry Port Classification and Functions

Dry Ports are located based on their assessment criteria, need and the center of gravity favorable to the shippers. Nevertheless, dry port development should be evaluated with its cost functions and also value added services that can be provided to every stakeholder in the logistics network. Roso et al. (2009) categorized inland nodes as close, mid-range & distance dry ports (Figures 1-3) and this classification has been used by numerous scholars in their works. In general, dry port plays a role of operations by rail or road to and from serving ports customs clearance, warehousing with temporary storage of cargo and containers and computerized processing of documents. Dry ports can also be sited in different location based on its distance to the seaport and the three types of geographical location of dry port also plays different role. A summary of these categories and functions is buttressed in Table 1.

The main role of close dry ports is to relieve the seaports from the burden of space shortage, congestion and environmental issues. With abundant land

available, all high space-consuming activities, such as warehousing or sorting, are shifted from seaports to dry ports. The customs clearance procedures could be carried out in these close dry ports.

Figure 1. *A Seaport with a Close Dry Port*

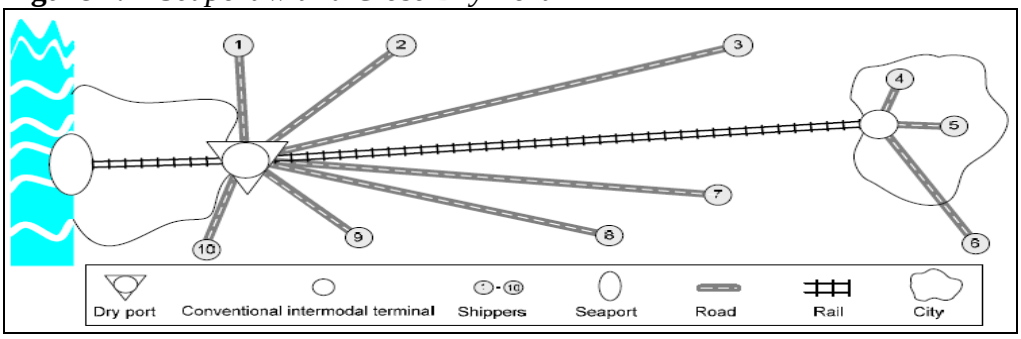

Source: Woxenius et al. (2004) The Dry Port Concept – Connecting Seaports with their Hinterland by Rail, p. 11.

Mid-range dry port functions as a consolidation center for diverse rail services, denoting technical and administrative equipment define for sea transport. It works as inter-modal centers to consolidate or deconsolidate cargo from shippers. It can also function as a trans-modal/trans-loading terminal before cargoes are being transported to their designated markets. These types of dry ports are more beneficial to the seaports because it increases the hinterland access in getting close to customers. Pollution and congestions are also tackled by the implementation of modal shift from trucks to barges/trains.

Figure 2. *A Seaport with Mid-Range Dry Port*

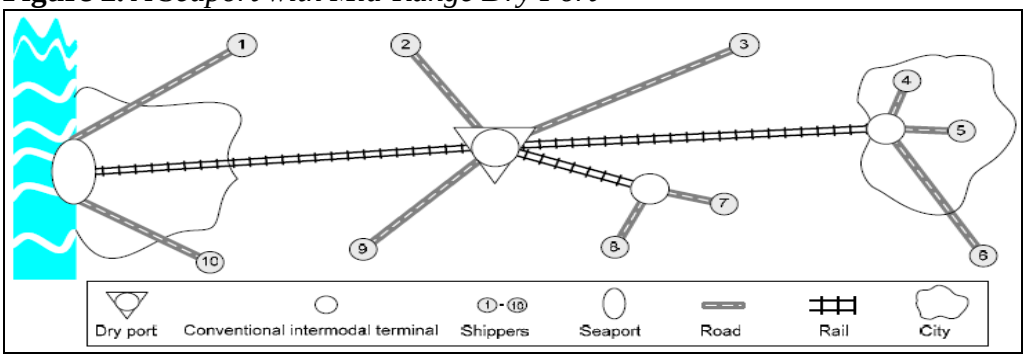

Source: Woxenius et al. (2004) The Dry Port Concept – Connecting Seaports with their Hinterland by Rail, p. 10.

The distant dry port is situated near the market, which might be the consuming area in import-based supply chains, or a core production location in export-based supply chains. This type of dry port plays an imperative role in the logistics system of landlocked countries to connect to international markets. In this case, the seaport will benefit from the connection to this type of dry port by gaining access to the inland market.

Figure 3. *A Seaport with a Distant Dry Port*

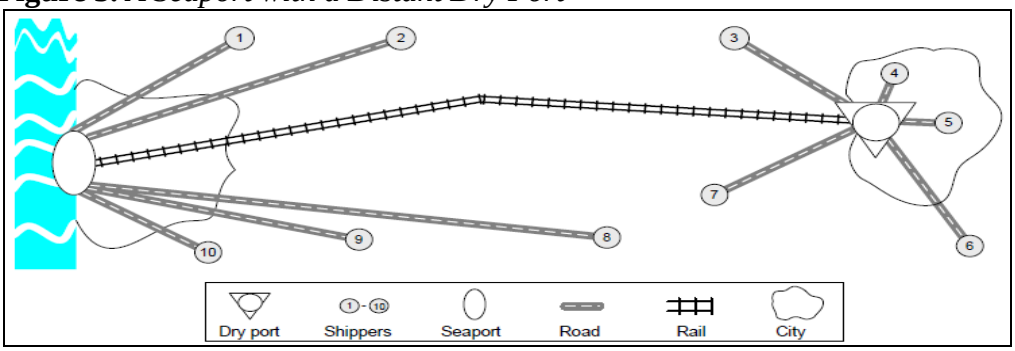

Source: Woxenius et al. (2004) The Dry Port Concept – Connecting Seaports with their Hinterland by Rail, p. 8.

Table 1. *Dry Port Categories and their Functions*

	Close dry port/ satellite terminal	Mid-range dry port/ transloading center	Distant dry port/load center
Development reason	Seaport constraints	Hinterland access	Economic zone facilitation
Position in hinterland supply chain	Start Point	Middle point	End point
Development driver	Sea-driven (Outside-in)	Sea or land driven	Land driven (inside out)
Role	- Relieve seaports from space shortage, congestion & environmental issues. - Handling cargo - Custom Clearance - Low value added service	- Transmodal -Tranloading cargoes - Modal shift - Consolidation & deconsolidation -Value added services	- Distribution - Consolidation for exported cargo - Reduce congestion - Modal Shift -High value added services
	Market derived		
	Direction of hinterland access		

Source: Nguyen C. L., Notteboom T. (2006) Dry Ports as Extensions of Maritime Deep-Sea Ports, p. 69.

Container Terminal Capacity

Container Terminal Capacity (CTC) has recently emerged as a foremost problem in several ports around the globe. Capacity measures are generally in units of output per time period and must signify the maximum throughput possible unimpeded by demand or other schemes: maximum crane moves per hour/day, TEU/acre, maximum TEU per hour/day/year and yard storage. Capacity problem happens when the input is larger than the probable output that can be produced by a terminal. Liu (2010) clarified that due to negative procedure variation in the sub-structural efficiency, excess or congestion has become a serious problem. Therefore, container port volume should be able to

handle the fast-tracking pace of demand in emergent economies and thus, it is the traffic development that energizes the expansion of ports' capacity. Some scholars have shown an intense apprehension about how to handle capacity problem. For example, Liu (2010) ascertain that terminals and container ports are obliged to cope with overcapacity because it has a substantial feature that indicates how dependable and significant the port relates to stakeholders and thus, it is important in defining traffic. Maloni and Jackson (2005) classify container capacity influence as endogenous and exogenous port capacity factors. The endogenous port capacity measures include technology, capital, waterways, labor, facilities, equipment, and efficiency while the exogenous port capacity dynamics include shipper efficiency, railroad truck capacity and efficiency, steamship line efficiency, capacity and efficiency, road congestion and OTI (Ocean Transportation Intermediaries) efficiency.

Solutions to the Container Terminal Capacity Issue

Conferring to Nguyen and Notteboom (2016) the following measures are proposed as solutions to container terminal capacity.

- Physical Expansion
- Using Automation and new technologies
- Improving the utilization of resources
- Floating and dry docks
- Investing in dry ports

Potential Benefits of a Dry Port

Some foremost benefits of developing dry port are elaborated with more collaboration with inland localities which will foster an increase in regional productivity using a more efficient and effective connection with inland transport nodes and stronger support for the cargo handling operation of the port because of adequate use of land space and augmented possibilities for a fruitful modal shift. Additionally, there is a development of the hinterland, and likelihood to capture a larger market share as competing ports as well as retaining customers in the hinterland markets. Other benefits are better understanding and level of service in the remote markets; increased prospects for intermodal services, even on shorter distances, more eye-catching hinterland services are offered because of an increased reliability, frequency and flexibility which will further reinforce the geographic concentration of logistics firms, thus, creating benefits for both seaports, inland terminals; and a more basic customs procedures.

Summary of Reviewed Literatures

Literatures concerning the study have been reviewed and it is undisputed that numerous outstanding studies have been conducted in the domain of dry port development but very few of these articles cover the West African sector.

There are numerous port expansion projects going on within the region. Therefore, there is a need for more substantial research to be conducted in order to address transport related problems that the region might be confronted with in the nearest future. Additionally, none of the studies reviewed have assessed political risk and the recent pirate attacks on the gulf of guinea as factors that can influence the development of dry port in West Africa.

Methodology

Transport Corridor Concept

The notion of "corridor" is not a new phenomenon, as this has existed for centuries ago. The ancient Silk Road is probably the best-known transit corridor globally, one that has had an enduring impact on the social and economic development on the expanses it crossed Kunaka and Carruthers (2014). Although the notion lacks an exact definition because of it physical and functional dimensions, it is generically understood to synchronize bundle of logistics and transport frameworks and services that accelerates trade and transportation which flows between centers of economic activities. A simple objective of a corridor project(s) include optimizing infrastructure connectivity, facilitating the efficient transit flow of freight and promoting economic growth by refining the effectiveness of exports commodities and reducing imports costs or emerging clusters of economic frameworks along the corridor strip supported by efficient and effective logistics systems (Arnold 2005). Additionally, a corridor is typically governed by national or regional body which constitute of a public or private sectors or an amalgamation of both.

Major Transit Corridors in West Africa

According to a report issued by Danida consulting group on Accelerating Trade in West Africa (Danida-Saana 2015), West African corridors can be categorized into "transit corridors and intra- regional corridors". In West Africa, transit corridors include; (1) Lagos [1](NG) - Jibiya the frontier with Niger and beyond (2) Cotonou (BN) – Niamey (NG), (3) Lomé (TG) – Ouagadougou (BF), (4) Tema (GH) - Ouagadougou (BF), (5) Abidjan (CI) - Ouagadougou (BF), (6) Abidjan (CI) - Bamako (ML), (7) San Pedro (CI) - Bamako (ML), (8) Conakry (GN) - Bamako, (ML) and (9) Dakar (SN) – Bamako (ML). The two principal West-East intra-regional transit corridors existing in the zone are; (10) Dakar, (SN) - Niamey, (NE) and (11) Dakar, (SN) - Lagos, (NG). These principal routes emanates from six major port cities; Abidjan-Cote d'Ivoire; Cotonou-Benin; Dakar-Senegal; Lagos-Nigeria (with three ports Apapa, Tin Can and Lekki); Lomé-Togo and Tema-Ghana (See Figure 4). Additionally, all corridors serve bilateral trade between ECOWAS member states as well as international trade. In

[1](NG)-Nigeria, (BN)-Benin Republic, (NG)-Niger, (TG)-Togo, (BF)-Burkina-Faso, (GH)-Ghana, (CI)-Cote-d'Ivoire, (ML)-Mali, (GN)-Guinea, (SN)-Senegal, (NE)-Niamey.

particular, they connect the three hinterland nations (Burkina-Faso, Mali and Niger) with coastal countries and market outside the region.

Figure 4. *Map of West Africa Indicating Major Transit Corridors*

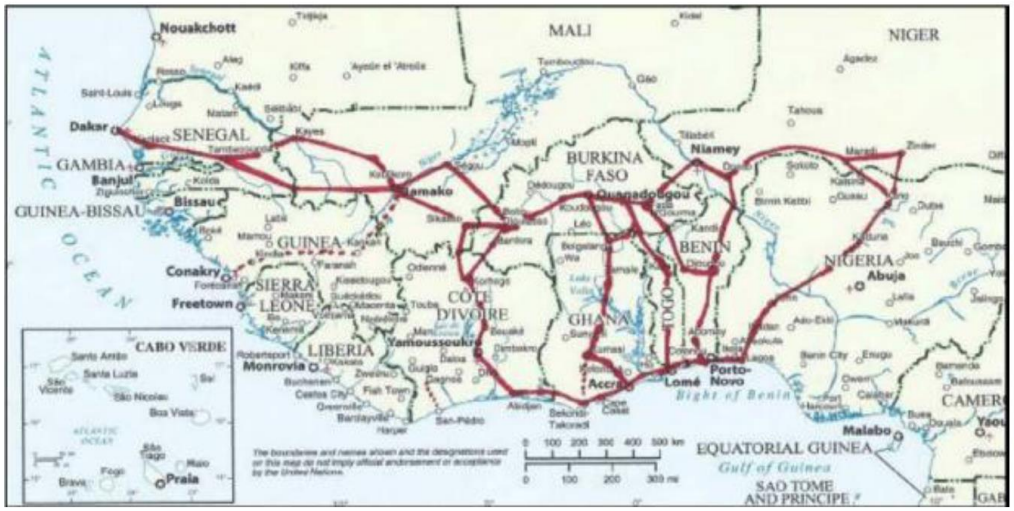

Source: Torres and Van Seters (2016), p. 24.

Factors Influencing the Growth of Transit Traffic in West Africa

The African continent is amid a transformative change and this will absolutely have a positive impact on its populations and thus increasing its market dimension. By 2020, Africa will have an approximated population of 2.1 billion people and a collective GDP of US$2.6 trillion and this is because the continent remains a minerals treasure house and it has about 60% of the world's uncultivated arable land. Additionally, the West African region is at the heart of Africa's economic transformation with a growth rate of 6.0% in 2014 (AFDB 2015). The dynamics enumerated below are considered as the major factors influencing the growth of transit trade in West Africa;

i. ***Sustainable Economic Growth*:** The averaged Africa's GDP growth was 5% from 2002 to 2012 and it is expected to significantly increase by 5.5% in 2018 which is higher than any other region except Asia and this has put Africa above America and Europe. Better economic sector accompanied with economic growth has tremendously improved its governance systems, lower foreign debt, lower inflation and lower budget deficit hence making African economies more resilient than in the past (CNBC Africa 2017).
ii. ***Implementation of Legal Instruments by Regional Bodies and Bilateral Transit Trade between Member Countries*:** Regional Trade Agreements (RTAs) in West Africa are basically in form of Free Trade Agreements (FTAs) and to a minimal extent Preferential Trade Agreements (PTAs) and the custom unions have been a principal façade of the global multilateral trading systems (see

iii. Table **2** 2). Within Sub-Saharan Africa, RTAs have principally involved nations belonging to a specific sub-region (i.e. "natural trading partners"). The main RECs in Sub-Saharan Africa are; Economic Community of West African States (ECOWAS), Economic Community of Central African States (ECCAS), West African Economic and Monetary Union (WAEMU), East African Community (EAC), Intergovernmental Authority on Drought and Development (IGADD) and Southern Africa Development Corporation (SADC).

Table 2. *Bilateral Trade Agreements between Landlocked and Transit Countries in W/A*

W/A LLC's	Selected West African Coastal Countries with Seaports					
	Benin	Cote d'Ivoire	Ghana	Nigeria	Senegal	Togo
B. Faso	a, b, c	a, b, c, d	a, b, c	N/A	a, b, c	a, b, c
Mali	a, b, c	a, b, c	N/A	N/A	a, b, c, d	a, b, c,
Niger	a, b, c, d	a, b, c	N/A	a, b, c	a, b, c	a, b, c

a = port agreement, b = transit agreement, c = road transport agreement, d = rail transport agreement.
Source: N'Guessan (2013) and Danida-Saana (2016).

iv. ***Port Infrastructure Development:*** Many African countries are tremendously investing in port infrastructures in order to meet growing demand and improve port performance and major international container operators are also eager to invest. New road and rail networks as well as the expansions at airports and harbors are also under construction so as to assist trade, while substantial capital investments which are internationally financed have demonstrated the strengths in these economies (AFDB 2010). Nearly three million containers were transported in West Africa in 2015 and this is quite a significant figure for the West African region.

v. ***Implementation of Joint Cross-Border Initiative:*** There is currently an ongoing optimism that the novel methodology to regionalization will have bigger success in Africa. An example of this novel methodology is the Regional Integration Facilitation Forum (RIFF) which originated as a Cross-Border Initiative (CBI) in 1992. The objective of this framework is to harmonize policies that can foster a market-driven concept of integration between Southern and Western Africa and the Indian Ocean countries. About fourteen member countries are active participants in the CBI/RIFF and it is co-sponsored by the European Union (EU), International Monetary Fund (IMF), African Development Bank (ADB), and the World Bank.

Port Selection Alternatives for Shippers in West African LLC's

This study takes into account three LLCs (Burkina-Faso, Mali, Niger) and six ports (Abidjan, Cotonou, Dakar, Lagos, Lomé & Tema) (see Figure 5); hence, a combination of 18 alternatives (See Table 6). The capitals of the three hinterland countries have also been considered as the major center of commercial activities;

namely, Bamako, Niamey and Ouagadougou. Additionally, the various transport infrastructure and intermodal transport is explained in Table 3 while a pictorial view is provided in Figure 6.

Figure 5. *LLCs' Shippers Port Selection Alternatives in West Africa*

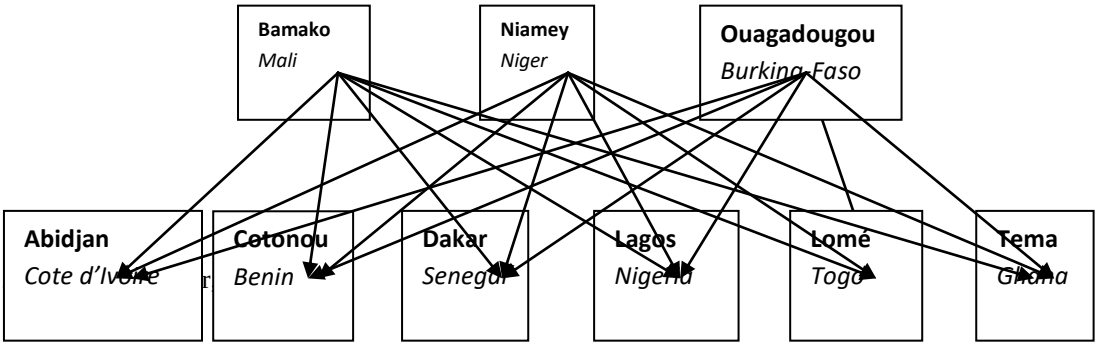

Table 3. *Transport Infrastructure in Selected West African Ports*

Transport Infrastructure	Rail Facilities	Rail Management	Road Access	Road Traffic Condition
Benin	Yes	N/A	Yes	congestion in port area
Cote d'Ivoire	Yes	SITARAIL - Bolloré/APMT	Yes	congestion in port area
Ghana	Yes	N/A	Yes	Congestion on access road
Nigeria	No	N/A	Yes	congestion in port area and exit points
Senegal	Yes	Senegal+Mali + Transrail	Yes	Congestion at port exit points
Togo	Yes	Togo-Rail	Yes	No Congestion at port but on roads

Source: Debrie (2012) and Researchers' Field Data (2018).

Figure 6. *Rail and Road Links in West Africa*

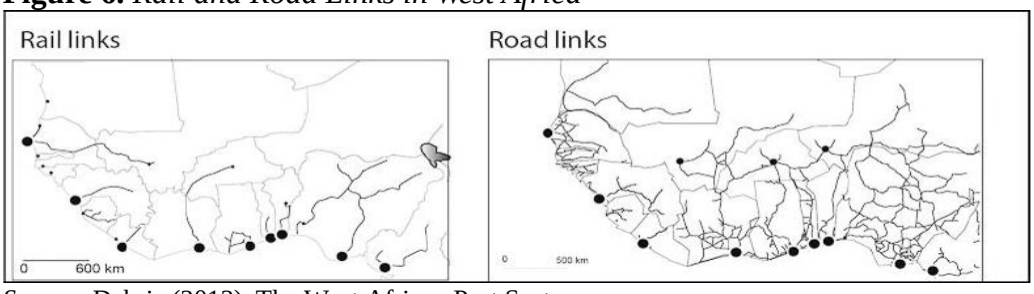

Source: Debrie (2012). The West African Port System.

Hinterland Transportation Cost Analysis for West African Countries

In this section, the total transport cost from various coastal ports to the different hinterland markets was analyzed, and this is because they remain the commercial centers in the LLC's. In total, six scenarios were analyzed per each

major port location and the transport cost determined. The distances of various locations of the commercial centers was used in part to determine the attractiveness of each proposed alternative port with regards to cost minimization for inland transport to key hinterland markets. The method takes into account the location of the coastal ports and markets, the shipping costs in US$ per ton kilometer and the volume of goods shipped or to be shipped to those locations (volume of imports and exports). The real road distances from ports to markets are used in this part of the study and the objective here is cost minimization. Hence, the port-market route that offers the least cost to transit traffic would be preferred by shippers in LLC's.

Data Analysis

The demand for each location is the sum of imports and exports in million tons. From Table 4, it can be observed that Mali recorded the highest tonnage of cargo in 2016 by 7.31 million tons and this was followed by Burkina-Faso and Niger which recorded 6.9 and 5.72 million tons of cargo respectively in 2016.

Table 4. *Demand (Imports and Exports) Data for West African LLC (Million Tons)*

	Year										
Country	2006	2007	2008	2009	2010	2011	2012	2013	2014	2015	2016
B-Faso	1.87	2.26	2.60	2.28	3.31	4.76	5.52	5.99	5.77	6.33	6.90
Mali	3.90	4.54	4.82	3.78	4.76	5.11	5.89	5.99	6.06	6.46	7.31
Niger	1.58	1.78	2.26	2.79	3.11	3.46	3.34	3.60	3.94	5.21	5.72

Source: Researchers' extraction from various ports website and PMAWCA, 2017.

Transport costs in ton km are represented in Table 5, Cote d'Ivoire and Ghana enjoys the cheapest transport cost of 0.17 US$ per ton km with Dakar recording the highest with 0.21 US$ per ton km. The pricing mechanism for such transport in West Africa is based on the cost of fuel along with road conditions, indirect costs and direct costs associated with inland transportation.

Table 4. *Average Transport Cost (US$/ton km. kilometer)*

Country	Transport cost – road (US$ ton km)	Transport cost – rail (US$ ton km)
Benin	0.18	N/A
Cote d'Ivoire	0.17	0.14
Ghana	0.17	N/A
Nigeria	0.20	N/A
Senegal	0.21	0.18
Togo	0.18	N/A

Source: Borderless West Africa 2016.

Corridor distances were derived from Sofreco and Nathan Associates and the distances range from about 928km from Lomé – Ouagadougou and 3250km for the Dakar-Lagos corridor.

Table 5. *Distances between Selected Transit Corridors in W/A*

Countries	Corridors	Distances (Km)
Benin	Cotonou – Bamako	1 947
	Cotonou – Niamey	1 070
	Cotonou – Ouagadougou	1 200
	Cotonou-Lagos	126
	Cotonou-Lomé	155
Cote d'Ivoire	Abidjan – Bamako	1 236
	Abidjan – Niamey	1 694
	Abidjan – Ouagadougou	1 232
	Abidjan-Tema	561
	Abidjan-Lomé	728
	Abidjan-Cotonou	870
	Abidjan-Lagos	955
Ghana	Tema – Bamako	1 967
	Tema – Niamey	1 576
	Tema – Ouagadougou	1 057
	Tema-Lomé	169
	Tema-Cotonou	311
	Tema-Lagos	436
Nigeria	Lagos-Bamako	1 942
	Lagos – Niamey	1 028
	Lagos-Ouagadougou	1 095
Senegal	Dakar – Bamako	1 053
	Dakar – Niamey	2 695
	Dakar – Ouagadougou	2 204
	Dakar -Tema	2 918
	Dakar -Lomé	3 135
	Dakar -Cotonou	3 194
	Dakar -Lagos	3 250
	Dakar-Abidjan	2 360
Togo	Lomé – Bamako	1 973
	Lomé – Niamey	1 222
	Lomé – Ouagadougou	928
Total (without overlaps)		46 383
Countries	Corridors	Rail Distance (km)
Abidjan	Abidjan-Ouagadougou	1 260
Dakar	Dakar-Bamako	1 230

Source: Researchers' Compilation from Sofreco and Nathan Associates (2011).
Note: Statistics is based on road length.

Analysis of Total Transport Cost via Selected Transport Corridors

Total transportation cost can be represented mathematically as:

$$TC = \sum_{n=1}^{k} d_n \; D_n \; F_n \qquad (1)$$

Where;
Dn = quantity in millions of tons
dn = distance between two locations
Fn = transportation cost in ton kilometers

The model makes the assumption that the cost per ton kilometer for rail transport is utilized instead of road where direct rail transport from a port location to a market is available, as rail cost is cheaper in line with the cost minimization objective. Abidjan's rail distance to Bamako is longer than the road route. However, the transport cost per ton kilometer is cheaper and hence the total transport cost via the rail route is the cheaper option and is used in this analysis (See Tables 7-12).

Table 6. *Scenario I – Suppose West African LLCs Choose Port of Abidjan*

Port	Hinterland Markets	Distance (km)	Quantity (million t.)	Cost (US$/km.ton)	Total cost (US$)
Abidjan (Cote d'Ivoire)	Bamako	1 236	7.31	0.17	1 535.91
	Niamey	1 694	5.72	0.17	1 647.25
	Ouagadougou*****	1 232	6.90	0.14	1 190.11
Total transport cost (million US$)					4 373.27

Source: Researchers 2018.

Table 7. *Scenario II – Suppose West African LLCs Choose Port of Cotonou*

Port	Hinterland Markets	Distance (km)	Quantity (million t)	Cost (US$/km.ton)	Total cost (US$)
Cotonou (Benin)	Bamako	1 947	7.31	0.18	2 561.86
	Niamey	1 070	5.72	0.18	1 101.67
	Ouagadougou	1 200	6.90	0.18	1 490.40
Total transport cost (million US$)					5 153.93

Source: Researchers 2018.

Table 8. *Scenario III – Suppose West African LLCs Choose Port of Dakar*

Port	Hinterland Markets	Distance (km)	Quantity (million t)	Cost (US$/km.ton)	Total cost (US$)
Dakar (Senegal)	Bamako *****	1 053	7.31	0.18	1 385.54
	Niamey	2 695	5.72	0.21	3 237.23
	Ouagadougou	2 204	6.90	0.21	3 193.60
Total transport cost (million US$)					7 816.37

Source: Researchers 2018.

Table 9. *Scenario IV – Suppose West African LLC's Chose Port of Lagos (Apapa)*

Port	Hinterland Markets	Distance (km)	Quantity (million t)	Cost (US$/km.ton)	Total cost (US$)
Lagos (Nigeria)	Bamako	1 942	7.31	0.20	2 839.20
	Niamey	1 028	5.72	0.20	1 176.03
	Ouagadougou	1 095	6.90	0.20	1 511.10
Total transport cost (million US$)					5 526.33

Source: Researchers 2018.

Table 10. *Scenario V – Suppose West African LLC's Chose Port of Lomé*

Port	Hinterland Markets	Distance (km)	Quantity (million t)	Cost (US$/km.ton)	Total cost (US$)
Lomé (Togo)	Bamako	1 973	7.31	0.18	2 596.07
	Niamey	1 222	5.72	0.18	1 258.17
	Ouagadougou	928	6.90	0.18	1 152.58
Total transport cost (million US$)					5 006.82

Source: Researchers (2018).

Table 11. *Scenario VI – Suppose West African LLC's Chose Port of Tema*

Port	Hinterland Markets	Distance (km)	Quantity (million t)	Cost (US$/km.ton)	Total cost (US$)
Tema (Ghana)	Bamako	1 967	7.31	0.16	2 300.60
	Niamey	1 576	5.72	0.16	1 552.36
	Ouagadougou	1 057	6.90	0.16	1 166.93
Total transport cost (million US$)					5 019.89

Source: Researchers (2018).

From the analysis above, the total transport cost with regards to inland transport of goods from ports to markets range between US$ 4,373.27 million for the port of Abidjan and US$ 7, 816.37 million for the Port of Dakar. Additionally, the ranking pattern of the cheapest route based on the total inland transportation cost is shown in Figure 7.

Figure 7. *Total Transport Cost for West African LLCs from Selected Transit Ports*

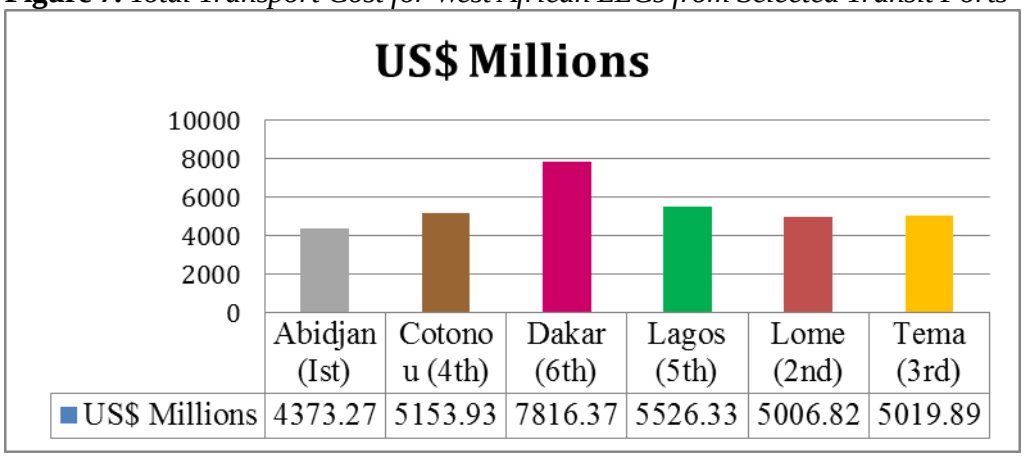

Analyzing Total Transport Cost with Forecasted Demand

A demand forecast for market regions is made, as dry port development should be based on expected demand of markets. The forecasted demand of the markets is based on multiple variables that include GDP, population and FDI of the countries in which the markets are located (see Table 13).

Table 12. *Economic Variables Used for Demand Forecast*

GDP US$ mil	‘06	‘07	‘08	‘09	‘10	’11	‘12	‘13	‘14	‘15	‘16
Benin	5142.1	5970.4	7133.8	7097.2	6970.5	7814.3	8117.6	9111.2	9575.0	9932.4	1064.5
[1]B. Faso	5845.7	6991.7	8378.4	8369.5	8969.5	10724.6	11166.4	11947.6	12377.5	10419.7	11693.1
Cote d’Ivoire	17801.3	20344.6	24255.6	24277.8	24885.3	25382.7	27041.5	31293.0	34242.6	36345.9	39101.5
Ghana	20409.8	24759.5	28527.1	25978.4	32175.9	39566.2	41940.3	47805.6	38617.5	41764.8	45231.7
Mali	6975.0	8146.3	9751.4	10181.7	10679.5	12978.7	12443.7	13246.9	14388.8	13176.8	14035.8
Niger	3664.6	4291.9	5403.6	5397.6	5719.7	6409.6	6942.5	7668.5	8245.4	7143.6	7509.5
Nigeria	145430.4	166451.8	208065.7	169481.3	369062.2	411744.0	460954.3	514965.9	568508.6	600125.3	649071.6
Senegal	9359.1	11285.7	13386.0	12813.4	12932.2	14441.6	14046.3	14952.9	15658.5	17002.7	18657.5
Togo	2203.6	2523.4	3163.0	3163.5	3173.3	3756.7	3916 .4	4339.8	4518.1	6734.8	8465.9

[1]Burkina Faso.

FDI US$ mill	‘06	‘07	‘08	‘09	‘10	‘’11	‘12	‘13	‘14	‘15	‘16
Benin	-12.4	139.0	48.0	-18.7	53.5	161.1	281.6	360.2	377.4	380.2	385.9
B.Faso	83.8	21.7	33.1	56.4	38.8	143.7	329.3	490.3	356.8	167.4	308.7
Cote d’Ivoire	350.7	443.2	466.5	396.0	358.1	301.6	330.3	407.5	462.0	466.8	499.1
Ghana	636.0	1383.2	2714.9	2372.5	2527.4	3247.6	3294.5	3227.0	3363.4	3501.0	3786.4
Mali	148.2	206.1	266.4	646.6	371.6	556.1	397.9	307.9	144.0	275.4	125.5
Niger	40.2	98.9	281.9	631.3	795.9	1066.5	841.3	719.1	821.9	529.3	292.8
Nigeria	4854.4	6035.0	8196.6	8554.8	6026.2	8841.1	7069.9	5562.9	4655.8	4895.7	5001.3
Senegal	289.6	351.0	453.9	330.1	266.1	338.2	276.2	311.3	342.7	378.4	390.0
Togo	91.3	62.3	50.7	46.1	124.9	727.8	121.5	195.8	292.1	335.8	378.5

[2]Pop mil	‘06	‘07	‘08	‘09	‘10	‘’11	‘12	‘13	‘14	‘15	‘16
Benin	8.4	8.7	9.0	9.2	9.5	9.8	10.0	10.3	10.6	11.0	11.7
B.Faso	13.8	14.2	14.7	15.1	15.6	16.1	16.6	17.1	17.6	18.1	18.6
Cote d’Ivoire	18.5	18.9	19.3	19.7	20.1	20.6	21.1	21.6	22.2	22.5	23.0
Ghana	22.0	22.5	23.1	23.7	24.3	24.9	25.5	26.2	26.8	27.6	28.3
Mali	13.2	13.6	14.1	14.6	15.1	15.5	16.0	16.5	17.0	17.5	18.0
Niger	14.1	14.7	15.2	15.8	16.4	17.1	17.7	18.4	19.1	19.9	20.7
Nigeria	143.3	147.2	151.1	155.2	159.4	163.8	168.2	172.8	177.5	180.3	188.6
Senegal	11.6	11.9	12.2	12.6	13.0	13.4	13.8	14.2	14.7	15.6	16.0
Togo	5.7	5.9	6.1	6.2	6.4	6.6	6.7	6.9	7.1	7.7	8.4

Source: Population, Foreign Direct Investment (Total Inflows), GDP (World Bank 2018).

[2]Population.

Linear Regression Model & Application

According to (Peng and Chu 2009), linear regression is one of the most common quantitative prediction methodologies and it has been extensively applied in port throughput literatures to ascertain indicators of throughput and forecast implementation. Tongzon (1995) and Tongzon and Wu (2005) employed linear regression to demonstrate the causal relationship between the determinants of cargo throughput and port performance. Seabrooke et al. (2003) also projected the level of cargo growth through the application of regression analysis techniques in Hong Kong. Additionally, a further study by (Chou et al. 2008) was conducted in projecting volumes of import containers in Taiwan where a modified regression model was developed to guarantee improved forecast accuracy. The prediction of throughput capacities has a substantial effect on port development strategy and the capacity to offer quality and effective services. Thus, a basic forecasting selection technique was adapted from Wang et al. (2009) (See Figure 8).

Figure 8. *Common Quantitative Forecasting Methods*

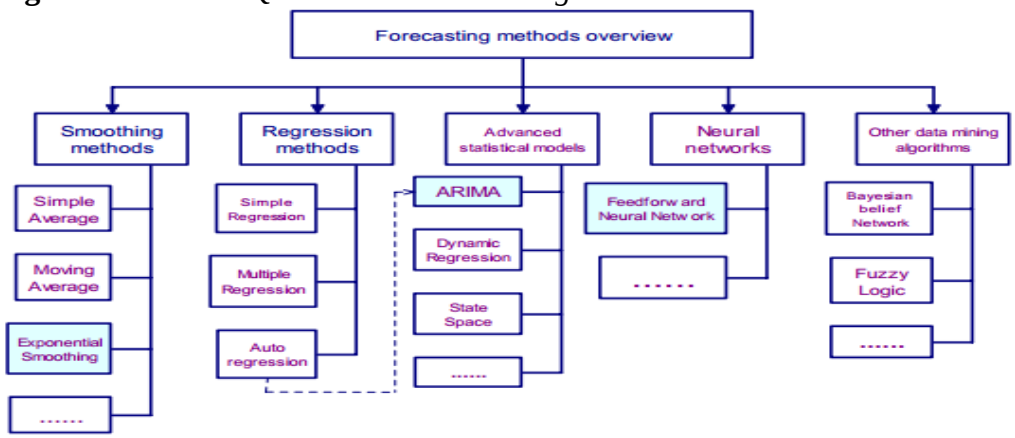

Source: Rule Induction for Forecasting Method Selection (Wang et al. 2014).

Sun (2010) suggested a dual forecasting model based on conditional expectation through probability dissemination of port cargo throughput. Alternatively, Huang et al. (2003) have applied the grey model in forecasting demand in a transportation network. An improved Grey theory using Fourier series FRMGM (1,1) for enhancing forecast accuracy of cargo throughput at Kaohsiung ports from 2013-2015 has also been applied by (Wang and Phan 2014). In this study, forecasting cargo throughput for the West African LLCs is executed using a classical time-series regression model.

Forecast Model and Analysis

In defining the economic indicators to be used in the regression model, numerous indicators were evaluated to check their level of correlation and the most remarkably used indicators in previous research include Population, Gross Domestic Product (GDP), Foreign Direct Investment (FDI) inflows and the level of imports and exports. The economic data used in the regression

model is based on the hypothesis that these drivers are the key factors of cargo throughput for West African LLCs.

$$Y = A + B_1X_1 + B_2X_2 + \dots BnXn \quad (2)$$

Where:

Y= dependent variable (container throughput)
Xn= independent variable
a=y- intercept (value of y when x=0)
b= slope or trend

$$b = \frac{N\sum XY - \sum X\sum Y}{N\sum X^2 - \left(\sum X\right)^2} \qquad a = \frac{\sum Y}{N} - b\left(\frac{\sum X}{N}\right) \quad (3)$$

Where N= number of period of data

The accuracy of the regression model was first checked by looking at the R square and adjusted R square figures from the output of the regression statistics. The R square values were verified to ensure that the variance of the output variable (cargo throughput) can be clarified by the variance of the input variables (GDP FDI and population). The adjusted R square, which is a more conservative form of the R square, was also verified and this indicates the model is very consistent for forecasting future cargo throughput levels. The coefficient, GDP and FDI were therefore found to be statistically significant at level that were much lower than 0.05. Cargo throughput, GDP and FDI are set respectively as, *Y* and X1 and X2 respectively in the model and based on the output. Deriving the expected GDP forecast and FDI forecast for the next period (2017) is required in order to derive the throughput for the next period and this is achieved by determining the GDP and FDI value depending on time *(t)* using a linear equation. In order to obtain the linear equation in the form ***x1t = a+b.t,*** (where *x1t* is the anticipated GDP forecast) and determine the coefficients *b* and *a*, the values for *t2* and *x1*t* need to be determined. The result of the forecasted data is presented Table 14 below.

Table 13. *Forecasted Demand of Economic Variables for West African LLCs*

[1]LLCs	'17	'18	'19	'20	'21	'22	'23
Benin	8.82	9.40	9.93	10.51	10.97	11..49	11.98
Burkina-Faso	7.64	8.23	8.72	9.41	9.89	10.38	10.91
Cote d'Ivoire	16.89	17.49	17.93	18.38	19.58	19.99	20.61
Ghana	12.30	12.84	13.41	13.98	14.52	14.99	15.45
Mali	7.95	8.68	9.02	9.78	10.44	10.97	11.63
Niger	6.39	6.82	7.30	7.81	8.20	8.69	9.01
Nigeria	21.67	22.32	22.86	23.41	23.94	24.49	24.98
Senegal	10.72	11.41	11.98	12.49	12.97	13.43	13.96
Togo	9.01	9.62	10.20	10.74	11.27	11.70	12.41
Total	34.28	36.59	38.45	40.98	43.05	45.03	47.01

Source: Researchers 2018.

From the year 2017-2023, a combined forecasted cargo throughput of 285.39 million tonnes of cargoes shall be loaded and discharged through port of Abidjan and cargo throughput has increased at an average of 9% per annum.

Port of Abidjan as a Gateway Port to West African Landlocked Countries

The Port of Abidjan is located in the economic capital of the Cote d'Ivoire, West Africa's largest French-speaking nation. It is one of the largest sea ports in West Africa lying on the Ebire Lagoon N $05^{o}.3$ and E -4.0^{o} connecting the Atlantic by the Vridi Channel. The port is located at the intersection of major shipping lines from U.S.A, Europe and Asia. It is one of the region's shipping hubs with a land surface area of 8,000 000 m2 housing 36 conventional berths located along its three main quays (Eastern, Southern and Northern Quays). Although the port has recently lost most of its market to neighboring competitors such as Tema, Lomé and Dakar due to the sporadic post electoral crisis in 2011, it still receives an average of 5217 vessels 2017, comprising of general cargo vessels, tankers, Ro-Ro, container vessels etc. and this implies that the port of Abidjan is expected to regain stability in the nearest future.

Recently, the port of Abidjan has expanded by building new terminals, upgraded its IT systems as well as widened its operational partnerships and networks in order to revive its port sector. This is reflected by the port's ability to handle increasing volumes of traffic from 19.6 million tonnes in 2016 to 20.2 million tonnes in 2017 (See Figure 9). Development projects completed in 2020 shall include expansion and dredging of the Vridi access channel, construction of a second container terminal, modernization of the fishing berth, installation of conveyor belt for cement and clinker vessels etc. Additionally, the Port of Abidjan generally runs a variety of the landlord port management system and the port authority is responsible for regulating port operations, in addition to building and maintaining infrastructures.

[1]LLCs- Land Locked Countries.

Figure 9. *Port of Abidjan Transit Traffic Statistics by Destination 2008 - 2017*

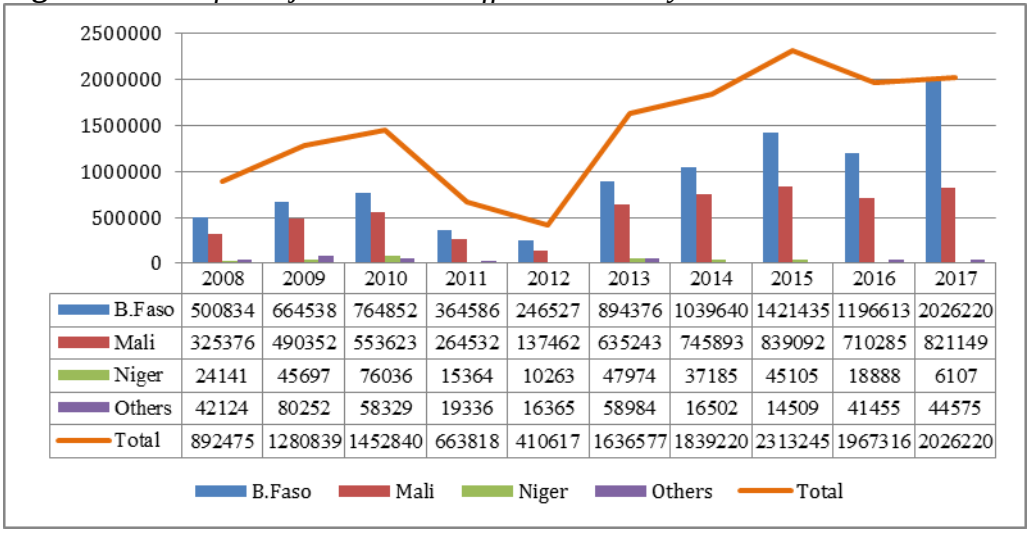

	2008	2009	2010	2011	2012	2013	2014	2015	2016	2017
B.Faso	500834	664538	764852	364586	246527	894376	1039640	1421435	1196613	2026220
Mali	325376	490352	553623	264532	137462	635243	745893	839092	710285	821149
Niger	24141	45697	76036	15364	10263	47974	37185	45105	18888	6107
Others	42124	80252	58329	19336	16365	58984	16502	14509	41455	44575
Total	892475	1280839	1452840	663818	410617	1636577	1839220	2313245	1967316	2026220

Source: Researcher's compilation from the port website (www.portabidjan.com).

Inland/Dry Port Location Selection

The gravity location model is used in this section to propose an optimum location of a dry port for the region with the Port of Abidjan as a gateway port. This is proposed in order to take further advantage of scale economies and increase the level of service for efficient distribution of cargo to hinterland markets in West Africa. The model is basically used in management science to determine the optimum location of a facility that has the function of either reducing transit time or lowering transport cost. The cost of distribution is seen as a linear function of the distance and the quantity or weight of cargo transported. The model uses a coordinate system superimposed on a visual map with the coordinates representing a set of numerical values when calculating averages. The grid map set up on a Cartesian plane identifies a set of coordinates which designates a location central to all other locations on the grid map. Using a map of West Africa, geometric locations of port and market are ascertained using *X* and *Y* axes.

The coordinates for the location of the dry port facility are computed using the following formula:

$$x = \frac{\sum_{i=1}^{n} x_i w_i}{\sum_{i=1}^{n} w_i} \quad y = \frac{\sum_{i=1}^{n} y_i w_i}{\sum_{i=1}^{n} w_i} \qquad (4)$$

Where,

x,y = coordinates of the dry port facility at the center of gravity
xi,yi = coordinates of gateway port and other competitive ports
Wi = annual demand shipped from gateway port to a particular market

In the Euclidean plane, the distance between two points is derived using a formula equivalent to the Pythagorean Theorem. Therefore, the distances between the regional hub port and markets are calculated using the formula:

$$d_n = \sqrt{(x - x_n)^2 + (y - y_n)^2} \quad (5)$$

Where,

xn,*yn* = coordinate location of either a market or supply source (gateway port)
Fn = cost of transporting one unit for one kilometer between the gateway port and market
dn = distance between the gateway port and the market *n*.

For this particular study, Euclidean distances are not used as real road distances from sources to markets are available. Euclidean distances do not show the real situation on the ground as such direct lines as measures of distance are more suited to air travel than road transport. It is quite unusual for roads leading from one point to another to be ultimately a straight line. Therefore, real distances will portray a more accurate picture and result in a more accurate outcome in determining a dry port location for consolidation and distribution of cargo as indicated on Figure 10 and Table 5.

Figure 10. *Grid Map of Regional Hub Port and Markets*

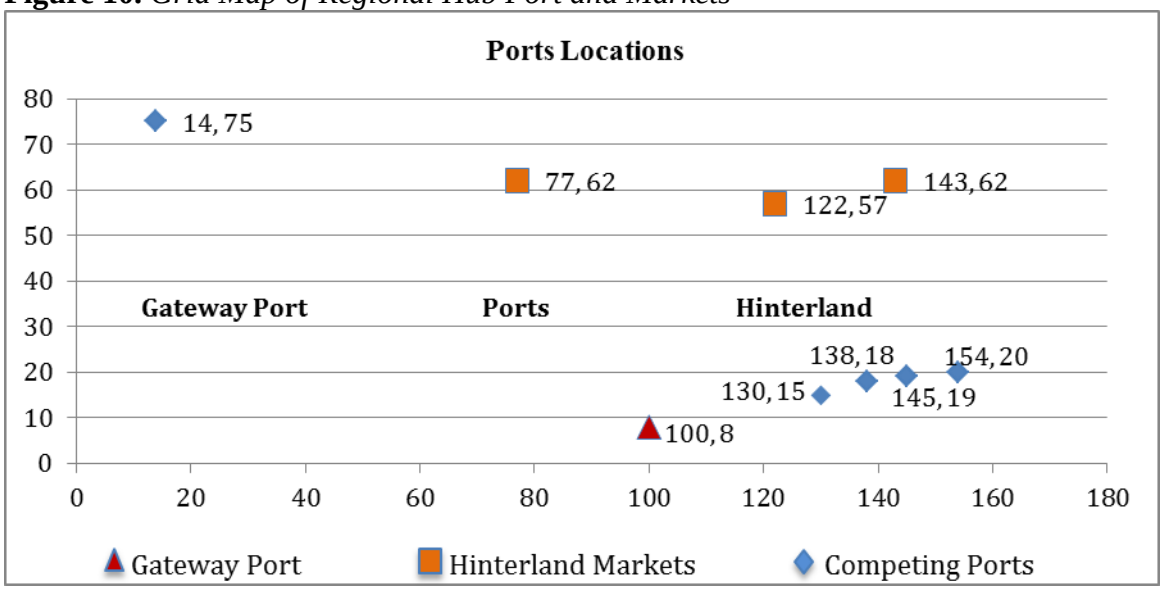

Source: Researchers 2018.

Table 14. *Derivation of Gravity Center*

Source/ Markets	$/Ton Km ($f_n$)	mTons D_n	Fi $/km	Coordinates y_n	x_n	Distance d_n	$D_nF_nx_n/d_n$	$D_nF_ny_n/d_n$	D_nF_n/d_n
Abidjan*	0.17	19.58	3.33	100	8	25	13.314	1.065	0.133
Accra (Tema)	0.17	14.52	2.47	130	13	561	0.572	0.057	0.004
Bamako	0.17	10.44	1.78	77	62	1236	0.111	0.089	0.001
Cotonou	0.17	10.97	1.86	138	19	870	0.296	0.041	0.002
Dakar	0.17	12.97	2.20	14	75	2360	0.013	0.070	0.000
Lagos	0.17	23.94	4.07	154	23	955	0.656	0.129	0.004
Lomé	0.17	11.27	1,92	130	19	728	0.324	0.050	0.002
Niamey	0.17	8.20	1.56	143	62	1694	0.118	0.051	0.000
Ouagadougou	0.17	9.89	1.68	122	57	1232	0.166	0.078	0.001
							15.570	1.630	0.148

Source: Researchers 2018.

The resulting dry port location can be obtained by:

X coordinate = 15.570/0.17 = 92.0*Y* coordinate = 1.630/0.17 = 10.0

Dry port can be located at point *(92, 11)* on the grid map.

Figure 11. *Dry Port Location on Grid Map*

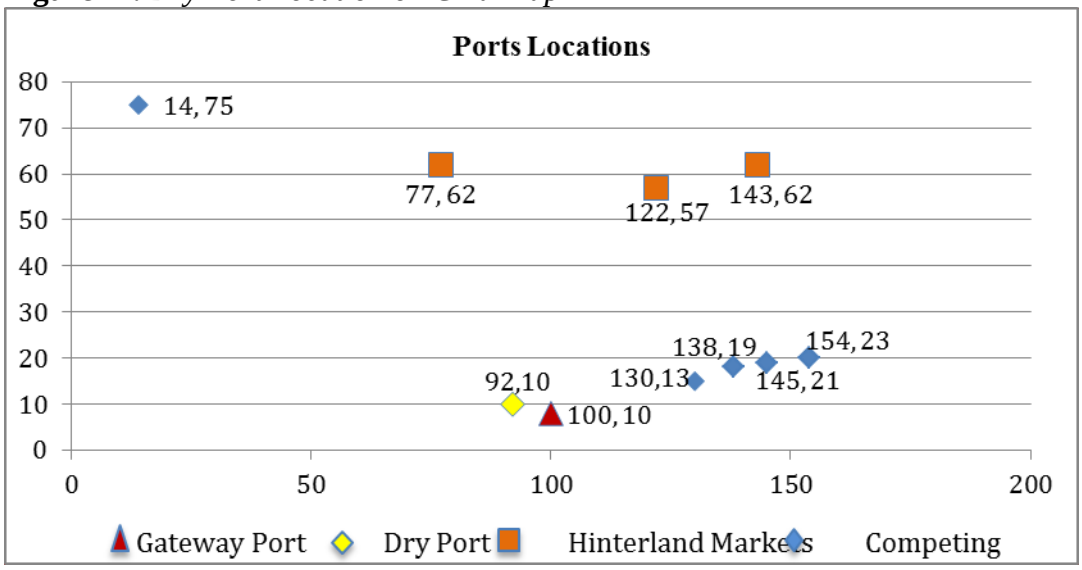

Source: Researchers 2018.

Figure 12. *Visual Map View of West African Cargo Distribution*

Source: Researchers 2018.

By superimposing the grid map (Figure 11) on the visual map (Figure 12), the optimum location for developing a regional dry port is a southern city in Cote d'Ivoire known as Divo. Divo is ranked the tenth most populated city in Cote d'Ivoire and a major advantage of this location is that it is connected to the port of Abidjan and other major cities within the country through the A2 highway. Transit cargo distribution from the regional hub port of Abidjan (Figure 12) would be transported to a dry port in Divo before an onward distribution to the various hinterland markets and commercial center within West Africa. This system would also decongest the port of Abidjan and enhance its productivity. Additionally, the Abidjan-Ouagadougou corridor remains a pivot transport framework for cargo destined for Burkina-Faso (Northbound and Southbound) via rail service as this may offset additional handling and facilitation costs that may arise from the utilization of the dry port. Also, direct shipments may leave the Port of Abidjan to the Dakar also due to distance constraints.

Findings

SWOT for Developing Dry Port Cote d'Ivoire

SWOT analysis is a corporate professional analytic technique applied by various institutions to assess their products and or services as well as the market situation when deciding the best way to attain a constant future growth. In the academic settings, numerous scholars have employed the SWOT as a major research methodology in undertaking their study and we refer readers with interest to Chen and Wang (2012), Augustin et al. (2018), Garnwa et al. (2009) and Wang (2011).

Strengths

- *Existence of Railway Network to Hinterland Markets:* The existing rail network along Abidjan-Ouagadougou corridor has made it the busiest corridor due to volume of cargo transported. Transportation cost is of essence to shippers in West African hinterland markets thus, most cargoes are transported via the port of Abidjan by train in order to minimize cost and this in return has made the port of Abidjan more competitive over other seaports in the region.
- *Port Expansion Projects and Dredging of Vridi Channel:* Ports in West African region have all embarked on enormous port expansion projects and the Port of Abidjan is not an exception. Additionally, the size of the Vridi channel has been a major limitation to the size of vessels calling the port of Abidjan therefore; its expansion will enable larger vessels calling at the port as well as increase the port's annual throughput.
- *Member of the same Regional Block with West African LLC's:* Cote d'Ivoire is an active member of the same regional block (West African Economic Monetary Union) with the three West African Landlord countries using a common language with relatively stable currency (franc CFA).
- *Strategic Location as a Gateway Port for West African Hinterland Markets:* The geographical position of the port of Abidjan has made its port and corridor accessible to all West African hinterland markets in relation to distance and this marginal adjustment from Abidjan to the hinterland market illustrates how strategically located Cote d'Ivoire has been for transit traffic to its landlocked neighbors (Burkina-Faso, Mali & Niger).

Weaknesses

- *Political Instability coupled with Ethnic and Regional Tensions:* A major weakness that has been a drawback for Cote d'Ivoire is the recent political crises and ethnic tensions which have saddled the country's economic sector and this has led to investors leaving the country to other neighboring West African nations.
- *Limited Terminal Capacity:* Most ports in the region are confronted with this problem thus, majority of them have embarked on massive port expansion projects. In response to this issue, the port of Abidjan has been concession to the French industrial conglomerate Bolloré so as to cater for the acute shortage of terminal needed for container handling operations at the port.
- *Poor State of Trucks applying Abidjan-Ouagadougou Corridor:* According to shippers from West African hinterland markets, trucks applying Abidjan - Ouagadougou corridor are currently in poor states thus, they are always confronted with constant breakdowns while in transit and this in return affects shippers lead time and competitiveness within the region.

Opportunities

- *Establishment of a Joint Border Post (JPB) with Landlocked Countries:* The establishment of JPB with Burkina-Faso and Mali will create a unique platform where information can be shared between the customs systems of all parties thus, harmonizing the clearance procedure and reducing truck waiting time at the border. An example is the existing Joint Border Post between Togo and Burkina-Faso at Cinkassé.
- *Efforts from Regional Blocks (ECOWAS & UEMOA) to Promote Transit Traffic:* West African regional bodies are making frantic efforts to ratify sustainable legislations that would promote intra-regional transit traffic. These legislations are aimed towards synchronizing and universalization of customs clearing procedures, insurance policies and transport frameworks between member states.
- *Encourage Public Private Partnership (PPP) in the Port Sector:* The participation of private entities in the Ivorian port sector is also a unique strategy that can be implemented by the port authority to boost productivity. The recent political crises has left the economy with very few foreign investors thus, deregulation of policies and privatization could help revamp its ports industry.

Threats

- *Growing Ports Competition among Competitors:* There is a continuous growing competition among ports located within the West African region and from competing neighboring corridors that are also part of same regional block (WAEMU) as Cote d'Ivoire. These corridor states include; Lomé-Ouagadougou, Dakar-Bamako and Cotonou-Ouagadougou. For example; Lomé-Ouagadougou transit corridor measures 928km and is currently the shortest distance to the West African hinterland markets. Additionally, there is also an existing rail network to between Dakar-Bamako transit corridor.
- *Burkina-Faso as a Second Transit Nation for Niger:* Burkina-Faso as a second transit state remains an inevitable bottleneck for shippers in Niger. Although Burkina-Faso is ranked 81st position on the 2016 global LPI, its customs procedure is known to be sagged with lengthy documentation process and illegal extortion of fees from commuters transiting through its territory.
- *Recent Pirate Attacks on Ships along the Gulf of Guinea:* Recent attacks along the West African maritime territory have raised major concerns from shipping lines calling various ports along the coast and countries mostly affected in the region include; Benin republic, Ghana, Nigeria and Togo with 11 attacks in the first quarter of 2013 (IMB 2015).

Discussion

The hinterland transport cost analysis conducted indicates that only few West African coastal countries offer cheap transit cost to shippers in hinterland markets and this has remained a major factor impeding the competiveness of landlocked countries with the global market in terms of international trade. Thus, there is an urgent need for stakeholders to implement measures that can reduce the transport cost and improve swift transportation of transit traffic along various transit corridors in West Africa. Adequate policies regarding the road-worthiness of trucks should also be implemented in order to reduce the number of damaged trucks on the corridor. The simple forecast conducted in this research indicates that the annual throughput for the port of Abidjan is going to experience a steady increase in the nearest future therefore, measures which could relieve the port during over capacity situations are instantly needed. Additionally, digitalizing most of the port's documentation systems will also reduce cargo clearance procedure at the port and at the various nodes along the corridor. Finally, there is a need to establish a joint regional force to protect West African maritime territories from pirate attacks and to ensure the safety and security of both vessels and cargoes calling at West African ports as this is a reliable measure to assure various shipping line the reasons for maritime businesses.

Conclusions

The Abidjan-Ouagadougou transit corridor is the only national transport network in Cote d'Ivoire that expedites cargoes designated for West African hinterland countries and it is also the principal route on the Ivorian territory that generates substantial revenue for the government. Thus, there is a need for the government to enhance an efficient and effective flow of transit traffic along the corridor. Additionally, the port of Abidjan is currently witnessing a tremendous development in port infrastructure due to its concession and this is coupled with a steadfast growth in the West African regional economy giving rise to a constant increasing demand for transport services. Hence, the development of a dry pot in Divo (Loh Djiboua district) remains a pilot program to promoting regional trade and sustainable transit traffic in Cote d'Ivoire and Sub-Saharan Africa.

References

African Development Bank - AFDB (2010) *Growing Forward: Developing Regional Hubs in Africa*. Retrieved from https://bit.ly/2Id6IR5.

African Development Bank - AFDB (2015) *Economic Transformation*. Retrieved from https://bit.ly/2I0EUjk.

Arnold J (2005) *Best Practice in Management of International Trade Corridor*. Washington, DC: World Bank. Retrieved from: https://bit.ly/2OCLjp1.

Arvis JF, Ojala L, Shephard B, Saslavky D, Busch C, Raj A (2014) *Connecting to Compete 2014: Trade Logistics in the Global Economy, the Logistics Performance Index and its Indicator*s. Washington, DC: World Bank.

Augustin DS, Akossiwa DL (2018) SWOT Analysis for Developing Dry Port in Togo. *American Journal of Industrial and Business Management* 8(6): 1407-1417.

Caballini C, Gattorna E (2009) The Expansion of the Port of Genoa: The Rivalta Scrivia Dry Port. *Transport and Communications Bulletin for Asia and the Pacific* 78: 103-125.

Chen JH, Wang Y (2012) SWOT-PEST Analysis in China's Dry Port. *Advance Materials Research* 479-481(Feb): 1004-1012.

Chou CC, Chu CW, Liang GS (2008) A Modified Regression Model for Forecasting the Volumes of Taiwan's Import Containers. *Mathematical and Computer Modelling* 47(9-10): 797-807.

Consumer News and Business Channel - CNBC Africa (2017). http://www.cnbcafrica.com/.

Danida-Saana Consulting (2015) *Accelerating Trade in West Africa-ATWA*. Retrieved from: https://bit.ly/2yF1N5m.

Debrie J (2012) *The West African Port System: Global Integration and Regional Particularities*. Retrieved from EchoGéo: https://bit.ly/2G2XMMK.

Garnwa P, Baredford A, Pettit S (2009) Dry Ports: A Comparative Study of the United Kingdom and Nigeria. *Transport and Communications Bulletin for Asia and the Pacific* 78: 58-81.

Huang W, Wu S, Cheng P, Yu Z (2003) Application of Grey Theory to the Transport Demand Forecast from the Viewpoint of Life Cycle-Example for the Container Port in Taiwan. *Journal of Maritime Sciences* 12: 171-185.

International Maritime Bureau - IMB (2015) *Piracy and Armed Robbery against Ships*.

Kunaka C, Carruthers R (2014) *Trade and Transport Corridor Management Toolkit. World Bank Training*. Washington, DC: World Bank. Retrieved from: https://bit.ly/2ME1Pm6.

Liu Q (2010) *Efficiency Analysis of Container Ports and Terminals*. PhD Thesis. UK: Centre for Transport Studies, University College of London.

Maloni M, Jackson EC (2005) North American Container Port Capacity: An Exploratory Analysis. *Transportation Journal* 44(3): 1-22.

N'Guessan (2003) *Improvement of Transit Transport in West Africa*. https//unctad.org/en/Docs/ldc20032_en.pdf.

Nguyen CL, Notteboom T (2016) Dry Ports as Extensions of Maritime Deep-Sea Ports: A Case Study of Vietnam. *Journal of International Logistics and Trade* 14(1): 65-88.

Peng WY, Chu CW (2009) A Comparison of Univariate Methods for Forecasting Container Throughput Volumes. *Mathematical and Computer Modelling* 50(7-8): 1045-1057.

Port Management Association for West and Central Africa - PMAWCA (2017) Accessed [January 21, 2014]. Retrieved from https://bit.ly/2FOzq80.

Roso V (2005) *The Dry Port Concept Applications in Sweden*. Proceedings of Logistics Research Network. Plymouth: International Logistics and Supply Chain Management.

Roso V, Woxenius J, Lumsden K (2009) The Dry Port Concept: Connecting Container Seaports with the Hinterland. *Journal of Transport Geography* 17(5): 338-345.

Seabrooke W, Hui E, Lam WA (2003) Forecasting Cargo Growth and Regional Role of Port of Hong Kong. *Cities* 20(1): 51-64.

Song DW, Cullinane K (1999) *The Stochastic Frontier Model: A New Approach to Efficiency Measurement in Logistics Chains*. Proceeding of the Universities Transport Group (UTSG) York, UK: University of York.

Sun L (2010) Research on a Double Forecasting Model for Port Cargo Throughput. *World Journal of Modelling and Simulation* 6(1): 57-62.

Tongzon J (1995) Determinants of Port Performance and Efficiency. *Transport Research A* 29(3): 245-352.

Tongzon J, Wu H (2005) Port Privatization, Efficiency and Competitiveness: Some Empirical Evidence from Container Ports (Terminals). *Transportation Research Part A* 39(2005): 405-424.

Torres C, van Seters J (2016) *Overview of Trade and Barriers to Trade in West Africa*. Discussion Paper 195. Maastricht: ECDPM

UNCLOS (1982) *United Nations Convention on the Law of the Sea*. Geneva, Switzerland. Retrieved from: https://bit.ly/1dSph2X.

UNESCAP (2012) *Introduction to the Development of Dry Ports in Asia*. Retrieved from: https://bit.ly/2TZAv21.

Veenstra A, Zuidwijk R, Asperen E (2012) The Extended Gate Concept of Container Terminals: Expanding the Notion of Dry Ports. *Maritime Economics & Logistics* 14(1): 14-32.

Wang M (2011) Analysis of SWOT for the Development of Dry Port in Wuyishan. *Journal of Wuyi University* 4.

Wang X, Smith-Miles K, Hyndman R (2009) Rule Induction for Forecasting Method Selection: Meta-Learning the Characteristics of Univariate Time Series. *Neurocomputing* 72(10-12): 2581-2594.

Wang CN, Phan VT (2014) An Improvement in the Accuracy of Grey Forecasting Model for Cargo throughput in International Commercial Ports of Kaohsuing. *WSEAS Transactions on Business and Economics* 11(1): 322-327.

Woxenius J, Roso V, Lunsden K (2004) *The Dry Port Concept- Connecting Seaports with their Hinterland by Rail*, 305-319. Proceedings of ICLSP 2004. Retrieved from: https://bit.ly/2HZoEPO.

A Practical Model of Godel–Planck–Hubble–Birch Universe

By UVS Seshavatharam[*] & S Lakshminarayana[†]

By considering 'Planck mass' as a characteristic massive seed and by replacing big bang with a growing Planck ball, an evolving model of quantum cosmology can be developed. With reference to increasing support for large scale cosmic anisotropy, preferred directions, quantum mechanical demand of cosmic spin and by considering a decreasing trend of angular velocity, from the beginning of Planck scale, we have developed a procedure for estimating the trend of all cosmic physical parameters. From and about the baby universe, in all directions, cosmic acceleration can be understood with increasing expansion velocity and decreasing total matter density ratio. We would like suggest that, from the beginning of Planck scale, 1) Dark matter can be considered as a kind of cosmic foam responsible for formation of galaxies. 2) Cosmic angular velocity decreases with square of the decreasing cosmic temperature. 3) Increasing ratio of Hubble parameter to angular velocity plays a crucial role in estimating increasing cosmic expansion velocity and decreasing total matter density ratio. 4) There is no need to consider dark energy for understanding cosmic acceleration. With further study, cosmological nucleosynthesis and dark matter synthesis along with mass generation mechanism can be reviewed in a quantum cosmological approach.

Keywords: *Angular Velocity, Critical Density, Dark Matter, Expansion Velocity, Hubble's Law, Ordinary Matter, Planck Scale, Quantum Cosmology.*

PACS Nos: *04.20.-q, 04.60.-m, 04.50.Kd, 98.80.Qc, 98.80.Bp, 98.80.Es*

Introduction

According to the current notion of modern cosmology, if the known laws of physics are extrapolated to the highest density regime, the result is a singularity which is typically associated with the big bang (Gamow 1948a, 1948b). Unfortunate thing is that, pre or post conditions and parameters of big bang physics are absolutely unknown. In this critical scenario, in a quantitative approach, it may not be wrong to consider a 'growing' or 'evolving' phase of 'Planck scale'. Even though massive nature is unclear - with known physical laws, Planck scale can be assigned with certain 'mass', certain 'radius', certain 'volume', certain 'density', certain 'temperature' and certain 'pressure'. Clearly speaking, Planck mass can be considered as a characteristic massive seed of the evolving universe and big bang can be replaced with an evolving Planck ball. Planck mass can be called as the 'baby universe'. Thinking in this way, by

[*]Honorary Faculty, I-SERVE, Survey no-42, Hitech city, Hyderabad, India.
[†]Retired Professor, Department of Nuclear Physics, Andhra University, Visakhapatnam-03, India.

replacing big bang (Mitra 2011, 2014) with a growing Planck ball, in a hypothetical approach, an evolving model of quantum cosmology can be developed (Bojowald 2015, Padmanabhan 2005, Sivaram 2000). Since Planck scale is associated with Quantum theory and 'spin' is a basic property of quantum mechanics, it may not be wrong to consider a growing and rotating model of a Planck ball (Whittaker 1945, Gamow 1946, Godel 1949, Raychaudhuri 1955, Narlikar and Hoyle 1963, Hawking 1969, Birch 1982, Korotky and Obukhov 1995, Nodland and Ralston 1997, Kuhne 1997, Li 1998, Singh 1999, Obukhov 2000, Carneiro 2002, Panov and Kuvshinova 2004, Barrow and Tsagas 2004, Szydlowski and Godlowski 2005, Su and Chu 2009, Godlowski 2011, Longo 2011, Cai et al. 2013, Chechin 2016, 2017). Since nothing is known, it is absolutely not possible to simulate a big bang, but with future science, engineering and technology, it is certainly possible to simulate any 'Planck scale' physical event. Till that time, cosmic observations can be analyzed with a notion of 'growing Planck ball'. Center of the growing universe seems to depend on the location of the assumed Planck seed under consideration. In this paper, with reference to our recent paper (Seshavatharam and Lakshminarayana 2019), by modifying our proposed set of assumptions we try to cover up the Mach's principle (Arbab 2004, Annila 2012, Grahn et al. 2018) and show that, observable cosmic radius is a geometric mean of Schwarzschild radius and Hubble radius (Tatum et al. 2015a, Seshavatharam and Lakshminarayana 2015). It needs further study.

Important demerits of big bang notion can be understood with the following points:

1) Preconditions of big bang are absolutely unclear and unknown.
2) No quantitative description is available for the matter content associated with the big bang event.
3) Physical reasons that led to big bang are unclear and unknown.
4) Quantitative description for big bang bursting force or pressure is unclear and unknown.
5) Whether big bang followed known physical laws are not - is also unclear and unknown.
6) Quantum information associated with big bang is unclear and unknown.
7) Within a fraction of second, how, big bang allowed 'inflation' to happen? - is still a puzzling issue.
8) Applying Planck scale physics to big bang notion is a confusing issue.
9) Whether pre big bang or post big bang constitutes dark matter – is unclear and unknown.
10) Role of dark energy in big bang - is another complicated and questionable issue.

We would like appeal that, proposed decreasing trend of angular velocity, increasing trend of expanding speed (without dark energy), plotted graphs for understanding the smooth decreasing trend of density ratios of dark matter and ordinary matter, estimated non-inflationary cosmic radius of 14.772 Gpc, early

stage fast cooling and later stage slow cooling seem to strengthen our proposed assumptions and semi empirical relations. Gamow's big bang model well established that, early stage nucleosynthesis plays a vital role in understanding the observed proportions of Hydrogen and Helium. Keeping this point in view, we plan to focus our future study on understanding Planck scale and nuclear scale baryonic and dark matter physical phenomena in a unified Gamow–Godel–Planck–Hubble–Birch universe.

Nomenclatures, Assumptions and Basic Relations

Nomenclatures

1) $H_t =$ Hubble parameter.
2) $\left(\rho_c c^2\right)_t \cong \left(3H_t^2 c^2 / 8\pi G\right) =$ Critical energy density.
3) $\left(\Omega_{OM}\right)_t =$ Ratio of ordinary matter density to critical density.
4) $\left(\Omega_{DM}\right)_t =$ Ratio of dark matter density to critical density.
5) $\omega_t =$ Cosmic angular velocity.
6) $\left(V_{\exp}\right)_t =$ Cosmic expansion velocity from and **a**bout the baby universe in all directions.
7) $\left(M_{OM}\right)_t =$ Cosmic ordinary mass content.
8) $\left(M_{DM}\right)_t =$ Cosmic dark matter content.
9) $\left(M_{OM} + M_{DM}\right)_t \cong M_t =$ Total matter content = Total mass of evolving Planck ball.
10) $R_t =$ Cosmic radius associated with M_t = Radius of evolving Planck ball.
11) $T_t =$ Cosmic temperature.
12) $\gamma_t =$ Ratio of Hubble parameter to angular velocity.
13) $\left(d_g\right)_t =$ Galactic distance from and about the baby universe.
14) $\left(v_g\right)_t =$ Galactic receding speed from and about the baby universe.

Note-1: For the above symbols, subscript 0 denotes current value and subscript pl denotes Planck scale value.

Proposed Assumptions

With respect to our earlier and recent publications (Seshavatharam and Lakshminarayana 2015, 2017, 2018a, 2018b), in this paper, we revise the proposed four assumptions for a better understanding and simplification.

1) Ratio of Hubble parameter to angular velocity is, $\gamma_t \cong \left(\frac{H_t}{\omega_t}\right) \cong \left[1 + \ln\left(\frac{H_{pl}}{H_t}\right)\right] \cong \sqrt{\frac{3H_t^2 c^2}{8\pi G\left(aT_t^4\right)}}$.

2) $\left(V_{\exp}\right)_t \cong R_t H_t \cong \gamma_t^{1/4} c$ can be considered as the increasing cosmic expansion velocity.
3) Total matter density ratio can be expressed with $\left(\Omega_{OM} + \Omega_{DM}\right)_t \cong \frac{c}{\left(V_{\exp}\right)_t} \cong \frac{1}{\gamma_t^{1/4}}$
4) Dark matter can be considered as a kind of cosmic foam responsible for formation of galaxies (Verlinde 2017, Levkov et al. 2018, Montes and Trujillo 2019, https://www.forbes.com[1]).

Note points-2:

(1) Assumption 1 indicates the role of Planck scale in entire cosmic evolution. Using the number γ_t, density ratios of dark matter and ordinary matter can be studied.
(2) Assumption 2 can be considered as a simplified form of Hubble's law applied to the expanding universe as whole. $\left(V_{\exp}\right)_t \cong \gamma_t^{1/4} c$ can be understood in terms of cosmic kinetic energy and temperature in the following way. During cosmic evolution,
   a) Kinetic energy of matter is inversely proportional to cosmic temperature.
   b) Based on assumption 1, cosmic temperature can be shown to be inversely proportional to $\sqrt{\gamma_t}$.
   c) Hence, cosmic expansion velocity can be shown to be proportional to $\gamma_t^{1/4}$.
(3) Assumption 3 plays a crucial role in estimating cosmic matter content.
(4) Assumption 4 may help in studying the nature of dark matter.

Role of the Planck Scale in Entire Cosmic Evolution

We make an attempt to implement the 'Planck scale' in the entire cosmic evolution. We define the Planck scale Hubble parameter, $H_{pl} \cong \sqrt{\frac{c^5}{G\hbar}} \cong 1.854921 \times 10^{43}$ sec^{-1}. To proceed further, we assume that,

$$\left(\frac{H_t}{\omega_t}\right) \cong \gamma_t \cong \left[1 + \ln\left(\frac{H_{pl}}{H_t}\right)\right] \cong \sqrt{\left(\frac{3H_t^2 c^2}{8\pi G\left(aT_t^4\right)}\right)} \tag{1}$$

$$\frac{3\omega_t^2 c^2}{8\pi G} \cong aT_t^4 \quad \text{and} \quad \omega_t \cong \sqrt{\frac{8\pi G\left(aT_t^4\right)}{3c^2}} \tag{2}$$

[1]https://www.forbes.com/sites/startswithabang/2019/02/22/the-wimp-miracle-is-dead-as-dark-matter-experiments-come-up-empty-again/#18c618f26dbc.

Based on relation (1), if defined $H_{pl} \cong 1.854921\times10^{43}$ sec^{-1} , one can choose different values of γ in between $\gamma_{pl} \cong 1$ and $\gamma_0 \cong 141.2564$ where $H_0 \cong 70$km/sec/Mpc$\cong 2.26853\times10^{-18}$ sec^{-1} (Planck Collaboration 2015, Riess 2016). For each assumed value of H_t, one can get a corresponding γ_t and all other physical parameters can be estimated.

For the Planck scale, $\gamma_{pl} \cong 1$ and $\omega_{pl} \cong \frac{H_{pl}}{\gamma_{pl}} \cong H_{pl} \cong 1.855\times10^{43}$ rad/sec.

For the current case, $\gamma_0 \cong 141.2564$ and $\omega_0 \cong \frac{H_0}{\gamma_0} \cong 1.606\times10^{-20}\ \frac{\text{rad}}{\text{sec}}$ $\cong 5.068\times10^{-13}\ \frac{\text{rad}}{\text{year}}$

This value can be compared with other estimates (Birch 1982).

In a simplified form, cosmic temperature can be expressed as,

$$T_t \cong \frac{1}{\sqrt{\gamma_t}}\left(\frac{3H_t^2c^2}{8\pi Ga}\right)^{\frac{1}{4}} \cong \left\{\frac{0.652632\hbar\sqrt{\omega_{pl}\omega_t}}{k_B}\right\} \tag{3}$$

Estimating the Trend of Density Ratios of Ordinary Matter, Dark Matter and Total Matter

With the help of defined $\left(\frac{H_t}{\omega_t}\right) \cong \gamma_t \cong \left[1+\ln\left(\frac{H_{pl}}{H_t}\right)\right]$ and with reference to the current observed values of $(\Omega_{OM})_0$ and $(\Omega_{DM})_0$, we are making an attempt to estimate the past values of $(\Omega_{OM})_t$ and $(\Omega_{DM})_t$.

Unless we know the physical nature and properties of dark matter, it may not be possible to thoroughly analyze the density ratios of dark matter and ordinary matter. Keeping the current values of $(\Omega_{OM})_0$ and $(\Omega_{DM})_0$ in view and guessing that, there exists $(\Omega_{OM})_{pl}$ and $(\Omega_{DM})_{pl}$ at Planck scale, we propose the following very simple 'model' relations. We ask readers not to show more focus on relations (4), (5) and (6). With further study, other such kind of relations can be developed in a verifiable approach and percentages of dark matter and ordinary matter can be explored (Verlinde 2017).

$$\frac{(\Omega_{DM})_t}{(\Omega_{OM})_t} \cong \gamma_t^{1/3} \tag{4}$$

$$(\Omega_{OM})_t \cong \left[\left(1+\gamma_t^{1/3}\right)\gamma_t^{1/4}\right]^{-1} \tag{5}$$

$$(\Omega_{DM})_t \cong \left[\left(1+\gamma_t^{-1/3}\right)\gamma_t^{1/4}\right]^{-1} \tag{6}$$

See Figure 1 plotted with relations (4) and (6). Blue curve represents a decreasing trend of ordinary matter density ratio, black curve represents a decreasing trend of dark matter density ratio and green curve represents a decreasing trend of total matter density ratio. Here, it is very important to note that, even though density ratios of ordinary matter and dark matter are assumed to have a decreasing trend, their mass content can be shown to be increasing with increasing cosmic volume. In terms of $(\Omega_{OM})_t$ and $(\Omega_{DM})_t$,

Figure 13. *Decreasing Trend of Density Ratios of Ordinary Matter, Dark Matter and Total Matter*

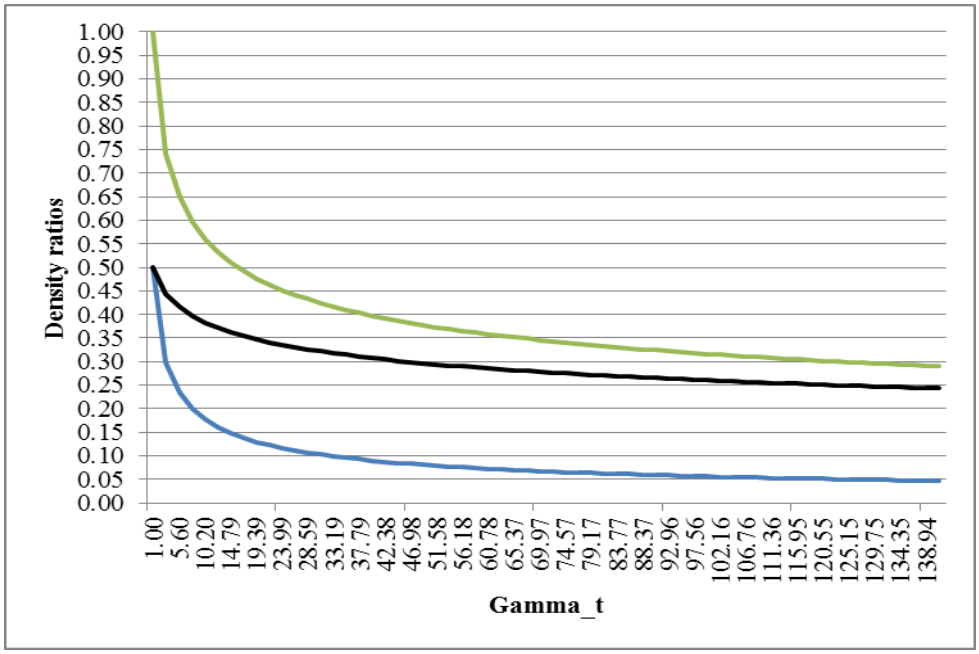

$$M_t \cong \left[(\Omega_{OM})_t + (\Omega_{DM})_t\right]\left(\frac{3H_t^2}{8\pi G}\right)\left(\frac{4\pi}{3}R_t^3\right) \cong \left(\frac{c\left(V_{\exp}\right)_t^2}{2GH_t}\right) \tag{7}$$

$$(M_{OM})_t \cong \left[\frac{(\Omega_{OM})_t}{(\Omega_{OM}+\Omega_{DM})_t}\right]\left(\frac{c\left(V_{\exp}\right)_t^2}{2GH_t}\right) \cong (\Omega_{OM})_t\left(\frac{\left(V_{\exp}\right)_t^3}{2GH_t}\right) \tag{8}$$

$$(M_{DM})_t \cong \left[\frac{(\Omega_{DM})_t}{(\Omega_{OM}+\Omega_{DM})_t}\right]\left(\frac{c\left(V_{\exp}\right)_t^2}{2GH_t}\right) \cong (\Omega_{DM})_t\left(\frac{\left(V_{\exp}\right)_t^3}{2GH_t}\right) \tag{9}$$

$$\left.\begin{aligned} \left(V_{\exp}\right)_t &\cong \sqrt{\frac{2GM_tH_t}{c}} \quad \text{and} \\ R_t &\cong \gamma_t^{1/4}\left(\frac{c}{H_t}\right) \cong \sqrt{\left(\frac{2GM_t}{c^2}\right)\left(\frac{c}{H_t}\right)} \end{aligned}\right\} \tag{10}$$

To Estimate the Current Cosmic Age

From the beginning of cosmic evolution, based on the proposed cosmic expansion velocities, cosmic age can be approximated with the following relation.

$$t \cong \frac{\left(R_t - R_{pl}\right)}{\left[\left(\left(V_{\exp}\right)_t + \left(V_{\exp}\right)_{pl}\right)\Big/ 2\right]} \tag{11}$$

where $\left[\left(\left(V_{\exp}\right)_t + \left(V_{\exp}\right)_{pl}\right)\Big/ 2\right]$ can be considered as average expansion velocity.

For the current case, $t_0 \cong 21.656$ BillionYears.

For a temperature of 3000 K, it is possible to show that,

$$\left.\begin{aligned} H_{3000K} &\cong 2.49\times10^{-12}\ \text{sec}^{-1} \\ \gamma_{3000K} &\cong 1+\ln\left(\frac{H_{pl}}{H_{3000K}}\right) \cong 127.34774 \\ Z_{3000K} &\cong \sqrt{\gamma_{3000K}} - 1 \cong 10.285 \\ z_{3000K} &\cong \sqrt{\frac{\gamma_0}{\gamma_{3000K}}\exp\left(\gamma_0 - \gamma_{3000K}\right)} - 1 \cong 1102.407 \end{aligned}\right\} \tag{12}$$

Cosmic age corresponding to a temperature of T=3000K can be estimated to be,

$$t_{3000K} \cong \frac{\left(R_{3000K} - R_{pl}\right)}{\left[\left(\left(V_{\exp}\right)_{3000K} + \left(V_{\exp}\right)_{pl}\right)\Big/ 2\right]} \cong 19613.65 \text{ Years} \tag{13}$$

where, $R_{3000K} \cong 4.0445\times10^{20}$ m and $\left(V_{\exp}\right)_{3000K} \cong 3.36c$. This estimation is 19.37 times less than the current estimations and needs further study with respect to early stage formation of galaxies.

Cosmic Scale Factor and Red Shift

With reference to the proposed relations (1) and (3) and with reference to the current definitions of cosmic redshift and scale factor, it is possible to show that,

$$\left.\begin{aligned}\left(\frac{1}{a}\cong(z+1)\cong\frac{T_t}{T_0}\right)&\cong\sqrt{\frac{\gamma_0 H_t}{\gamma_t H_0}}\cong\sqrt{\frac{\gamma_0}{\gamma_t}}\sqrt{\frac{H_t}{H_0}}\\ \cong\sqrt{\frac{\gamma_0}{\gamma_t}}\left\{\exp\left(\frac{\gamma_0-\gamma_t}{2}\right)\right\}&\cong\sqrt{\left(\frac{\gamma_0}{\gamma_t}\right)\exp(\gamma_0-\gamma_t)}\end{aligned}\right\} \quad (14)$$

$$z\cong\sqrt{\left(\frac{\gamma_0}{\gamma_t}\right)\exp(\gamma_0-\gamma_t)}-1 \quad (15)$$

See Table 1 for various cosmic physical parameters associated with current and Planck scales.

Table 1. *Current and Planck Scale Cosmic Physical Parameters*

Current scale	Planck scale
$H_0\cong 70$km/sec/Mpc $\cong 2.26853\times10^{-18}sec^{-1}$	$H_{pl}\cong\sqrt{\frac{c^5}{G\hbar}}\cong 1.855\times10^{43}$ sec^{-1}
$\gamma_0\cong\left[1+\ln\left(\frac{H_{pl}}{H_0}\right)\right]\cong 141.2564$	$\gamma_{pl}\cong\left[1+\ln\left(\frac{H_{pl}}{H_{pl}}\right)\right]\cong 1$
$(\Omega_{OM})_0\cong 0.04673$	$(\Omega_{OM})_{pl}\cong 0.5$
$(\Omega_{DM})_0\cong 0.2433$	$(\Omega_{DM})_{pl}\cong 0.5$
$(\Omega_{OM})_0+(\Omega_{DM})_0\cong 0.290$	$(\Omega_{OM})_{pl}+(\Omega_{DM})_{pl}\cong 1.0$
$T_0\cong\left(\frac{1}{\sqrt{\gamma_0}}\right)\left(\frac{3H_0^2c^2}{8\pi Ga}\right)^{\frac{1}{4}}\cong 2.721$ K	$T_{pl}\cong\left(\frac{1}{\sqrt{\gamma_{pl}}}\right)\left(\frac{3H_{pl}^2c^2}{8\pi Ga}\right)^{\frac{1}{4}}$ $\cong 9.247\times10^{31}$ K
$R_0\cong\gamma_0^{1/4}\frac{c}{H_0}\cong 4.556\times10^{26}$ m $\cong 14.772$ Gpc	$R_{pl}\cong\gamma_{pl}^{1/4}\left(\frac{c}{H_{pl}}\right)\cong 1.616\times10^{-35}$m
$(V_{\exp})_0\cong R_0H_0\cong 3.4475c$	$(V_{\exp})_{pl}\cong R_{pl}H_{pl}\cong c$
$(M_{OM})_0\cong 1.7035\times10^{53}$ kg	$(M_{OM})_{pl}\cong 5.441\times10^{-9}$ kg
$(M_{DM})_0\cong 8.87195\times10^{53}$ kg	$(M_{DM})_{pl}\cong 5.441\times10^{-9}$ kg
$\left[(M_{OM})_0+(M_{DM})_0\right]$ $\cong M_0\cong 1.0575\times10^{54}$ kg	$\left[(M_{OM})_{pl}+(M_{DM})_{pl}\right]$ $\cong M_{pl}\cong 1.0882\times10^{-8}$ kg
$t_0\cong\frac{R_0}{\left[\left((V_{\exp})_0+(V_{\exp})_{pl}\right)/2\right]}$ $\cong 21.656$ BillionYears	$t_{pl}\cong 0$

Velocity and Distance Relation

In all directions, from and about the hypothetical baby universe, current galactic receding speeds can be approximated with,

$$\left(v_g\right)_0 \cong \left(\frac{\left(d_g\right)_0}{R_0}\right)\left(V_{\exp}\right)_0 \cong \left(\frac{\left(V_{\exp}\right)_0}{R_0}\right)\left(d_g\right)_0 \cong H_0\left(d_g\right)_0 \tag{16}$$

a) Relation (16) can be compared with currently believed Hubble's law for any receding galaxy in the current expanding universe.

b) For a distance of $\frac{c}{H_0}$, receding speed is c.

c) When, $\left(d_g\right)_0 \to R_0$, $\left(v_g\right)_0 \cong H_0 R_0$

Results and Discussion

Cosmological Constant Problem

With reference to proposed concepts, ratio of the Planck scale critical density to the current critical density is,

$$\left(\frac{3H_{pl}^2c^2}{8\pi G}\right) \div \left(\frac{3H_0^2c^2}{8\pi G}\right) \cong \left(\frac{H_{pl}}{H_0}\right)^2 \cong 6.685\times10^{121} \tag{17}$$

This idea can be considered as a characteristic tool for constructing a model of 'quantum gravity' with cosmic evolution.

Horizon Problem

If one is willing to consider the concept of 'matter causes the space-time to curve', 'horizon problem' can be understood. According to big bang model, during its evolution, as the universe is expanding, thermal radiation temperature decreases and matter content increases. As matter content increases, at any stage of evolution, it is possible to have an increasing radius of curvature. For the current case, $R_0 \cong \gamma_0^{1/4}\left(\frac{c}{H_0}\right) \cong \sqrt{\left(\frac{2GM_0}{c^2}\right)\left(\frac{c}{H_0}\right)} \cong 14.772$ Gpc and there is no scope for 'causal disconnection' of distant visible matter (Vardanyan 2011).

Cosmic Inflation

In our model, without considering 'inflation' concepts (Guth 1981, Linde 1982, Steinhardt 2011, Ijjas et al. 2014), starting from the Planck scale, it is possible to have a current cosmic radius of 14.772 Gpc and it is consistent with

current observations of 14.25 Gpc. Our estimated cosmic age corresponding to 2.7 K is around 21.66 billion years whereas big bang model estimation is 13.8 billion years. At lower time scales, our estimated cosmic age corresponding to 3000 K is around 19,614 years whereas big bang model estimation is 3,80,000 years.

Point to be discussed in depth is, with big bang and inflation, after 3,80,000 years of evolution, cosmic temperature is 3000 K where as in our model, without big bang and inflation, after 19,614 years of cosmic evolution, temperature is 3000K. From this, it is very clear to say that, compared to big bang and inflation, in our model, temperature drop is faster in the beginning and slower in the later stages. This can be considered as a hint for the observed large scale 'Isotropic' nature of Cosmic microwave back ground radiation (CMBR).

Cosmic Acceleration and Expansion Velocity

By considering a decreasing trend of ordinary matter and dark matter density, starting from the Planck scale, it is possible to get an expression for cosmic expansion velocity. It can be expressed as follows.

$$\frac{\left(V_{\exp}\right)_t}{c} \cong \gamma_t^{1/4} \cong \left[1+\ln\left(\frac{H_{pl}}{H_t}\right)\right]^{1/4} \cong \left(\frac{3H_t^2c^2}{8\pi G\left(aT_t^4\right)}\right)^{1/8} \cong \frac{1}{(\Omega_{OM})_t+(\Omega_{DM})_t} \tag{18}$$

Based on this expression, for the Planck scale, $\left(V_{\exp}\right)_{pl} \cong c$ and for the current scale, $\left(V_{\exp}\right)_0 \cong 3.4475c$. After 21.66 billion years of cosmic expansion, increment in expansion velocity seems to be $\left[\left(V_{\exp}\right)_0 - \left(V_{\exp}\right)_{pl}\right] \cong 2.45c$. (See Figure 2).

Figure 2. *Increasing Trend of Cosmic Expansion Velocity*

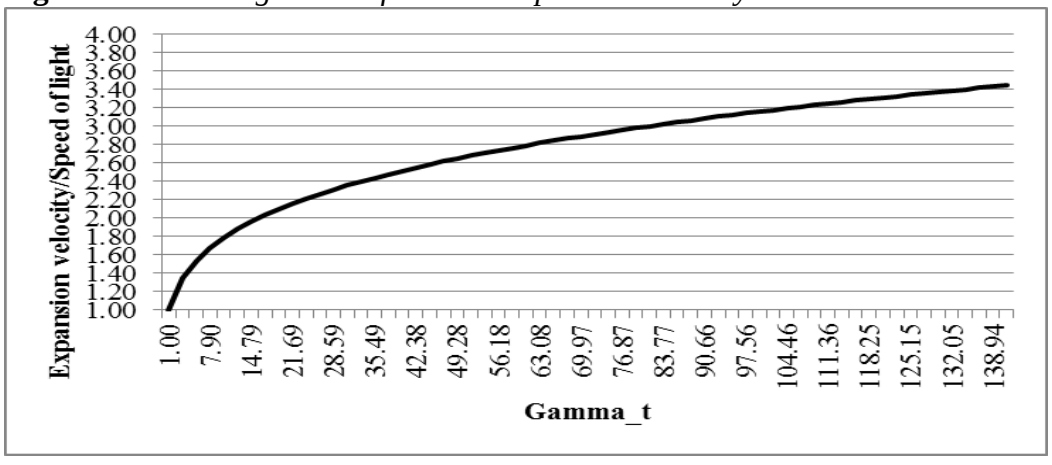

From Figure 2, it is very clear that, right from the beginning of cosmic evolution, cosmic expansion velocity seems to have an increasing trend.

Interesting point to be noted is that, expansion velocity seems to depend on $\frac{1}{(\Omega_{OM})_t + (\Omega_{DM})_t}$. In near future, if decrease in $(\Omega_{OM})_t + (\Omega_{DM})_t$ is found to be insignificant, one can expect cosmic 'constant rate of expansion' (Nielsen et al. 2016, Colin et al. 2018, Dam et al. 2017) and if decrease in $(\Omega_{OM})_t + (\Omega_{DM})_t$ is found to be significant, one can expect 'acceleration' (Haridasu et al. 2017). It is for further study.

Cosmic Angular Velocity

With reference to our assumptions and relations, defined Planck scale angular velocity is 1.855×10^{43} rad/sec and current angular velocity seems to be $\omega_0 \cong 1.606\times10^{-20}$ rad/sec $\cong 5.068\times10^{-13}$ rad/year. Here, interesting point to be noted is that, cosmic angular velocity decreases with decreasing cosmic temperature and decreasing Hubble parameter. The first experimental evidence of the Universe rotation was done by Birch in 1982 evidently. According to Birch, there appears to be strong evidence that the Universe is anisotropic on a large scale, producing position angle offsets in the polarization and brightness distributions of radio sources. These can probably be explained on the basis of a rotation of the Universe with an angular velocity of approximately 10^{-13} rad/year. Observational effects of current cosmic rotation can be understood with the works of Obukhov (2000), Godlowski (2011) and Longo (2011). Nowadays Chechin (2016, 2017) is seriously working on cosmic rotation.

About Dark Matter

Considering the very nature of Dark matter, new studies suggest that, a) Dark matter can be eliminated with emerging gravity concept (Verlinde 2017). b) Dark matter can be considered as a Bose-Einstein condensate (Levkov et al. 2018). c) Dark matter distribution can be understood through the distribution of intracluster light (Montes and Trujillo 2019). d) Evidence for considering dark matter as a characteristic weakly interacting massive particle (WIMP) is getting ruled out (https://www.forbes).[1] In this critical situation, our proposal of considering dark matter as a kind of 'galactic foam' can be given some consideration. With further study, mystery of 'dark matter density ratio' can be explored with respect to different theoretically extended ideas of general theory of relativity or quantum cosmology.

[1]https://www.forbes.com/sites/startswithabang/2019/02/22/the-wimp-miracle-is-dead-as-dark-matter-experiments-come-up-empty-again/#18c618f26dbc.

General Discussion

Schwarzschild radius (Seshavatharam 2010, Tatum et al. 2015b) is one of the iconic relation underlying general theory of relativity and can be given a priority in developing a workable or unified model of cosmology. We would like to suggest that, by considering a relation of the, $R_t \cong \gamma_t^{1/4}\left(\frac{c}{H_t}\right) \cong \sqrt{\left(\frac{2GM_t}{c^2}\right)\left(\frac{c}{H_t}\right)}$ currently believed 'horizon' problem can be reviewed and resolved.

Cosmic expansion, Lambda term, dark matter, cosmic temperature, inflation, cosmic acceleration and dark energy and vacuum energy are different concepts, by using which alternative models of GTR are emerging and are being extended in many ways. In this sequence, quantum cosmology can also be given some consideration.

Quantum cosmology is a wide range physical model intended for understanding the in-built cosmological quantum phenomena on small scale as well as large scale distances. So far, progress in this direction is very nominal and 'GTR' needs a serious review with reference to 'quantum cosmology'.

When universe is able to give birth to atoms, elementary parrticles and photons that show quantrum behaviour, universe can certainly be considered as a quantum gravitational object for ever.

What to quantize? How to quantize? When to quantize? and What to measure? are some interesting questions in current quantum cosmology and need a special focus. In this context, cosmic temperature can be considered as a characteristic feature of quantum cosmology.

With reference to particle physics, current technological limits on particle colliding energy, unidentified/unseen particles, unknown particle interactions and incomplete final unification scheme - to some extent, one can hopefully believe in the existence of dark matter (Barkana 2018).

Basically, 'dark energy' was proposed for understanding cosmic acceleration. Careful analysis of improved supernovae data suggets that universe is coasting at constant veleocity and evidence for acceleration is only marginal. In this context, now a days, a great debate has been initiated among mainstream cosmologists on the existence of dark energy (Haridasu et al. 2017, Racz et al. 2017, Berezhiani et al. 2017, Smoller 2017). According to a recent study (Zhao et al. 2017), the nature of dark energy is 'dynamic' and conceptually seems to deviate from the famous cosmological constant or vaccum energy. According to another new study (Wang and Meng 2017), evidence for dynamical dark energy is very poor.

Density perturbations and interaction between dark mtter and baryons seem to play a crucial role in understanding observed cosmic acceleration and need of introducing dark energy seems to be ad-hoc.

Even though redshift is an index of cosmic expansion, without knowing the actual galactic distances and actual galactic receding speeds, with 100% confidence level, it may not be possible to decide the absolute nature of cosmic expansion rate.

If the universe is the same in all directions, as the big bang models require,

the hot spots and cold spots of CMBR in the afterglow of the big bang should be randomly splattered about the sky - the big temperature splotches and the small temperature goose pimples should have no preferred direction. The fact that they are aligned along the axis of evil leads Land and Magueijo (2005) to suggest that, may be the assumptions behind the big bang models are wrong. In other words, the Universe is not the same in all places or directions, but has a special direction.

Considering a sample of 355 optically polarized quasars with accurate linear polarization measurements, (Jain et al. 2004, Hutsemekers et al. 2005), demonstrated that quasar polarization angles are definitely not randomly oriented over the sky. Polarization vectors appear coherently oriented over very large spatial scales, in regions located at both low and high redshifts and characterized by different preferred directions. These characteristics make the alignment effect difficult to explain in terms of local mechanisms, namely a contamination by interstellar polarization in our Galaxy.

According to Ghosh et al. (2016) - The tantalizing possibility that the cosmological principle may be violated is indicated by many observations. The most prominent of these effects is the so-called Virgo alignment, which refers to a wide range of phenomena indicating a preferred direction pointing towards Virgo. The Square Kilometer Array has the capability to convincingly test several of these effects. These include the dipole anisotropy in radio polarization angles (Jain and Ralston 1999), the dipole in the number counts and sky brightness (Blake and Wall 2002, Singal 2011, Gibelyou and Huterer 2012, Tiwari and Jain 2015a, Rubart and Schwarz 2013) and in the polarized number counts and polarized flux (Tiwari and Jain 2015b). These observations may indicate that we need to go beyond the standard Big Bang cosmology. Alternatively they may be explained by pre-inflationary anisotropic and/or inhomogeneous modes (Aluri and Jain 2015, Rath et al. 2013). In either case, confirmation of this alignment effect is likely to revolutionize cosmology.

According to Zhao and Santos (2015) - The foundation of modern cosmology relies on the so-called cosmological principle which states a homogeneous and isotropic distribution of matter in the universe on large scales. However, recent observations, such as the temperature anisotropy of the cosmic microwave background (CMB) radiation, the motion of galaxies in the universe, the polarization of quasars and the acceleration of the cosmic expansion, indicate preferred directions in the sky. If these directions have a cosmological origin, the cosmological principle would be violated, and modern cosmology should be reconsidered.

Nature loves symmetry. Subject of cosmic ‘rotation’ is not new and not against to General theory of relativity. Quantum mechanics point of view, ‘spin’ is a basic and characteristic property. Quantum gravity point of view, it is reasonable to review the currently believed ‘standard cosmology’ with reference to cosmic rotation.

Proposed coefficient γ_t seems to have an attractive feature of connecting the density ratios of ordinary matter and dark matter throught the cosmic evolution. With further study, such kind of other coefficients can also be developed with

possible physics.

Without considering the currently belived dark energy, cosmic expnasion velocity can be shown to be increasing with a drcreasing trend of total matter density ratio. To some extent, this can be compared with currently believed cosmic acceleration concept (Riess et al. 1998, Perlmutter et al. 1999, Weinberg et al. 2013).

Considering the updated supernovae redshift data, in 2016, cosmologists noticed that, universe is coasting at constant speed rather than acceleration. In this way, nowadays, a great debate is going on among various groups of cosmologists on 'cosmic acceleration' (Li et al. 2011, Rubin and Hayden 2016). Another group of cosmologists are developing models with speed of light (Tsagas 2011, Wei et al. 2015, Melia and Fatuzzo 2016, John 2016, Tutusaus et al. 2018). In this context, we would like suggest that, observationally, by finding the trend of total matter density ratio, actual expansion speed can be figured out.

Dark matter may exist or may not exsit, gravity may be emerging or may not be emerging, based on assumption 3 and Figure 1, observationally believed current total matter density ratio can be fitted and can be extrapolated to past and future in a verifiable approach. With further study, mystery of 'total matter density ratio' can be explored with respect to different theoretically extended ideas of general theory of relativity or quantum cosmology.

The discovery of the accelerating universe in the late 1990s was a radical idea in modern cosmology. To account for the observed cosmic acceleration, cosmologists hypothesized the presence of a hidden and dominating energy reservoir of the universe and called it as 'Dark energy'. Evidence for dark energy, the new component that causes the acceleration, has since become extremely strong, owing to an impressive variety of increasingly precise measurements of the expansion history and the growth of structure in the universe. Very unfortunate thing is that, till today, no one could understand the mechanism for the observed cosmic acceleration. It is one of the central challenges of modern observational cosmology (Huterer and Shafer 2018). Another puzzling issue is that, even though the standard Friedmann-Lemaitre-Robertson-Walker cosmological model (FLRW) is gaining a great success in explaining most of the modern observations, till today, observationally no one could identify a probable means or carrying agent for the well believed dark energy. It casts a serious doubt on the actual physical existence of dark energy and raises a general doubt on the scope of FLRW model to cosmic acceleration. In this context, our proposed method of 'increasing cosmic expansion velocity connected with decreasing total matter density ratio', i.e. relation (18) can be given some consideration in reviewing and relinquishing (Buchert et al. 2018) the currently believed dark energy concept.

In a cosmological approach, so far no physical model is successful in understanding the mass generation and proliferation mechanism for the observed photons, leptons, neutrinos, baryons, mesons and Higgs bosons from the cosmic energy reservoir. In this context, one can see a great initiative taken by Schwinger (1998), Bulnes (2018) and Robson (2017).

Conclusions

By considering the proposed concepts, asumptions, relations, result oriented discussion and general discussion, an outline picture of a workable model of quantum cosmology can be developed. With further study, nucleosynthesis and dark matter synthesis along with mass generation mechanism can be reviewed in a quantum cosmological approach. We are working in this direction and it will be published elsewhere.

Acknowledgements

Author Seshavatharam is indebted to Dr. E. Terry Tatum for his kind technical and helpful discussions, to Profs Brahmashri M. Nagaphani Sarma, Chairman, Shri K.V. Krishna Murthy, to Founder Chairman, Institute of Scientific Research in Vedas (I-SERVE), Hyderabad, India and to Shri K.V.R.S. Murthy, Former Scientist IICT (CSIR), Govt. of India, Director, Research and Development, I-SERVE, for their valuable guidance and great support in developing this subject. Both authors are very much thankful to the anonymous reviewers for their helpful suggestions in improving the quality and presentation of this subject.

References

Aluri PK, Jain P (2012) Large Scale Anisotropy due to Pre-Inflationary Phase of Cosmic Evolution. *Modern. Physical Letters A* 27(4).

Annila A (2012) Probing Mach's Principle. *Monthly Notices of Royal Astronomical Society* 423(2).

Arbab AI (2004) Quantization of Gravitational System and its Cosmological Consequences. *Gen. Rel. Grav. Grav* 36(Jan): 2465-2479.

Barkana R (2018) Possible Interaction between Baryons and Dark-matter Particles Revealed by the First Stars. *Nature* 555(Feb): 71-74.

Barrow JD, Tsagas CG (2004) Dynamics and Stability of the Godel Universe. *Classical and Quantum Gravity* 21(7): 1773-1790.

Berezhiani L, Khoury J, Wang J (2017) Universe without Dark Energy: Cosmic Acceleration from Dark Matter-baryon Interactions *Physical Review* 95(12-15): 123530.

Birch P (1982) Is the Universe rotating? *Nature* 298(Jul): 451-454.

Blake C, Wall J (2002) A Velocity Dipole in the Distribution of Radio Galaxies. *Nature* 416(6877): 150-152.

Bojowald M (2015) Quantum Cosmology: A Review. *Reports on Progress in Physics* 78(2): 023901

Buchert T, Coley AA, Kleinert H, Roukema BF, Wiltshire DL (2016) Observational Challenges for the Standard FLRW Model. *International Journal of Modern Physics* 25(3): 1630007.

Bulnes F (2018) Gravity, Curvature and Energy: Gravitational Field Intentionality to the Cohesion and Union of the Universe. In T Zouaghi (ed), *Gravity - Geoscience*

Applications, Industrial Technology and Quantum Aspect. http://dx.doi.org/10.5772/intechopen.71037.

Cai RG, Ma YZ, Tang B, Tuo ZL (2012) Constraining the Anisotropic Expansion of the Universe. *Physical Review D* 87(12).

Carneiro S (2002) Open Cosmologies with Rotation. *General Relativity and Gravitation* 34(6): 793-805.

Chechin LM (2016) Rotation of the Universe at Different Cosmological Epochs. *Astronomy Reports* 60(6): 535-541.

Chechin LM (2017) Does the Cosmological Principle Exist in the Rotating Universe? *Gravitation and Cosmology* 23(4): 305-310.

Colin J, Mohayaee R, Rameez M, Sarkar S (2018) Apparent Cosmic Acceleration due to Local Bulk Flow. arXiv:1808.04597v1.

Dam LH, Heinesen A, Wiltshire DL (2017) Apparent Cosmic Acceleration from Type Ia Supernovae. *Monhtly Notices of the Royal Astronomical Society* 472(1): 835-851.

Gamow G (1946) Rotating Universe? *Nature* 158(4016): 549.

Gamow G (1948a) The Evolution of the Universe. *Nature* 162(4122): 680=682.

Gamow G (1948b) The Origin of Elements and the Separation of Galaxies. *Physical Review* 74(4): 505.

Ghosh S, Jain P, Kashyap G, Kothari R, Nadkarni-Ghosh S, Tiwari P (2016) Probing Statistical Isotropy of Cosmological Radio Sources using Square Kilometre Array *Journal of Astrophysics and Astronomy* 37(4): 25.

Gibelyou C, Huterer D (2012) Dipoles in the Sky. *Monthly Notices of the Royal Astronomical Society* 427(3): 1994-2021.

Godel K (2000) An Example of a New Type of Cosmological Solutions of Einstein's Field Equations of Gravitation. *General Relativity and Gravitation* 32(7): 1409-1417.

Godlowski W (2011) Global and Local Effects of Rotation: Observational Aspects. *International Journal of Modern Physics* 20(9): 1643-1673.

Grahn P, Annila A, Kolehmainen, E *(*2018) On the Carrier of Inertia. *AIP Advances* 8(3): 035028.

Guth AH (1981) Inflationary Universe: A Possible Solution to the Horizon and Flatness Problems. *Physical Review D* 23(2): 347-356.

Haridasu BS, Lukovic VV, D'Agostino R, Vittorio N (2017) Strong Evidence for an Accelerating Universe. *Astronomy & Astrophysics* 600. Doi: 10.1051/0004-6361/201730469.

Hawking SW (1969) On the Rotation of the Universe *Monthly Notices of the Royal Astronomical Society* 142(2): 129-141.

Huterer D, Shafer DL (2018) Dark Energy Two Decades After: Observables, Probes, Consistency Tests. *Reports on Progress in Physics* 81(1): 016901.

Hutsemekers D, Cabanac R, Lamy H, Sluse *D* (2005) Mapping Extreme-Scale Alignments of Quasar Polarization Vectors. *Astronomy & Astrophysics* 441(3): 915-930.

Ijjas A, Steinhardt PJ, Loeb A (2014) Inflationary Schism. *Physics Letters B* 736(Sep): 142-146.

Jain P, Ralston JP (1999) Anisotropy in the Propagation of Radio Polarizations from Cosmologically Distant Galaxies. *Modern Physics Letters A* 14(6): 417-432.

Jain P, Panda S, Sarala S (2004) Pseudoscalar-Photon Mixing and the Large Scale Alignment of QSO Optical Polarizations. *PRAMANA Journal of Physics* 62(3): 679-682.

John MV (2016) Realistic Coasting Cosmology from the Milne Model. arXiv:1610.09885.

Korotky VA, Obukhov YN (1995) Polarization of Radiation in a Rotating Universe. JETP

108: 1889-1898.
Kuhne RW (1997) On the Cosmic Rotation Axis. *Modern Physics Letters A* 12(32): 2473-2474.
Land K, Magueijo J (2005) Examination of Evidence for a Preferred Axis in the Cosmic Radiation Anisotropy. *Physical Review Letters* 95(7): 071301.
Levkov DG, Panin AG, Tkachev II (2018) Gravitational Bose-Einstein Condensation in the Kinetic Regime. *Physical Review Letters* 121(15): 151301.
Li LX (1998) Effect of the Global Rotation of the Universe on the Formation of Galaxies. General Relativity and Gravitation 30(3): 497-507.
Li Z, Wu P, Yu H (2011) Examining the Cosmic Acceleration with the Latest Union2 Supernova Data. *Physics Letters B* 695(1-4): 1-8.
Linde AD (1982) A New Inflationary Universe Scenario: A Possible Solution of the Horizon, Flatness, Homogeneity, Isotropy and Primordial Monopole Problems. *Physics Letters B* 108(6): 389-393.
Longo MJ (2011) Detection of a Dipole in the Handedness of Spiral Galaxies with Redshifts z ~ 0.04. *Physics Letters B* 699(4): 224-229.
Melia F, Fatuzzo M (2016) The Epoch of Reionization in the R_h=ct Universe. *Monthly Notices of Royal Astronomical Society* 456(4): 3422-3431.
Mitra A (2011) Why the Big Bang Model Cannot Describe the Observed Universe Having Pressure and Radiation. *Journal of Modern Physics* 2(12): 1436-1442.
Mitra A (2014) Why the Rh = ct Cosmology is Unphysical and in fact a Vacuum in Disguise Like the Milne Cosmology. *Monthly Notices of Royal Astronomical Society* 442(1): 382-387.
Montes M and Trujillo I (2019) Intracluster Light: A Luminous Tracer for Dark Matter in Clusters of Galaxies. *Monthly Notices of Royal Astronomical Society* 482(Oct): 2838-2851.
Narlikar J V, Hoyle F (1963) Newtonian Universes with Shear and Rotation. *Monthly Notices of Royal Astronomical Society* 126(2): 203-208.
Nielsen JT, Guffanti A, Sarkar S (2016) Marginal Evidence for Cosmic Acceleration from Type Ia Supernovae. *Scientific Reports* 6(Oct): 35596.
Nodland B, Ralston JP (1997) Indication of Anisotropy in Electromagnetic Propagation over Cosmological Distances. *Physical Review Letters* 78(16): 3043-3046.
Obukhov YN (2000) On Physical Foundations and Observational Effects of Cosmic Rotation Colloquium on Cosmic Rotation. In M Scherfner, T Chrobok, M. Shefaat (eds). Colloquium on Cosmic Rotation, 23. Berlin: Wissenschaft und Technik Verlag.
Padmanabhan T (2005) Dark Energy: the Cosmological Challenge of the Millennium. *Current Science* 88: 1057.
Panov VF, Kuvshinova EV (2004) Quantum Birth of the Universe with Rotation. *Gravitation & Cosmology* 10: 37-38.
Perlmutter S, Aldering G, Goldhaber G, Knop RA, Nugent P, Castro PG, Deustua S, Fabbro S, Goobar A, Groom DE, Hook IM, Kim AG, Kim MY, Lee JC, Nunes NJ, Pain R, Pennypacker CR, Quimby R, Lidman C, Ellis RS, Irwin M, McMahon RG, Ruiz-Lapuente P, Walton N, Schaefer B, Boyle BJ, Filippenko AV, Matheson T, Fruchter AS, Panagia N, Newberg HJM, Couch WJ (1999) Measurements of Ω and Λ from 42 High-Redshift Supernovae. *The Astrophysical Journal* 517(2): 565.
Planck Collaboration (2015) Planck 2015 Results XIII Cosmological Parameters.
Racz G, Dobos L, Beck R, Szapudi I, Csabai I (2017) Concordance Cosmology without Dark Energy. *Monthly Notices of Royal Astronomical Society Letters* 469(1): L1-L5.
Rath PK, Mudholkar T, Jain P, Aluri PK (2013) Direction Dependence of the Power Spectrum and its Effect on the Cosmic Microwave Background Radiation. *Journal of*

Cosmology and Astroparticle Physics 2013(Apr).

Raychaudhuri AK (1955) Relativistic Cosmology I. *Physical Review* 98(4): 1123-1126.

Riess AG, Filippenko AV, Challis P, Clocchiatti A, Diercks A, Garnavich PM, Gilliland RL, Hogan CJ, Jha S, Kirshner RP (1998) Observational Evidence from Supernovae for an Accelerating Universe and a Cosmological Constant *The Astronomical Journal* 116(3): 1009-1038.

Riess AG, Macri LM, Hoffmann SL, Scolnic D, Casertano S, Filippenko AV, Tucker BE, Reid MJ, Jones DO, Silverman JM, Chornock R, Challis P, Yuan W, Brown PJ, Foley RJ (2016) A 2.4% Determination of the Local Value of the Hubble Constant. *The Astrophysical Journal* 826(1): 56.

Robson BA (2017) Cosmological Consequences of a Quantum Theory of Mass and Gravity. In AJ Capistrano de Souza (ed), *Trends in Modern Cosmology*. http://dx.doi.org/10.5772/intechopen.68410.

Rubart M, Schwarz DJ (2013) Cosmic Radio Dipole from NVSS and WENSS. *Astronomy & Astrophysics* 555(Jul): 117.

Rubin D, Hayden B (2016) Is the Expansion of the Universe Accelerating? All Signs Point to Yes. *The Astrophysical Journal Letters* 833(2): L30.

Schwinger J (1998) Particles, Sources, and Fields. In *Advanced Book Program* 1. USA: Perseus Books.

Seshavatharam UVS (2010) Physics of Rotating and Expanding Black Hole Universe. *Progress in Physics* 2(Apr): 7-14.

Seshavatharam UVS, Lakshminarayana S (2015) Primordial Hot Evolving Black Holes and the Evolved Primordial Cold Black Hole Universe. *Frontiers of Astronomy, Astrophysics and Cosmology* 1(1): 16-23.

Seshavatharam UVS, Lakshminarayana S (2017) Toy Model of Spinning Quantum Cosmology. *Physical Science International Journal* 15(4): 1-13.

Seshavatharam UVS, Lakshminarayana S (2018a) On the Eternal Role of Planck Scale in Machian Cosmology. *SF J Astrophysics* 1:5.

Seshavatharam UVS, Lakshminarayana S (2018b) Toy Model of Evolving and Spinning Quantum Cosmology – A Review. *International Journal of Astronomy Astrophysics and Space Science* 5(1): 1-13.

Seshavatharam UVS, Lakshminarayana S (2019) An Outline Picture of a Growing and Rotating Planck Universe with Emerging Dark Foam. *Asian Journal of Research and Review in Physics* 2(2): 1-13.

Singal AK (2011) Large Peculiar Motion of the Solar System from the Dipole Anisotropy in Sky Brightness due to Distant Radio Sources. *The Astrophysical Journal* 742(2): L23-L27.

Singh S (1999) Cosmological Models with Shear and Rotation. *Journal of Astrophysics and Astronomy* 20(1-2): 67-77.

Sivaram C (2000) Some Implications of Quantum Gravity and String Theory for Everyday Physics. *Current Science* 79(4): 413-420.

Smoller J, Temple B, Vogler Z (2017) An Instability of the Standard Model of Cosmology Creates the Anomalous Acceleration without Dark Energy. *Proceeding of the Royal Society A* 473(2207): 20160887. Doi: 10.1098/rspa.2016.0887.

Steinhardt PJ (2011) The Inflation Debate: Is the Theory at Heart of Modern Cosmology Deeply Flawed? *Scientific American* 304(4): 1-25.

Su SC, Chu MC (2009) Is the Universe Rotating? *The Astrophysical Journal* 703(1): 354.

Szydlowski M, Godlowski W (2005) Dynamics of the Universe with Global Rotation. *General Relativity and Gravitation* 37(5): 907-936.

Tatum ET, Seshavatharam UVS, Lakshminarayana S (2015a) Thermal Radiation Redshift in Flat Space Cosmology. *Journal of Applied Physical Science International* 4(1): 18-26.

Tatum ET, Seshavatharam UVS, Lakshminarayana S (2015b) The Basics of Flat Space Cosmology. *International Journal of Astronomy and Astrophysics* 5(2): 116-124.

Tiwari P, Jain P (2015a) Dipole Anisotropy in Integrated Linearly Polarized Flux Density in NVSS Data. *Monthly Notices of Royal Astronomical Society* 447(3): 2658-2670.

Tiwari P, Jain P (2015b) Extracting Spectral Index of Intergalactic Magnetic Field from Radio Polarizations. *Monthly Notices of Royal Astronomical Society* 460(3): 2698-2705.

Tsagas C (2011) Apparent Cosmic Acceleration due to Large-scale Peculiar Motions. *J. Phys: Conf. Ser.* 283(1): 012040.

Tutusaus I, Lamine B, Blanchard A (2018) Model-Independent Cosmic Acceleration and Type Ia Supernovae Intrinsic Luminosity Redshift Dependence. *Astronomy & Astrophysics* 625(A15): arXiv:1803.06197.

Vardanyan M (2011) Applications of Bayesian model Averaging to the Curvature and Size of the Universe. *Monthly Notices of Royal Astronomical Society Letters* 413(1): L91-L95.

Verlinde E (2017) Emergent Gravity and the Dark Universe. *SciPost Phys.* 2, 016.

Wang D, Meng XH (2017) No Evidence for Dynamical Dark Energy in Two Models. *Physical Review D* 96(10): 103516.

Wei JJ, Wu XF, Melia F, Maier RS (2015) Comparative Analysis of the Supernova Legacy Survey Sample with ΛCDM and the Rh=ct Universe. The Astronomical Journal 149(3).

Weinberg DH, Mortonson MJ, Eisenstein DJ, Hirata C, Riess AG, Rozo, E (2013) Observational probes of cosmic acceleration. *Physics Reports* 530(2): 87-255.

Whittaker ET (1945) Spin in the Universe. *Yearbook of Royal Society.* Edinburgh: 5-13.

Zhao GB, Raveri M, Pogosian L, Wang Y, Crittenden RG, Handley WJ, Percival WJ, Beutler F, Brinkmann J, Chuang CH, Cuesta AJ, Eisenstein DJ, Kitaura FS, Koyama K, L'Huillier B, Nichol RC, Pieri MM, Rodriguez-Torres S, Ross AJ, Rossi G, Sánchez AG, Shafieloo A, Tinker JL, Tojeiro R, Vazquez JA, Zhang H (2017) Dynamical Dark Energy in Light of the Latest Observations. Nature Astronomy 1(9): 627-632.

Zhao W, Santos L (2015) The Weird Side of the Universe: Preferred Axis. *International Journal of Modern Physics: Conference Series* 45: 1760009.